FZR-428

Annual Report 2003/04

Radiation Source ELBE

Forschungszentrum Rossendorf

Annual Report 2003/04

Radiation Source ELBE

Editor: Dr. Ulf Lehnert

ZR Forschungszentrum
Rossendorf

Contents

Development of a Superconducting RF photo Gun   53

Appendix   59

Preface

At Forschungszentrum Rossendorf (FZR) near Dresden research is performed using radiation and radioactivity in the **Life Sciences** as well as in research on the **Structure of Matter** and in the fields of **Environment and Safety**. The center belongs to the Wissenschaftsgemeinschaft G. W. Leibniz (WGL), one of the German institutions devoted to extra-university research. Among the six large research facilities run by the FZR the Radiation Source ELBE plays a special role as it offers interesting possibilities for investigations in all the three research programs of the FZR.

During year 2003/2004 significant milestones were acchieved at ELBE. In January, 2003 the first user's operation with scientific purpose started using the bremsstrahlung facility for nuclear spectroscopy. The experiments were mostly run in the night shifts to allow for construction and completion of the facility during the day.

After technical completion of the beamline in October, 2003 the electron beam could be delivered to the radiation physics target chamber. Immediately afterwards the generation of channeling radiation was demonstrated. This was followed by measurements to characterize the used crystals and to optimize radiation efficiency and background supression.

In both years under report a major part of the technical capacity was used for the free-electron laser U27 and it's peripheral facilities. All necessary components could be completed by the end of March, 2004. Due to the preceding carefull and systematic installation and alignment and the use of advanced beam diagnostic methods the generation of infrared radiation was acchieved very quickly. Lasing at a wavelength of 19.6 μm was demonstrated at May 7th, 2004 for the first time. Subsequently, many optimization and characterization runs were performend on both the electron and the infrared beam and the optical resonator. In summer 2004 the first scintifically oriented experiments started using infrared beams in the 15–21 μm wavelength range. Since December, 2004 the laser can be operated at full electron beam power (cw-mode) as well.

Thus, during years 2003/2004 three out of five initially planned secondary radiation targets went into routine user operation. The set-up of the second accelerator module which will increase the available electron beam energy to approximately 40 MeV could be advanced so far that it's installation will take place during January, 2005. Extending the beam energy range and with it the possible spectral range of both the X-ray and the infrared radiation will substantially increase the range of applications of both facilities and will make ELBE even more attractive to scientific users.

Results from Scientific Work at ELBE

The first two years of ELBE operation not only were devoted to the commissioning of the electron accelerator, the various secondary beams and the equipment installed for the experiments, they also brought the first interesting scientific results. Here the outstanding properties of ELBE with its high brilliance beams and the narrow pulse width available in various bunch sequences have played an important role.

For the research on the subatomic structure of matter ELBE delivered intense bremsstrahlung with variable endpoint energies and the respective beam port allowed to take high statistics data on nuclear resonance fluorescence with low non-resonant background. The nuclei studied span the range from ^2H to the doubly magic ^{208}Pb, where the high brilliance of ELBE even allowed the study of polarized photon scattering. Among the other nuclides investigated the Mo-isotopes attracted special interest because of their non-understood high cosmic abundance. They were studied intensively by photon scattering as well as by photo activation and the data give hints for a more detailed understanding of element production in the cosmos, especially with respect to the p-process occurring in high temperature environments.

At the second beam station to become operational, the channeling X-rays source, intense efforts led to the success of a quasi monochromatic X-ray spectrum. This monochromatization was achieved by the channeling process and by Bragg reflection in polycrystalline graphite. The peak has a width of few percent and its energy can be varied in the range from around 10 to 100 keV by changing the electron energy. Since such photon radiation is widely used in diagnostic and therapeutic radiology, precise measurements of the relative biological effectiveness of these X-rays and its dependence on photon energy are prepared. Especially interesting for future experiments at this X-ray beam is its picosecond time resolution.

The one secondary ELBE beam expected to attract the most users is the infrared (IR) radiation from the Free Electron Laser FELBE. Starting in May 2004 IR was produced regularily by sending electron bunches through its undulator U27. The undulator period of 27 mm in combination with electron energies between 15 and 35 MeV allows to cover IR wavelengths from around 4 to 22 μm. Longer wavelengths up to the THz range will become available after the installation of a new undulator (U100) in about one year. In a first life science study a 17 μm FEL beam was focused to a spot size of ~100 μm onto a thin layer of DNA simultaneously irradiated with polarized probe pulses of 0.63 μm. Probably due to IR-induced changes in the DNA the reflectivity as observed by Brewster Angle Microscopy changed synchronously to the FEL. A second pump-probe experiment at the FEL was in the field of semiconductor physics; it used 21.4 μm to determine the relaxation times of superlattices and self assembled quantum dots. In both cases indications of an exponential decay were observed encouraging extended studies at different and especially lower temperatures. In a third application of the intense IR-FEL radiation a very sensitive characterization of environmental samples containing toxic metals was achieved by a collaboration of radiochemists and nuclear physicists of the FZR.

Photodisintegration of the Deuteron

R. Beyer[1], E. Grosse [2], A.R. Junghans[1], G. Rusev[1], K.D. Schilling[1], R. Schwengner[1], A. Wagner[1]

Experimental investigations of the deuteron-photo-disintegration [1] have mainly been performed at energies near and above 100 MeV, where inelastic channels like nucleon resonances and meson production open up and where many partial waves contribute. At photon energies below 10 MeV the situation seems much simpler with only two channels (photon scattering and $d\gamma \to pn$) and only $l = 0$ and $l = 1$ beeing of importance. Nevertheless an exact knowledge of the cross section near the disintegration threshold is of great importance in the field of nuclear astrophysics, as it - together with the inverse reaction $pn \to d\gamma$, related to it by detailed balance - determines [2, 3] the reaction rate of the first step in the big bang nucleosynthesis (BBN).

A detailed quantitative understanding of BBN allows to calculate the primordial abundance ratio of the lightest elements and their isotopes as a function of the photon-to-baryon ratio. From now available observations of abundances in distant and thus young stars a big bang photon-to-baryon ratio can be determined to be compared to the value obtained for the later photon decoupling phase of the universe. This value was determined with high accuracy from the inhomogenity of the cosmic microwave background radiation (CMB) [4].

Most previous photodisintegration experiments at near threshold energies were performed with mono-chromatic photons, delivered either by radioactive decay or by Compton backscattering of a laser beam. In both cases the low photon intensity and systematic errors in determining it accurately have limited the quality of the results. Especially in the region below the maximum cross-section data have been published which are inconsistent within their error bars. One experiment has been reported from a conventional bremsstrahlung facility [5]. Within the range of 7-20 MeV the actual center-of-momentum (CM) energy was determined by a measurement of the outgoing proton energy.

As already pointed out in early theoretical work by Bethe et al. [6], the $l = 0$ (M1) disintegration predominant at energies below 100 keV above threshold can be predicted from the nucleon magnetic moments by an extrapolation from the thermal n-capture on H, which was rather well determined at 295 K. Similarly, the $l = 1$ (E1) disintegration, determinin the cross section above 500 keV, can be connected to the processes thoroughly investigated in the multi MeV range. Proton-neutron potentials (of type Argonne-Urbana, Bonn etc.) [7] as well as effective field theories [8]

have made different predictions for the energy range around 100 keV. This range has been shown to be of special importance for the nucleosynthesis at 10^9 K. Here the cross section is governed by the competition between M1 and E1 [1].
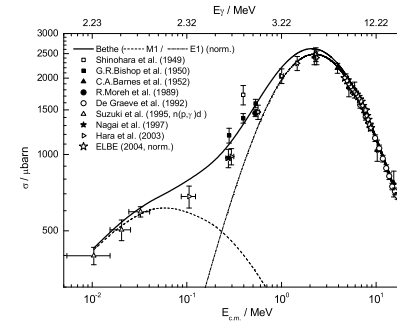
Fig. 1: *Cross section for the Photodisintegration of the deuteron vs. photon energy (top scale) resp. c.m. energy above threshold (bottom scale).*

First studies have been undertaken at the IKH to find out if the electron beam parameters at ELBE - repetition rate in the MHz range and sub-nanosecond pulse width - allow us to improve the data base and thus the comparison to the CMB results. For an extraction of the CM-energy from the nucleon velocities the good time resolution allows a rather short flight path and consequently large solid angle. In an preparative experiment we could show that the low emittance of the electron beam together with the complex photon collimation system allows a proton energy measurement over an extended range (cf. Fig. 1). The energy dependence of these data from ELBE agrees very well to an extended study of the same process at the Ghent linac [5]; obviously the determination of the c. m. energy via the measurement of only one dissociation product delivers consistent results. In future runs at ELBE a normalization to the energy dependent-photon flux can be attained by a simultaneous measurement of photon scattering from added target nuclei with previously determined resonance widths. This method was already successfully applied for the nuclear resonance fluorescence experiments at ELBE.

[1] H. Arenhövel, M. Sanzone, Few Body Systems, Suppl. 3 (1991)

[2] R. H. Cyburt, Phys. Rev. D 70 (2004) 023505

[3] K. M. Nollet, S. Burtes, Phys. Rev. D 61 (2000) 123505

[4] WMAP Coll., Astroph. I., Suppl. Ser. 148 (2003) 1, 175

[5] A. DeGraeve et. al., Nucl. Phys. A 530 (1991) 420 and Phys. Rev. C 45 (1992) 860

[6] H. A. Bethe, G. E. Brown et. al., Nucl. Phys. A 324 (1979)

[7] I.E. Marcucci, Nucl. Phys. A, in press

[8] G. Rupak, Nucl. Phys. A 678 (2000) 405

[1] FZR, Institute of Nuclear and Hadron Physics
[2] also Technische Universität Dresden

First Measurement with Polarised Photons at ELBE

R. Schwengner[1], M. Erhard[1], E. Grosse[1], A. R. Junghans[1], K. Kosev[1], G. Rusev[1], K. D. Schilling[1],
A. Wagner[1]

The excitation of nuclear states by linearly polarised photons in connection with the measurement of the azimuthal asymmetry of the scattered photons is one method to distinguish between electric and magnetic radiation at high photon energies ($E_\gamma > 5$ MeV) and, hence, to determine the parity of nuclear states. For the production of a beam of linearly polarised photons we use the fact that an off-axis portion of the spatial distribution of the bremsstrahlung photons is partly polarised [1, 2]. Using steering magnets the electron beam can be deflected from the normal direction and then deflected back such that it hits the radiator in the centre under a selected angle [3]. As a consequence, an off-axis portion of the spatial distribution of the photons is transmitted through the collimator. The optimum deflection angle for the production of polarised bremsstrahlung is $\theta = m_0 c^2 / E_e$, the ratio of the rest energy to the full energy of the electron. The steering magnets were designed such that the electron beam can be deflected at four azimuthal angles of $0°$, $90°$, $180°$ and $270°$, thus defining four different polarisation planes. A cyclical use of these four directions enables us to reduce the influence of fluctuations of the electron current and of systematic uncertainties.

The applicability of polarised bremsstrahlung was tested by irradiating a ^{208}Pb target at an electron energy of 15 MeV. The deflection of the electron beam was switched between the four possible directions each hour. Fig. 1 shows the degree of polarisation deduced as $P_\gamma = (N_{p\perp} - N_{p\parallel})/(N_{p\perp} + N_{p\parallel})$, where $N_{p\perp}$ and $N_{p\parallel}$ are the intensities of protons resulting from the disintegration of deuterons [4] and measured perpendicular or parallel to the polarisation plane, respectively, assuming an analysing power of one. The energies of these protons were rescaled to the energies of the incident photons as described in Ref. [4]. Spectra measured with those detectors, which belong to the same orientation relative to the polarisation plane, were added up. The maximum degree of polarisation in this first experiment is about 12 % and has still to be optimised in further experiments. Asymmetries deduced for known transitions in ^{208}Pb as $(I_{\gamma\perp} - I_{\gamma\parallel})/(I_{\gamma\perp} + I_{\gamma\parallel})$, where $I_{\gamma\perp}$ and $I_{\gamma\parallel}$ are the intensities of γ transitions observed perpendicular or parallel to the polarisation plane, respectively, are shown in Fig. 2. Positive asymmetry values are expected for electric dipole ($E1$) transitions and negative asymmetry values for magnetic dipole ($M1$) transitions. The deduced values are consistent with those deduced in previous work [5] and hence demonstrate that the facility for polarised bremsstrahlung at ELBE can be used to measure the linear polarisations of many γ transitions in a wide energy range simultaneously.
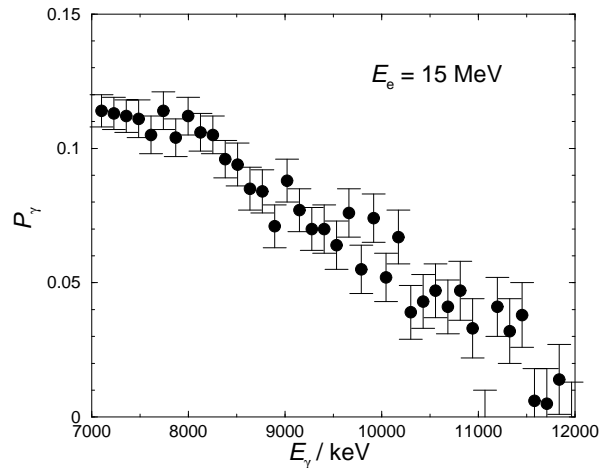
Fig. 1 *Degree of polarisation as a function of the photon energy as deduced from spectra of protons emitted from disintegrated deuterons. Data below $E_\gamma \approx 7$ MeV cannot be used because the proton spectra are at low energy contaminated by scattered photons.*
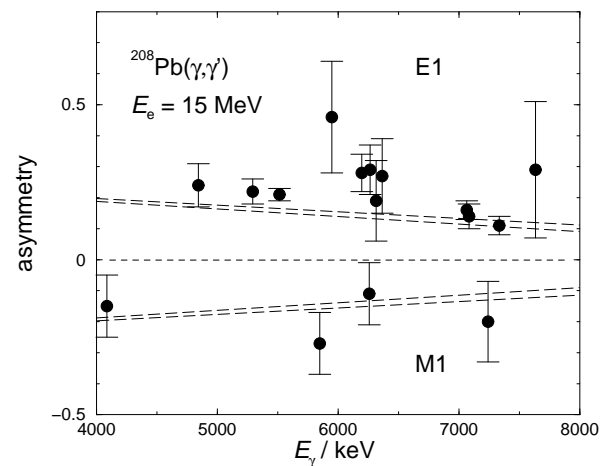
Fig. 2 *Experimental asymmetries of transitions in ^{208}Pb. The bands marked with dashed lines indicate the degree of polarisation as derived from Fig. 1. Note that the bands are extrapolations below 7 MeV.*

[1] U. Kneissl, H.H. Pitz, A. Zilges, Prog. Part. Nucl. Phys. 37 (1996) 349.
[2] K. Govaert et al., Nucl. Instr. Meth. A 337 (1994) 265
[3] K.D. Schilling et al., Wiss.-Techn. Berichte FZR-272 (2003) 31
[4] R. Schwengner et al., this report p. 45
[5] K. Wienhard et al., Phys. Rev. Lett. 49 (1982) 18

[1] Institute of Nuclear and Hadron Physics

Search for E1-Pygmy Strength in Molybdenum Isotopes Close to the Particle Separation Energies

G. Rusev[1], R. Beyer[1], M. Erhard[1], F. Dönau[1], E. Grosse[2], A. Hartmann[1], A.R. Junghans[1], K. Kosev[1], C. Nair[1], N. Nankov[1], K.-D. Schilling[1], W. Schulze[1], R. Schwengner[1], A. Wagner[1]

Within a series of experiments at the new superconducting electron accelerator ELBE devoted to questions of the cosmic element generation (e. g. the problem of overproduction of neutron-deficient stable molybdenum isotopes) a search for E1 resonance strength located close to the particle thresholds was performed. In a detailed study of elastic photon scattering from ^{92,98,100}Mo such strenght as concentrated in so called "pygmy" resonances was searched. A bremsstrahlung continuum with an endpoint energy of 13.6 MeV was used and the scattered photons were detected in 4 large escape-suppressed high-purity germanium detectors. Due to the good background suppression of the experiments more than 90 % of all photons observed in the range of 7 - 12 MeV stem from scattering through resonances (about 300 per isotope). Due to the high density of these partially overlapping resonances only around 20 % of the scattered photons can

be clearly assigned to originate from well isolated resonances. Therefore, an analysis is needed which goes beyond the fitting of distinct "peaks". After a correction for cascading multi-step photon emission a ground state dipole strength function can be constructed from the experimental data using a standart underleveldensity formelism [1]. The resulting strength function can be extrapolated across the particle separation threshold. This extrapolation compares well to the dipole strength extrapolated from experimental (γ, n)-data [2]. An enhancement of the strength near 9 MeV is observed in ^{98}Mo and ^{100}Mo roughly in agreement to predictions from RPA-calculations [2].

[1] A. Gilbert & A.G.W. Cameron, Can. J. Phys. 43 (1965) 1446

[2] H. Beil, et al., Nucl. Phys. A 227 (1974) 427

[3] N. Paar et al., Phys. Lett. B 606 (2005) 288
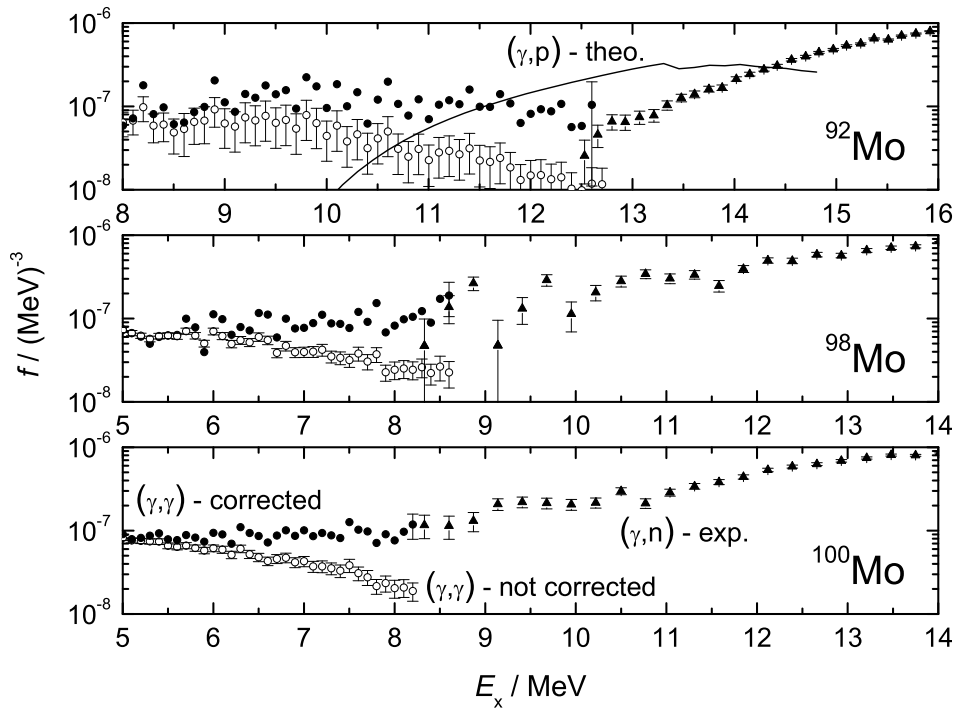
Fig. 1: *Dipole strength functions in ^{92,98,100}Mo as determined from photon scattering data (corrected for multistep decay) and from nuclear photo effect (γ,n) data taken at Saclay [1]. Apparently the two data sets are in accordance in the region of the particle emission thresholds. The ELBE data points are averaged over intervals of 100 keV; for the corrected points a typical error bar is shown for the data point at the highest energy. In ^{92}Mo the strength going into the (γ, p)-channel has to be taken into account.*

below S_n : $\quad f(E, \lambda) = \frac{1}{3(\pi \hbar c)^2 \Delta_E} \sum_i \frac{\int \sigma_{i,\gamma}^{corr} dE}{E_i}$

above S_n : $\quad f(E, \lambda) = \frac{1}{3(\pi \hbar c)}^2 \left\langle \frac{\sigma_{\gamma,n}(E)}{E} \right\rangle$

[1] FZR, Institute of Nuclear and Hadron Physics
[2] also Technische Universität Dresden

Dipole-Strength Distributions in ^{92,98,100}Mo and ^{88}Sr up to the Neutron-Separation Energies

G. Rusev[1], R. Schwengner[1], K. D. Schilling[1], A. Wagner[1], F. Dönau[1],

M. Erhard[1], E. Grosse[1], A. R. Junghans[1], K. Kosev[1], N. Nankov[1]

The response of atomic nuclei to photons has attracted increasing interest in recent years. In particular, the structure of dipole excitations close to the neutron-separation energy is expected to reveal information on new types of collective excitation modes posing a challenge to the theoretical description of the nuclear many-body system [1]. Besides, the distribution of the dipole strength around the neutron-separation energy influences reaction rates in specific processes of the nucleosynthesis and is therefore of importance for astrophysical problems [2].

Dipole-strength distributions close to the neutron-separation energies have been studied for only few nuclides until now. The new bremsstrahlung facility at the ELBE accelerator of the FZR opens up the possibility to investigate dipole excitations with a sensitive detector setup at energies above 10 MeV.

In the course of a systematic study of dipole-strength distributions in nuclei around $A = 90$ we initiated the investigation of the nuclides ^{92}Mo, ^{98}Mo and ^{100}Mo. The investigation of such a chain of isotopes allows us to study the evolution of the dipole-strength distribution with increasing ratio of neutron number to proton number, N/Z.

The nuclei ^{98}Mo and ^{100}Mo had previously been investigated in photon-scattering experiments up to 3.8 MeV [3, 4] at the Stuttgart Dynamitron accelerator. The present photon-scattering experiments at the ELBE accelerator enabled the study of dipole excitations in Mo isotopes to higher energies up to the neutron-separation energies. We performed photon-scattering experiments on ^{92}Mo at electron energies of 6.0 and 13.2 MeV, on ^{98}Mo at 8.5 and 13.2 MeV and on ^{100}Mo at 7.8 and 13.2 MeV. The neutron-separation energies of ^{92}Mo, ^{98}Mo and ^{100}Mo are $S_n = 12.7$, 8.7 and 8.3 MeV, respectively. Samples of 2035.7 mg ^{92}Mo, 2952.5 mg ^{98}Mo and 2916.8 mg ^{100}Mo were used as targets in the experiments. These targets were combined with elementary ^{11}B for photon-flux calibration. Four HPGe detectors of 100 % relative efficiency were used in the measurements, two of them placed at 127° and the other two at 90° relative to the incident photon beam in order to deduce the angular distributions of resonantly scattered γ-rays. Parts of the spectra measured at 127° for the three isotopes are shown in Fig. 1. The closed-shell nucleus ^{92}Mo shows prominent peaks up to 11 MeV while the heavier isotopes ^{98}Mo and ^{100}Mo have weak transitions up to 8.5 MeV. The peaks above 4 MeV in ^{98}Mo and ^{100}Mo were observed for the first time in photon-scattering experiments, while ^{92}Mo was previously investigated at the former linac at Ghent at an electron energy of 10 MeV [5]. The multipolarities of the observed transitions were obtained by comparing the ratios of the γ-ray intensities observed at 90° and 127° with the expected values for dipole and quadrupole transitions, 0.73 and 2.28, respectively. Most of the transitions show dipole character.
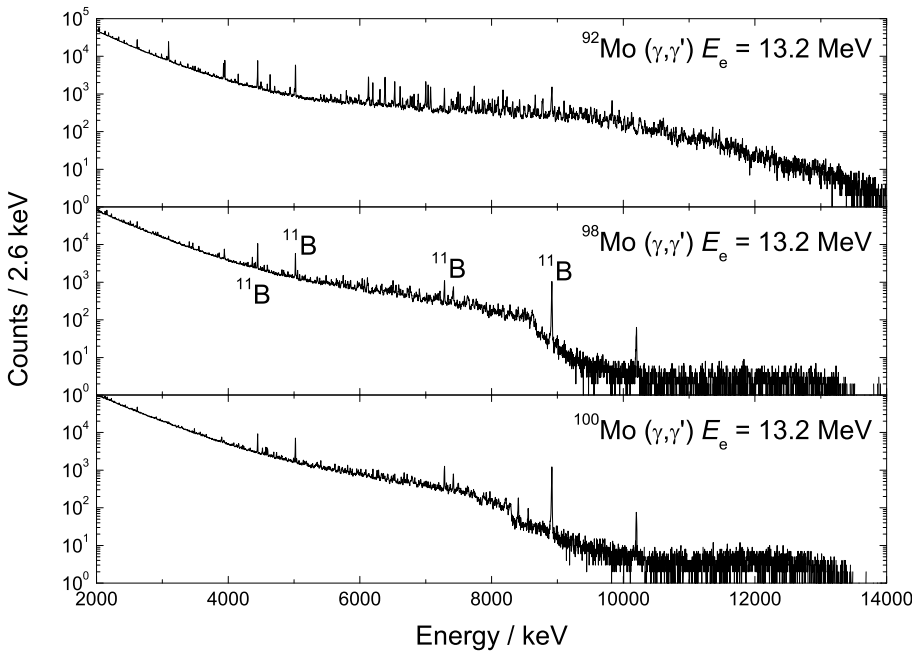

Fig. 1: *Partial photon-scattering spectra from ^{92}Mo, ^{98}Mo and ^{100}Mo measured at 127° relative to the beam axis.*

---

[1]Institute of Nuclear and Hadron Physics

The reduced partial widths Γ_0/E_γ^3 of the observed transitions, which are proportional to the reduced transition strengths, were deduced for the three isotopes. A comparison of the dipole-strength distributions for ^{92}Mo, ^{98}Mo and ^{100}Mo is shown in Fig. 2. The three isotopes display broad distributions up to the respective neutron-separation energies.
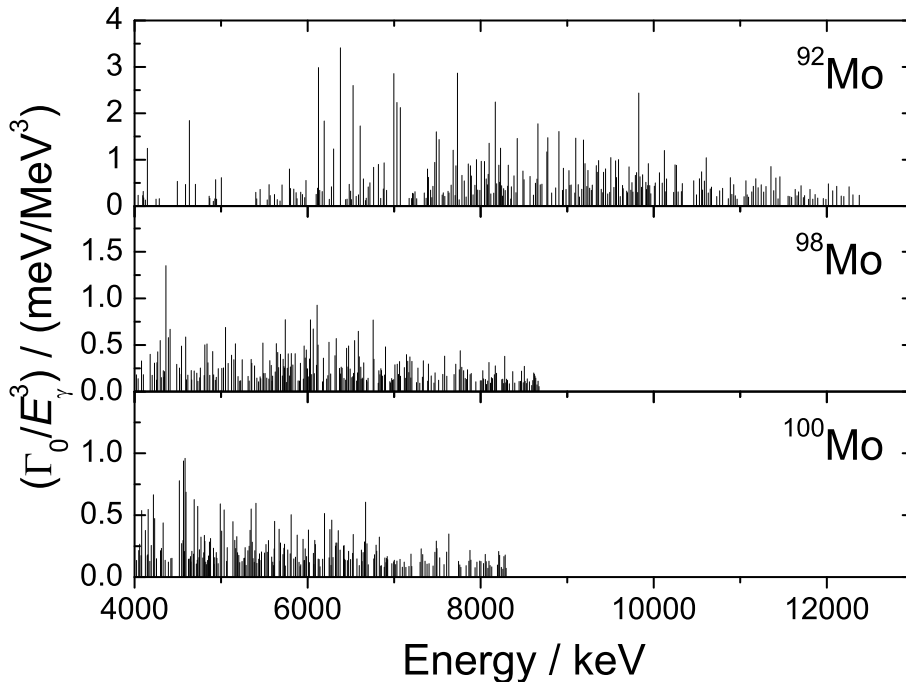
Fig. 2: *Distribution of reduced level widths for the dipole transitions in ^{92}Mo, ^{98}Mo and ^{100}Mo, respectively.*

From the dipole-strength distributions of the three Mo isotopes we deduce the summed strength and study its dependence on the ratio N/Z. The sum of the $E1$ strength has been calculated under the assumption that all transitions above 5 MeV are $E1$ transitions. This sum was calculated over all transitions with an energy above 5 MeV or with energy in the range between 5 and 8.3 MeV (the neutron-separation energy for ^{100}Mo), respectively. Fig. 3 shows the dependence of the energy-weighted $B(E1)$ strength for the three isotopes. The summed $E1$ strength drops by a factor of about five with the number of neutrons changing from 50 to 58.
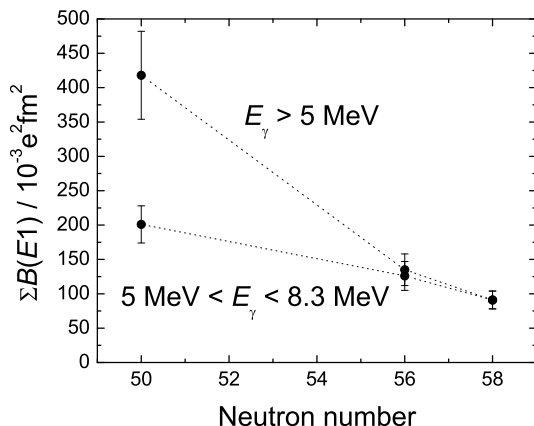
Fig. 3: *Energy-weighted sums of E1 strength for all transitions with an energy above 5 MeV or with an energy in the range between 5 and 8.3 MeV, respectively.*

Such a dependence is in contrast to the understanding of pygmy resonances being due to the vibration of the excessive neutrons against an inert proton-neutron core [1]. The interpretation of the observed behavior requires further experimental and theoretical investigations.

The experiment on the $N = 50$ nuclide ^{88}Sr was carried out with bremsstrahlung produced with an electron beam hitting a niobium radiator of 7 μm thickness. The kinetic energy of the electrons was 13.2 MeV and the average electron current was 400 μA. A 10 cm thick aluminium absorber was placed behind the radiator in order to reduce the low-energy part of the bremsstrahlung spectrum. The target consisted of 2731.8 mg of ^{88}SrCO$_3$ with an enrichment of 99.9 %, combined with 455.5 mg of ^{11}B used for the calibration of the photon flux. γ rays were measured with four high-purity germanium detectors of 100 % efficiency relative to a 3"$\times$3" NaI detector. All detectors were surrounded by escape-suppression shields of bismuth germanate scintillation detectors. Two detectors were placed at 90° relative to the photon-beam direction while the other two were positioned at 127° to deduce angular distributions of the γ rays. About 150 γ transitions in the energy range from 7 to 12 MeV were observed for the first time. Fig. 4 shows ratios of integrated cross sections obtained from the present measurement at $E_e^{kin} = 13.2$ MeV and from our previous measurement at 6.8 MeV [7] for states with excitation energies E_x between 3.5 and 6.5 MeV.
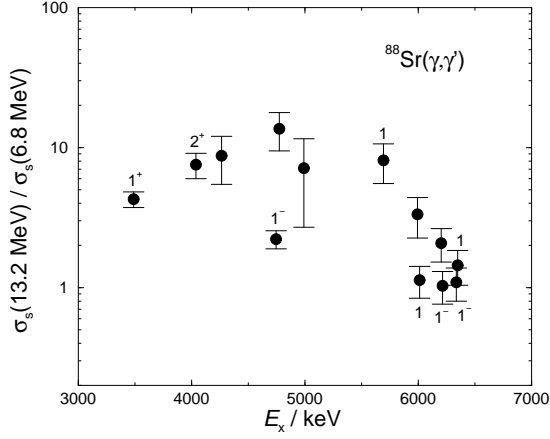
Fig. 4: *Ratios of integrated cross sections obtained in measurements at electron energies of 13.2 and 6.8 MeV.*

Ratios of 2 to 10 for states below 6 MeV indicate a considerable feeding of these states by transitions from higher-lying states in the measurement at 13.2 MeV. However, the feeding becomes small for states with $E_x > 6$ MeV.

The reduced partial widths Γ_0/E_γ^3 deduced from the γ-ray intensities under the assumption, that all transitions are ground-state transitions, are shown in Fig. 5.
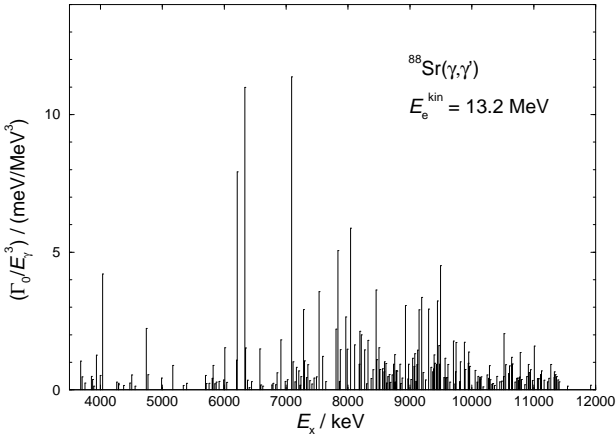
Fig. 5: *Reduced partial widths for transitions in ^{88}Sr.*

These reduced partial widths are proportional to the reduced transition strengths of dipole transitions ($B(E1)$ or $B(M1)$). The dipole-strength distribution is characterised by little strength below 6 MeV and few prominent transitions accompanied by many transitions of small strength at higher energies. The transition with large strength at 7088 keV may be related to the $\nu(g_{9/2} \rightarrow g_{7/2})$ spin-flip transition which is predicted at about this energy by shell-model calculations. The sum of the $B(E1)\uparrow$ strengths for transitions from states between 6 MeV and the highest observed level in ^{88}Sr is compared with the one obtained for the $N = 50$ isotone ^{92}Mo in Fig. 6. This sum seems to increase with the ratio of neutron number to proton number, N/Z. However, the study of further $N = 50$ isotones is necessary to learn about this tendency of dipole strength which has implications for the synthesis of nuclei in explosive stellar events [2].
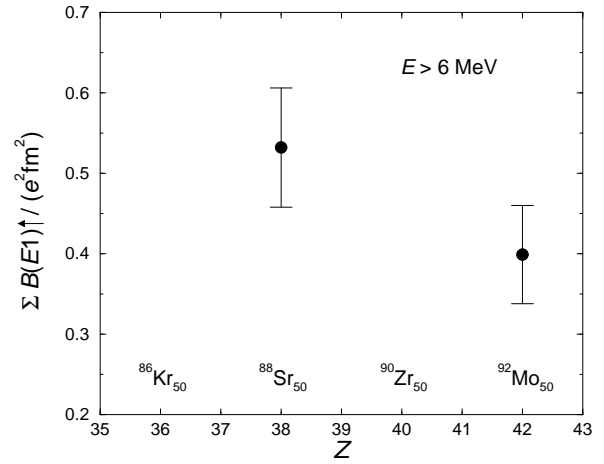
Fig. 6: *Sums of $B(E1)\uparrow$ values for the $N = 50$ isotones ^{88}Sr and ^{92}Mo.*

[1] A. Zilges et al., Phys. Lett. B 542 (2002) 43
[2] S. Goriely, Phys. Lett. B 436 (1998) 10
[3] G. Rusev et al., Wiss.-Tech. Berichte FZR-372 (2003) 34
[4] G. Rusev et al., Wiss.-Tech. Berichte FZR-372 (2003) 35
[5] F. Bauwens, Ph. D. thesis, University of Ghent, 2000
[6] R. Schwengner, G. Rusev et al., Wiss.-Tech. Berichte FZR-401 (2004) 9
[7] L. Käubler, H. Schnare et al., Phys. Rev. C 70 (2004) 064307

$E1$ and $M1$ Strength in ^{92,98,100}Mo Calculated by RPA

F. DÖNAU[1]

The photon beam of the bremsstrahlung facility at ELBE has been used to measure the spin $I = 1$ (dipole) excitations between 4 to 9 MeV excitation energy in ^{92,98,100}Mo in a high resolution experiment. Due to the magic $N=50$ neutron configuration in the ground state the ^{92}Mo nucleus is spherical whereas the occupation of open neutron shells in ^{98,100}Mo is known to lead to deformed shapes [1]. An interesting question is how the distribution of the dipole excitations changes when considering this isotopic series. A further question concerns the suggestion of possible Pygmy resonances for growing neutron excess, i.e. whether the dipole-excitation strength in the vicinity of the neutron threshold increases with the neutron number.

Defining the energy-weighted sum rule $EWSR(E)$ as the integrated $E1$ strength up to the energy E, the ratio $EWSR(E)/EWSR(E_{\max} = 30\,\text{MeV})$ as a function of the energy is shown in Fig. 2. The function $EWSR(E)/EWSR(E_{\max})$ provides a more quantitative measure of the fragmentation effect of the transition strength originated by the structural change in the isotopic series ^{92,98,100}Mo. One notices the stepwise increase of the ratio in ^{92}Mo reflecting again the spherical degeneracy which is modified in ^{98}Mo to a more regular curve in accordance with the more smooth level density in the deformed ^{98}Mo which is seen also in the ratio for ^{100}Mo. The same tendency was found for the analogous ratio of the $M1$ transition strengths.

Fig. 1 *Calculated strength for an $E1$ excitation from the the ground state to a vibrational state at the energy E in ^{92}Mo (solid lines) and ^{98}Mo (dashed lines), respectively. A Lorentzian width $\Gamma = 10$ keV 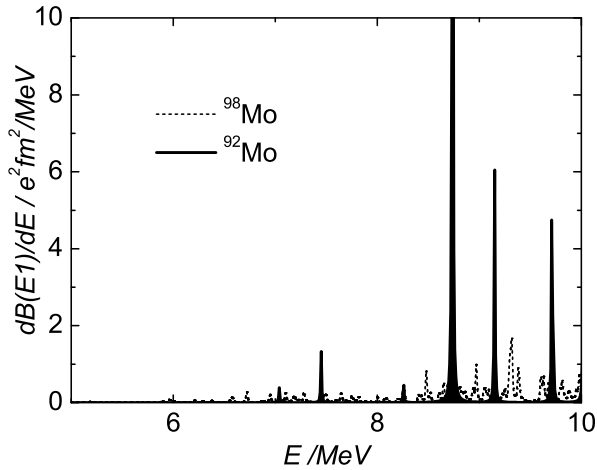is used in both nuclei. The strength distribution in ^{100}Mo which is not shown here is qualitatively quite similar to the one in ^{98}Mo.*

The RPA code [2] has been applied to investigate what the mean field plus RPA is predicting for this case. In Fig. 1 we present the calculated $E1$-strength distribution for ^{92}Mo and ^{98}Mo as obtained for an isovector dipole-plus-octupole interaction. The strength of the residual interaction was chosen to fit the position of the giant dipole resonance. The selfconsistently calculated shape of the Nilsson potential changes from $\varepsilon = \gamma = 0$ in ^{92}Mo to $\varepsilon = 0.19, \gamma = 16°$ in ^{98}Mo. The resulting $E1$ strengths found in the RPA calculation are shown in Fig 1. The transition strength in the spherical ^{92}Mo is distributed into a few strong lines corresponding to the degeneracy of the spherical shells and their strong selection rules for $E1$ transitions. In contrast, the transition strength in ^{98}Mo appears strongly fragmented due to the shell splitting in a deformed field.

Fig. 2 *Ratio of the calculated energy-weighted sum rule $EWSR(E)/EWSR(E_{\max} = 30$ MeV$)$ as a function of the energy E. Note, that $EWSR(E)$ amounts at $E = 10$ MeV only to about 2 % of the total $EWSR$.*

Comparing the $EWSR$ ratios in detail one finds that the values in the spherical case are fluctuating with a large period about the more smoothed values in the deformed case. It seems suggestive to perform a similar analysis of the experimental data by extracting the fractional $EWSR$s in order to obtain information about the shell structure in the isotopic series which can be compared with the calculation. It is evident that for such a comparison the experimental transition strength need to be measured for a large enough energy interval in order to obtain a sensitive $EWSR$ ratio. A comparison of such ratios at an arbitrarily selected excitation energy E is probably not very conclusive because of the fluctuating character of this ratio.

[1] P.F. Mantica, A.E. Stuchbery *et al.*, Phys. Rev. C 63 (2001)034312

[2] F. Dönau, this report, p. 8

---

[1]Institute of Nuclear and Hadron Physics

Measurements of Photodisintegration Yields of Mo and Au at Different Energies

M. Erhard[1], E. Grosse[1], A.R. Junghans[1], K. Kosev[1], C. Nair[1], N. Nankov[1], G. Rusev[1], K.D. Schilling[1], R. Schwengner[1], A. Wagner[1]

The aim of photoactivation studies with bremsstrahlung at ELBE is the investigation of p-nuclei like ^{92}Mo [1] to determine photodisintegration cross sections of astrophysical interest [2]. The measured photoactivation yield is proportional to the integral of the photon flux times the photodisintegration cross section. The γ decay of the photodisintegration products is used to identify the number of nuclei produced. The photon flux can be deduced from the known ^{11}B transition strengths and from the activation of Au samples irradiated together with natural molybdenum.

In ^{92}Mo, the proton-separation energy is $S_p = 7.456$ MeV, and the (γ, p) process populates the 105-keV state ^{91m}Nb with a half-life $T_{1/2} = 60.86$ d [1]. The neutron-separation energy is $S_n = 12.672$ MeV, and the (γ, n) process decays to the 64.6 s isomer of ^{91}Mo. Calculations with TALYS [3] show that the direct population of the ground states (g.s.) for both, ^{91}Mo and ^{91}Nb, is strongly reduced due to the high spin difference between the decaying ^{92}Mo continuum states and the corresponding g.s. If the activation energy is below S_n, a unique signature of the (γ, p) process is the electron-capture decay of ^{91m}Nb (branching ratio $K = 2.9\%$) into an excited level of ^{91}Zr, which deexcites into the stable g.s. by emitting a 1205 keV γ quantum.

From the intensity of the full-energy peak measured with an HPGe detector [4], the photoactivation yield was derived by taking into account the total deposited beam charge, target mass, isotopic abundance, decay and measurement time, full-energy peak efficiency, and dead time as well as coincidence-summing corrections.
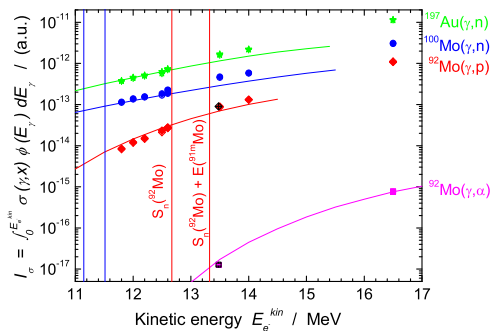

Fig. 1: *Integrated excitation functions of photodisintegration processes in Mo isotopes (points) and theoretical predictions from a Hauser-Feshbach model [5] folded with the photon-energy distribution [6] up to the endpoint energy E_e^{kin}. Theoretical curves are adjusted to the low-energy points in $^{197}Au(\gamma, n)$.*

In Fig. 1, the measured photoactivation yields are compared to model calculations. The theoretical curves are normalised to fit the simultaneously measured ^{197}Au(γ, n) data at low energies. At the highest

activation energy at ≈ 16.5 MeV, we observed the ^{92}Mo$(\gamma, \alpha)^{88}$Zr reaction for the first time $[T_{1/2}(^{88}$Zr$) = 83.4$ d; $E_\gamma = 393$ keV; $K = 97.24\%]$. The photoactivation of enriched ^{92}Mo (97.31%) at 13.48 MeV was used to get a second value for the (γ, α) yield. This value was normalised relative to the yield of the 1205-keV transition from ^{92}Mo(γ, p). The reaction ^{100}Mo(γ, n) was observed by analysing the transition at 740 keV. Photoactivation of ^{92}Mo at energies above the neutron threshold plus the excitation energy of the isomeric state of ^{91m}Mo leads to a contribution of the (γ, n) channel in the measured yield, since ^{91m}Mo decays to ^{91m}Nb via β^+ decay with a probability of 50%. Because of the short half-life this contribution cannot be separated by measuring γ quanta from the ^{91m}Mo decay. The ^{91}Mo g.s. decay branch, however, can be used to separate the (γ, n) contribution. The g.s. itself decays with a half-life of $T_{1/2} = 15.5$ min predominantly to the g.s. of ^{91}Nb via β^+ decay. The decay of the Mo sample was measured in several short runs directly after the irradiation, the result is shown in Fig. 2. The transitions at 1582 and 1637 keV in ^{91}Nb allow to deduce the number of ^{91}Mo nuclei produced from ^{92}Mo(γ, n).
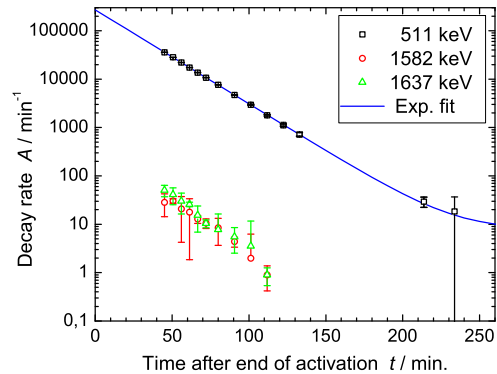
Fig. 2: *Decay of ^{91}Mo. Photoactivation of 677 mg ^{nat}Mo ($E_e^{kin} \approx 16.5$ MeV, $t_{irr} \approx 7$ h, $I_e \approx 350$ μA). The data point of the 511 keV annihilation peak measured after 234 min gives an upper limit of the background contribution. The half-life $T_{1/2} = (15.49 \pm 0.04)$ min [statistical error] deduced from the fit reproduces exactly the literature value of $T_{1/2} = (15.49 \pm 0.01)$ min.*

[1] M. Erhard, A. Wagner et al., Wiss.-Techn. Berichte FZR-401 (2004) 13

[2] M. Arnould, S. Goriely, Phys. Rep. 384 (2003) 11

[3] A.J. Koning et al., program TALYS-0.64 (Dec 2004), NRG Report 21297/04.62741/P FAI/AK/AK

[4] M. Erhard, E. Grosse et al., this report, p. 12

[5] T. Rauscher, F.-K. Thielemann, Atom. Data and Nucl. Data Tables 88 (2004) 1

[6] L.I. Schiff, Phys. Rev. 83 (1951) 252

[1]Institute of Nuclear and Hadron Physics

Measurement of Channeling Radiation at ELBE

W. Wagner[1], A. Panteleeva[1], J. Pawelke[1], W. Enghardt[1]

The beamline for Radiation Physics at ELBE was put into operation in October 2003. Research work on the production of channeling radiation (CR) has been started in view of its feasibility for application as a non-conventional quasi-monochromatic X-ray source to be used for biomedical investigations [1].

The experimental setup consisted in a 42.5 μm thick diamond type IIa crystal fixed on a 3-axes goniometer. This device was constructed by FMB Berlin and especially designed to meet the rather strong demands for handling it under the extremely clean UHV conditions in line with the superconducting electron accelerator ELBE.

Spectrometry of the CR observed has been carried out using Si-pin-diodes as well as CdZnTe detectors. For shielding against the intense background radiation the detectors were housed inside a 10 cm thick Pb collimator with a diaphragm of 5 mm diameter which was positioned under zero degree with respect to the beam direction at a distance of 3.2 m from the target crystal. To avoid a high energy threshold due to the attenuation of radiation in air an evacuated (2 mbar) auxiliary pipe was mounted between the Be-window (127.5 μm) of the UHV electron beamline and the detector station.

Fig. 1: *Energy spectrum (lower one) of (110) planar CR at an electron energy of 17 MeV. For clearness, the spectra measured at aligned and random (grey) crystal orientation are shifted on the ordinate scale by +1000.*
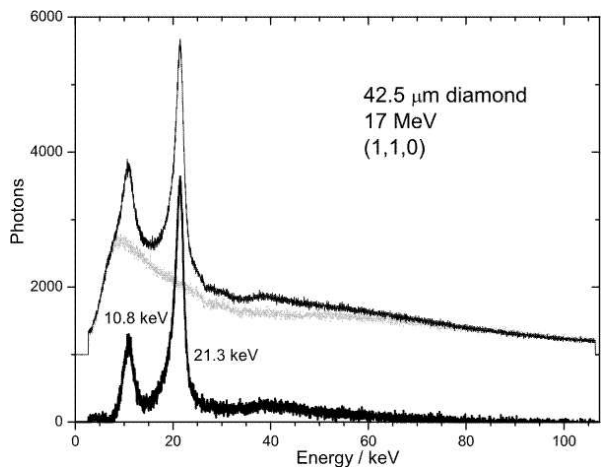
Measurements of planar and axial CR spectra have been performed for the zone of the crystal axis [110] at electron energies (E_e) of 14.6 and 17 MeV. For illustration, the spectrum measured for the (110) plane at 17 MeV is given in Fig. 1 together with the related spectrum of bremsstrahlung which has been registered at slightly non-aligned crystal orientation and was normalized to the (110) spectrum at its high-energy tail.

The spectral distribution of CR (also shown in Fig. 1) is then obtained as the difference of both these spectra. It consists of two CR lines representing the lowest transitions between bound channeling states (1–0 and 2–1) as well as a weaker and broader peak from a free-to-bound transition. The energy values (E_x) measured for some prominent CR lines are listed in Tab. 1.

Tab. 1: *Energies of prominent CR lines.*

E_e/MeV	Index	Transition	E_x/keV
14.6	(110)	1–0	16.5
	(111)	2–1	11.1
17.0	(100)	1–0	13.3
	(110)	1–0	21.3
		2–1	10.8
	(111)	2–1	13.7
		3–2	10.8
		1–0	8.5
	(113)		11.2
17.0	[110]	2p–1s	68.6
		3d–2p	44.0
		3p–2s	28.2

During the first run absolute monitoring of the electron beam current which typically amounted to about 1 nA was not yet available. The installation of a secondary electron monitor (SEM) [2] directly behind the source crystal to avoid electron losses due to the scattering in the target was still in progress.

Some very rough estimation of the CR yield, however, could be carried out by calculating the number of electrons from the output of bremsstrahlung registered simultaneously with CR. Partial integration of the measured spectrum has been performed at an energy larger than 70 keV where possible coherent contributions from free-to-bound transitions are negligible. The resulting yield for the 1–0 transition of planar CR at 17 MeV (Fig. 1) amounts to 0.088 photons/sr e$^-$. Although the uncertainty of this estimation is rather high (about 70%) and systematic errors for the time being ignored may lead to a substantial underestimation of the CR yield, this value converts into a CR rate of 1.6×10^{10} photons/s 10%BW if one assumes an average beam current of 100 μA. By the order of magnitude, such CR rates meet the requirements to investigate RBE values of soft X-rays on living cells [3].

[1] W. Neubert, W. Enghardt, U. Lehnert, E. Müller, B. Naumann, A. Panteleeva, J. Pawelke, Proc. Conf. Monte Carlo 2000, Lisbon 2000, Eds. A. Kling, F. Barão, M. Nakagawa, L. Távora, P. Vaz, Springer-Verlag Berlin-Heidelberg-New York(2001)123

[2] V.V. Morokhovskyi, PhD-Thesis D17, TU-Darmstadt, 1998

[3] A. Panteleeva, W. Enghardt, U. Lehnert, J. Pawelke, Wiss.-Techn. Berichte FZR-271 (1999) 95

[1]FZR, Institute of Nuclear and Hadron Physics

15

Yield Dependence of Electron Channeling Radiation on the Crystal Thickness

W. Wagner[1], B. Azadegan[1], J. Pawelke[1], W. Enghardt[1]

The dependence of the yield of channeling radiation (CR) on the thickness (d) of the diamond crystal has been investigated at ELBE.

In earlier works [1,2] the dissipative ansatz for the population of bound states $P_n(z)$ defined an energy dependent occupation length l_{occ} from the integral

$$N_{ch} \propto \int_0^d P_n(z)dz = 1 - e^{-z/l_{occ}}, \qquad (1)$$

where the intensity of a CR line N_{ch} is given by the product of thin-target transition probability and the occupation probability of a channeling state (Eq. 1). First systematic investigations on diamond at low electron energies (5-10 MeV) have been extended to a crystal thickness of $200\,\mu m$ [3]. It has been shown that the population dynamics is governed by multiple scattering of the electrons in the crystal. Especially at larger crystal thickness the intensity rather follows

$$N_{ch} \propto \Theta_{MS}(d) \sim \sqrt{d}, \qquad (2)$$

where $\Theta_{MS}(d)$ is the mean angle of multiple scattering. To prove such behaviour a further series of CR measurements has been carried out. The electron beam of ELBE with an energy of $14.6\pm0.2\,MeV$ was focused at the crystal position into a spot of 1 mm diameter with a divergence of about 0.1 mrad $\langle rms \rangle$. Three perfect diamond crystals, all of type IIa, with the thicknesses $42.5\,\mu m$, $102\,\mu m$ and $168\,\mu m$ have been used for the measurement of the yield of the 1-0 transition of planar (110) CR.

The CR as well as random bremsstrahlung spectra have been registered by a $300\,\mu m$ thick Si-pin-diode positioned 3 m away from the target at zero degree with respect to the beam direction inside a thick Pb collimator with an aperture of 1 mm. An auxiliary vacuum line (1.6 mbar) has been installed between the $127.5\,\mu m$ thick Be-window of the accelerator beamline and the detector to minimize X-ray absorption. The total beam charge was monitored with the help of a secondary electron monitor (SEM) [4] positioned directly behind the crystal to diminish losses due to electron scattering in the target.

The measured spectra were corrected for detector efficiency, self absorption and attenuation in window materials on the path to the detector. After subtraction of the bremsstrahlung background (Fig. 1) an appropriate function has been fitted to the profile of the 1–0 CR line. To calculate the CR yield the number of electrons was obtained by integration of the respective SEM-scaled differential bremsstrahlung flux [5] which was found to increase linearly with target thickness. The resulting CR yields versus the crystal thickness are shown in Fig. 2 together with the curves obtained in accordance with Eq. (1) (thin line) and Eq. (2) (thick line). It is obvious that the $\sqrt{d}$-dependence better fits the data points confirming the results of ref. [3]. The effect of multiple scattering also leads to a broadening of the CR line width which amounted to $1.54\,keV$ and $2.5\,keV$ for $42.5\,\mu m$ and $168\,\mu m$, respectively, and a slight shift of the peak centroid (Fig. 1).

When Eq. (1) accounts for the depopulation of channeling states with thickness, multiple scattering seems to come into play at larger crystal thickness (or at lower electron energies) and partly compensates dechanneling leading to a more steep increase of the CR yield with increasing crystal thickness than prescribed by Eq. (1). This is due to contributions from in-plane scattered electrons as well as due to the redistribution of the population of channelling states. If l_{occ} depends linearly on the electron energy, Eq. (1) is able to describe the dependence of the CR yield on the crystal thickness to approximately $2 \times l_{occ}(E)$ only.
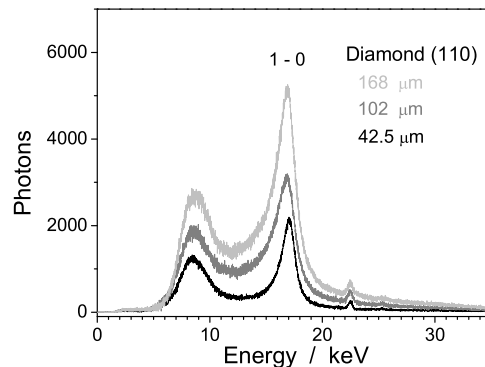
Fig. 1: *CR spectra of (110) diamond at 14.6 MeV.*

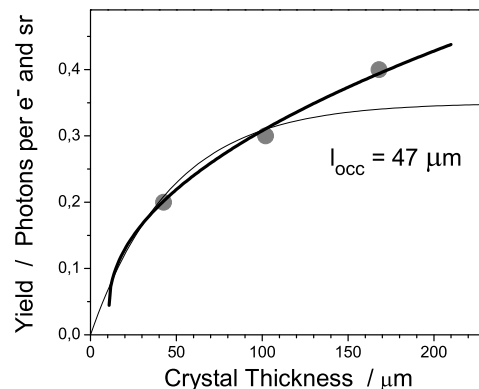**Fig. 2:** *CR yield versus crystal thickness.*

[1] J.O. Kephart, R.H. Pantell et al., Phys. Rev. B40 (1989) 4249
[2] U. Nething, M. Galemann et al., Phys. Rev. Lett. 72 (1994) 2411
[3] I. Reitz, Diplomarbeit, TU Darmstadt (1999)
[4] W. Neubert, K. Heidel et al., this report p. 39
[5] J.D. Jackson, Classical Electrodynamics, Wiley, New York (1975)

[1]FZR, Institute of Nuclear and Hadron Physics

Monochromatisation of Channeling X-rays at ELBE Using HOPG Crystals

J. Pawelke[1], B. Azadegan[1], W. Wagner[1], W. Enghardt[1]

The application of channeling radiation (CR) as an unconventional X-ray source to be used for radiobiological research requires the separation of the quasi-monochromatic CR line from the unavoidable polychromatic bremsstrahlung background [1]. Monochromatisation on the base of Bragg reflection in highly oriented pyrolytic graphite (HOPG) mosaic crystals was chosen in order to retain as much as possible of the CR intensity. A first monochromator has been manufactured whose curved surface was designed for optimal separation of the CR peak of 18.4 keV mean energy from the 1-0 transition of the (110) electron planar channeling in diamond [2]. First test measurements at ELBE, however, have been performed with a planar HOPG crystal since the curved monochromator requires a change of the beam line beforehand.

The electron beam of ELBE with an energy of 14.6 ± 0.2 MeV was focussed at the position of the CR crystal into a spot of 1 mm diameter with a divergence of about 0.1 mrad (rms). The CR spectrum has been measured by a Si-PIN photodiode positioned 3.2 m away from the 42.5 μm thick diamond crystal at zero degree with respect to the beam direction (X-axis) inside a thick Pb collimator with an aperture of 1 mm. The energy spectrum of the CR is presented in Fig. 1, showing the CR peak at 16.5 keV with a width of 1.8 keV FWHM.
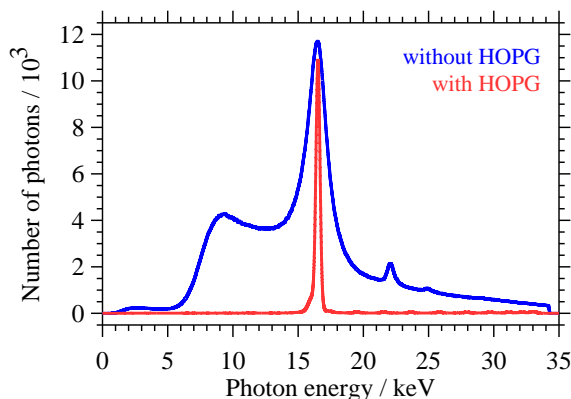

Fig. 1: *Energy distribution of (110) planar CR at zero degree (upper line) and after reflection in the HOPG crystal at 13.1 degree (lower line). Both spectra are scaled for the same electron beam charge, measurement time and detector solid angle.*

Thereafter, a planar HOPG crystal of 10×8 cm^2 size, 1 mm thickness and 0.8 degree mosaicity (Optigraph Ltd., Moscow, Russia) was moved to the centre of the CR cone along the horizontal line (Y-axis) perpendicular to the beam direction by a stepping motor unit. For this purpose, a HOPG crystal from the same batch as used for covering the curved monochromator described in [2] was directly deposited on a 1 cm

thick polymethyl methacrylate plate and positioned with its 10 cm side parallel to the horizontal beam direction, the 8 cm side being vertically oriented and the centre of the crystal being at a distance of 1.7 m from the diamond. The stepping motor unit also allowed the rotation of the crystal about its two axes, parallel to the 10 cm ($\theta_{max} = \pm 6°$) and the 8 cm ($\phi_{max} = \pm 180°$) side, respectively. The energy spectrum after reflection has been measured by a second Si-PIN photodiode positioned 1.7 m away from the centre of the HOPG at $\phi = 13.0 \pm 0.5°$ inside a thick Pb collimator with an aperture of 3 mm. With the HOPG crystal at an angle $\phi = 6.5°$ the Bragg reflection condition for 16.5 keV photons of the CR peak (cf. Fig. 1) is fulfilled. The spectrum after reflection is shown in Fig. 1 as well, demonstrating a high peak reflectivity of the HOPG crystal. However, the considerably reduced peak width of 0.4 keV FWHM denotes a rather low integral reflectivity and is smaller than the energy spread of about 2.0 keV FWHM expected from the HOPG mosaicity. The reason for that is the small angular acceptance of the HOPG crystal (about 0.15°) in the CR cone. By moving the HOPG crystal along the Y-axis but keeping the angles constant the peak position and height in the reflected spectrum are changed. In Fig. 2 the peak energy and area of the reflected spectrum are shown for several Y-positions and are compared with the width of the CR peak at zero degree. The width of 1.0 keV FWHM demonstrates the reflection of an HOPG monochromator of optimised geometry with high integral reflectivity which retains the intensity of the rather broad CR peak as much as possible.
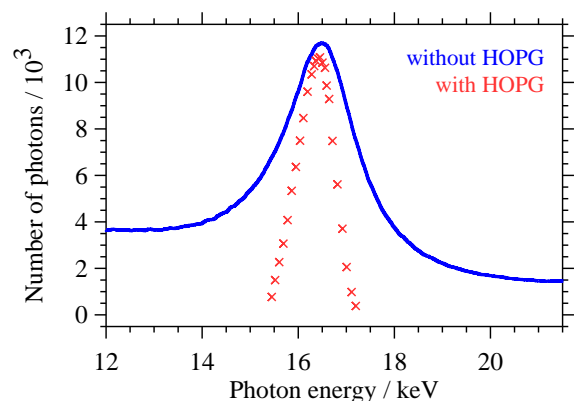

Fig. 2 *Peak-width comparison of (110) planar CR at zero degree (line) with the spectrum obtained by scanning the HOPG crystal 20 mm along the Y-axis (symbols).*

[1] W. Wagner, A. Panteleeva et al., Wiss.-Techn. Berichte FZR-401 (2004) 56

[2] J. Pawelke, A. Heitsch et al., Wiss.-Techn. Berichte FZR-372 (2003) 68

[1]FZR, Institute of Nuclear and Hadron Physics

Degenerate Pump-Probe-Experiments on Semiconductor-Heterostructures

D. Stehr[1], M. Krenz[1], S. Winnerl[1], T. Dekorsy[1], M. Helm[1], F. Schrey[2], K. Unterrainer[2], G. Strasser[2]

We performed time-resolved measurements on two kinds of III-V-semiconductor-heterostructures, namely superlattices (SL) and self-assembled quantum dots (QD). In the case of superlattices two semiconductors with different bandgaps, here pure GaAs and $Al_{0.3}Ga_{0.7}As$, are grown alternating epitaxially on a semi-insulating GaAs wafer. Due to the conduction band offset between these two materials so called *quantum wells* are formed in which the electrons are confined. If the barriers between each quantum well are thin enough, the states will be coupled and a *miniband*-structure in the conduction band is established (for an schematic illustration, see Fig. 1b). These minibands are much narrower than the energy bands in bulk materials. The dispersion is plotted from the center of the *mini*-Brillouin-zone to its edge, which is located at π/d (d = superlattice period, see Fig. 1a).
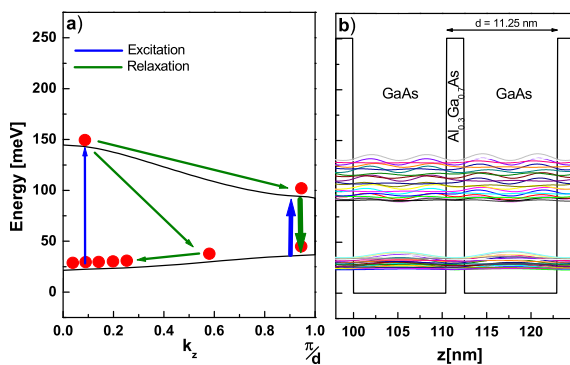

Fig. 1: *(a) Miniband dispersion with a sketch of the relaxation processes. The arrows on the very right ($k_z = \pi/d$) reflect our experiment. (b) A short section of the superlattice with conduction band edge and wavefunctions*

In this picture we briefly discuss the aim of our experiments. After excitation with a strong (10-100 MW/cm^2) pump pulse, we will probe the absorption with a (weaker) second pulse with the same wavelength (probe pulse). As one can see from Fig.1, in this n-doped superlattice there will be a broad absorption regime from 55-110 meV ($22 - 10\,\mu m$). For this experiment the FEL was tuned to $21.4\,\mu m$, so electrons are excited near the edge of the mini-Brillouin-zone.

After excitation to the second miniband, the relaxation occurs mainly via the emission of longitudinal-optical (LO) phonons ($\hbar\omega_{LO} \approx 36$ meV) on a picosecond timescale.

For measuring these decay times a degenerate ($\lambda_{pump} = \lambda_{probe}$) pump-probe setup has been established, which is sketched in Fig. 2.
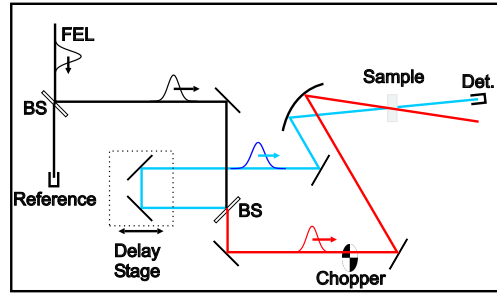
Fig. 2: *Degenerate pump-probe setup*

First, the beam is split into an experiment beam and a reference beam (ratio 95/5) for recording possible instabilities of the FEL. Afterwards, the beam is split into a pump and probe beam, the latter sent through a mechanical delay stage. Depending on the time delay we can record a change in the transmission of the probe beam. If the probe pulse arrives at the sample after the pump pulse, we can monitor the relaxation from the second to the first miniband. Behind the sample the two beams are separated from each other, and the intensity of the probe beam is recorded with a LN_2-cooled HgCdTe Detector. For obtaining a better S/N-ratio, optical chopping of the pump beam has been applied to record the signal using lock-in techniques.
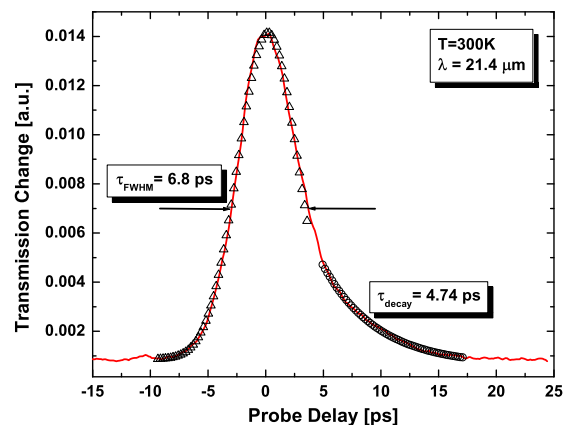
Fig. 3: *Pump-probe signal from the superlattice sample.*

The pump-probe signal from the superlattice is shown in Fig. 3. The curve is dominated by a symmetrical contribution, which reflects the pulse duration of the FEL and is simply its autocorrelation. Extracting the full width at half maximum (FWHM) of 6.8 ps indicates a pulse length of 4.2 ps. However, the curve is slightly asymmetric and on the positive delay side a longer tail is evident. This can be fitted with an expo-

---

[1] Institute of Ion Beam Physics and Materials Research, FZR
[2] TU Wien, Vienna, Austria

nential of $\tau = 4.7$ ps. Though this appears somewhat too long for LO phonon relaxation, we note that relaxation times of a few picoseconds have been predicted for electrons at the edge of the mini Brillouin zone (however at $T = 5$ K)[1]. In the future we plan to extend these experiments to lower temperatures and of course to different excitation wavelengths. In addition, somewhat shorter FEL pulses are desirable. This will allow us to gain more information about the electron relaxation in the excited miniband, relevant for so-called superlattice quantum cascade lasers.

In case of QDs one grows lattice-*mismatched* semiconductors on top of each other, in this case InAs on GaAs, and small islands of InAs are formed due to strain relaxation (see Fig. 4a). In these QDs *discrete* energy levels are formed (e_1 and e_2, Fig. 4b), where the ground state wavefunction has s-type symmetry while the first excited state has p-symmetry. For usual dot sizes of 10-20 nm diameter the transition energy from e_1 to e_2 (ϵ_{12}) lies between 50 and 60 meV (25-20 μm).
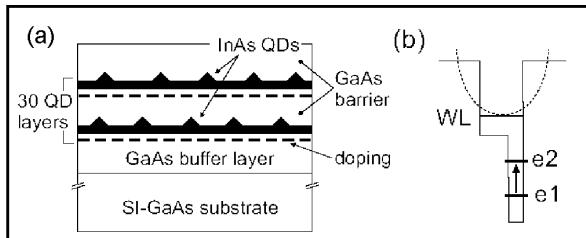
Fig. 4: *Growth scheme (a) and energetic properties (b) of self-assembled quantum dots (compare [2]).*

Due to its character of a zero-dimensional system, direct relaxation via LO-phonon-scattering like in case of a superlattice is prohibited, if the energies are not matched, and thus the relaxation time is expected to

be much longer, in the 10-100 ps range. Furthermore the relaxation mechanism of the $e_1 \rightarrow e_2$ transition has been discussed for several years, in particular the strong-coupling polaron formed in the quantum dots [3].

The aim of our experiment is to determine the relaxation time of doped QDs using degenerate pump-probe-measurements with the FEL.
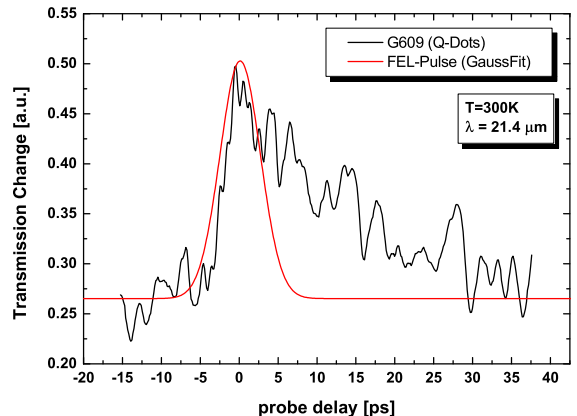
Fig. 5: *Pump-probe signal from the quantum-dot sample.*

The result of our first experiments is shown in Fig. 5. Due to the very low absorption of the sample ($< 5\%$), the signal to noise-ratio is much smaller than in the case of superlattices. Still we were able to record a weak transmission change in the probe beam under conditions where the FEL was running continuously with 13MHz repetition rate (no macrobunches). The decay time is of the order of 15 ps, but obviously more experiments have to be performed, in particular at low temperatures.

[1] F. Compagnone et al., Appl. Phys. Lett. **80**, 920 (2002)

[2] L. Rebohle et al., Appl. Phys. Lett. **81**, 2079 (2002)

[3] S. Hameau et al., Phys. Rev. Lett. **83**, 4152 (1999)

FEL-light induced changes in thin organic films observed by dynamic Brewster Angle Microscopy

M. Sczepan[1], G. Furlinski[1], D. Wohlfarth[1], W. Seidel[1], K. Fahmy[1]

Brewster angle microscopy is a proven technique for the evaluation of thin organic films [1], especially for the observation of phase transitions in monolayers [2]. If a sample is observed under Brewster angle conditions, small changes in the refractive index of the surface can be observed and thus thin layers on the surface can be made visible. Coupling a Brewster angle microscope with a powerful light source like the FEL allows investigation of the IR induced changes in thin organic films. Using the temporal characteristics of the pump light, fast processes (down to $20\,\mu s$ using an electronic delay system for the camera shutter or even down to some nanoseconds using a synchronized pulsed illumination source and an optical delay line) can be tracked.

The microscope setup (Fig. 1) consists of an illumination system, an imaging system and a pump beam delivery system. The angle of the illumination and imaging systems can be adjusted to work with substrates with different refractive indices and Brewster angles.

The Brewster angle illumination system uses a HeNe-cw-laser as a light source. An additional optical delay line can be used for work with a pulsed illumination source. The light is focussed onto the sample using a $250\,mm$ focal length off-axis paraboloid mirror. A thin film polarizer allows only p-polarized light to illuminate the sample.

Fig. 1: *Schematic view of the Brewster angle microscope setup. The sample is illuminated by a polarized HeNe laser beam and observed using a home built 20-fold magnification microscope. The FEL pump-light is focussed onto the observed spot using a short focal length off axis parabolic mirror.*
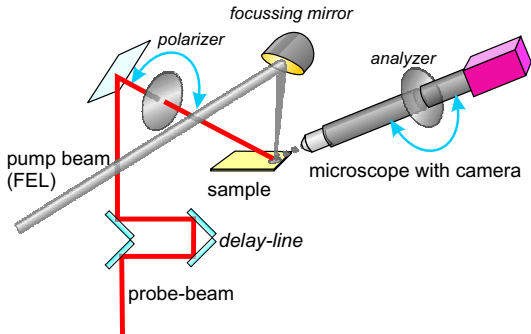
The sample is mounted on a 3-axis translation stage for easier alignment. It is observed using a microscope constructed from a 10x microscope lens (Zeiss A-Plan), a $200\,mm$ focal length tube lens and a $25\,mm$ focal length projection lens. An internal analyzer eliminates scattered and thus depolarized light emerging from the sample. The image (field of vision is about $300\,\mu m$ wide) is captured by a 780x582 pixel monochrome CCD camera (AVT Marlin 046B). An electronic delay system allows to synchronize the camera with the FEL macropulse structure. The microscope tube can be adjusted in object distance, angle and x and y directions.

The sample is irradiated with the FEL light using an off axis parabolic mirror (focal length $37\,mm$). With an initial beam diameter of $15\,mm$ the pump beam can be focused down to a spot size of about $100\,\mu m$. For easier alignment a HeNe-Laser based co-alignment system has been set up.

We are interested in the study of IR-pulse induced structural changes in biopolymers. A large number of superstructures is particulary important for DNA function. Our experiments aim at the induction and kinetic analysis of the IR-induced transitions between such states.

First tests of the systems have been performed using thin layers of DNA. A small drop $(20\,\mu l)$ of DNA solution (concentration $1\,mg/ml$) was applied on a zinc selenide substrate. After drying a thin layer (some micrometers) was formed. This sample was irradiated with infrared light from the FEL ($17.0\,\mu m$ wavelength, $400\,\mu s$ macro bunch length, $2\,Hz$ repetition rate, single pulse energy $100\,nJ$). A change in reflectivity in the irradiated spot of the layer following the temporal modulation of the FEL light could be observed (Fig. 2). This reflectivity change is probably the result of changes in the refractive index of the DNA film but changes in the thickness of the layer and effects of higher order harmonic wavelengths, which sometimes can be present in the FEL generated light, cannot be excluded at this early stage of the experiments.

However, the preliminary experiments demonstrate the feasibility of high signal/noise detection of IR-pulse induced processes in biofilms.

[1] S. Hénon, J. Meunier; Rev. Sci. Instr. 62, 936 (1991)
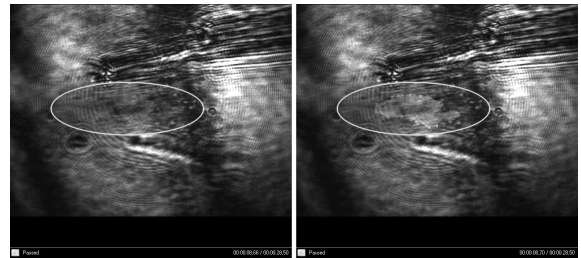[2] S. Riviére, S. Hénon et al.; J. Chem. Phys. 101(11), 10045 (1994)

Fig. 2: *Microscopic image of the sample surface without and with FEL illumination. At the irradiated spot a change in reflectivity during illumination (picture right) can be observed.*

[1]FZR, Institute of Nuclear and Hadron Physics

Infrared characterization of environmental samples by pulsed photothermal spectroscopy - First experiment at FELBE

H. Foerstendorf[1], W. Seidel[2], F. Glotin[3], R. Prazeres[2], J.M. Ortega[2]

Detailed knowledge of the interaction of toxic radioactive metals in biosphere is important to assess the environmental risk and the exposure paths of people e.g. from residues of uranium mining activities. The low concentration of these metals in environmental samples make them extremely difficult to measure with conventional FT-IR devices. This is why we are studying an alternative method, such as the photothermal beam deflection (PTBD) technique using a free electron laser (FEL) as a tunable heating source.

The PTBD technique is based on the theory of photothermal spectroscopy which describes the conversion of absorbed energy of a light beam incident on a sample into heat by nonradiative deexcitation processes [1].

In typical PTBD experiments (see Fig. 1) a solid sample is irradiated by a modulated beam of monochromatic light produced by a tunable infrared laser and a probe beam (e.g. a HeNe laser) which is reflected from the sample. Depending on the modulated intensity of the pump beam, the probe beam is deflected due to the photoinduced displacement which can be observed by a position detector [1].
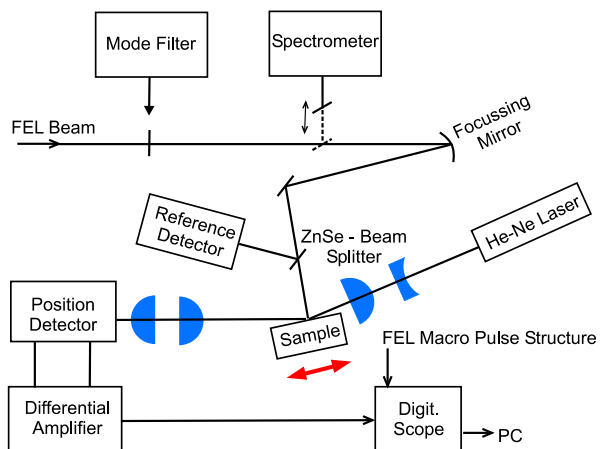

Fig. 1 *Layout of the PTBD experiment setup used at CLIO and FELBE.*

The amplitude of the observed signal is proportional to the slope of the induced displacement of the sample surface. Additionally, it can be shown that there is direct proportionality between the observed signal and the absorption coefficient of the material under investigation [3]. Therefore, a direct access to acquisition of absorption spectra is provided [2]. PTBD spectroscopy potentially provides spatial information about surfaces of samples since generation and detection occur in the sub-millimeter length scale. With a sufficient small laser probe it should therefore be possible to obtain a spatial resolution of a few micrometers. In our previous PTBD experiment using the FEL at CLIO/Orsay as an infrared pump source we investigated a distinct pattern of O^+-implanted and untreated regions of germanium (Ge) substrates serving as a model surface for the investigation of the spatial resolution of the PTBD technique.

Recently we have started the investigation with PTBD technique at FELBE with model compounds showing optical absorption bands at 17.8 μm. For the first time, we have used the new optical beam transportation system of the FELBE facility from the diagnostic station to the radiochemistry laboratory.

Figure 2 shows the obtained beam deflection signal (pink) together with the macropulse (green) and the signal from the reference detector (blue). It has to be mentioned that the power of the laser pulses of the FEL at CLIO is about 100 times higher compared to those of FELBE. Therefore, the high quality of the first results of this work demonstrate that the FEL at FELBE facility is suitable for future PTBD investigations.
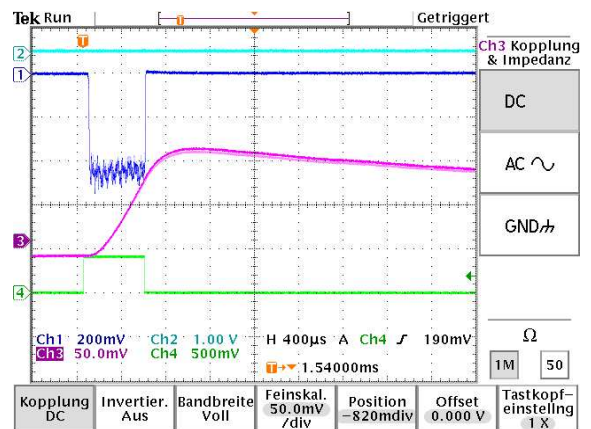
Fig. 2 *A snapshot from the screen of a digital oscilloscope for one macrobunch. The time scale is 400 μsec/div. The length of the electronical macrobunch signal (lower green curve) is 550 μsec but for the laser we measured 500 μsec (upper blue curve). The deflection signal (after difference amplifier, middle pink curve) raises about 50 μsec after the laser pulse.*

[1] A. Rosencwaig, A. Gersho, J. Appl. Phys. 47 (1976) 64
[2] W. Seidel, H. Foerstendorf et al., Eur. Phys. J. Appl. Phys. 25 (2004) 39
[3] M.A. Olmstead et al., Appl. Phys. A 32 (1983) 141

[1] *Institute of Radiochemistry, FZR, Dresden, Germany*
[2] *Institute of Nuclear and Hadron Physics, FZR, Dresden, Germany*
[3] *LURE, Université de Paris-Sud, Orsay, France*

Status of the Neutron Time-of-Flight Source at ELBE

E. Altstadt[1], C. Beckert[1], R. Beyer[2], H. Freiesleben[3], V. Galindo[1], M. Greschner[3], E. Grosse[2,3],
A.R. Junghans[2], J. Klug[2], B. Naumann, K. Noack[1], S. Schneider, K. Seidel[3], A. Wagner[2], F.-P. Weiss[1]

The ELBE electron beam of up to 40 MeV can be used to produce intense neutron beams in a liquid lead radiator. The extremely short beam pulses (5 ps) provide the basis for an excellent time resolution of neutron time of flight (tof) experiments. The design of the photoneutron source has been described in [1].

Due to the very short neutron pulses, an energy resolution of about 1% can be reached with a flight path of only 3.9 m. The usable energies range from 200 keV to ca. 10 MeV with an electron beam repetition rate of 1.6 MHz. This is an interesting energy interval to measure neutron cross sections needed e.g. in the context of minor actinide transmutation. Lower neutron energies from 30-100 keV are accessible with a reduced intensity for possible nuclear astrophysics experiments. The long-term needs for nuclear data have been formulated, e.g. in ref. [2]
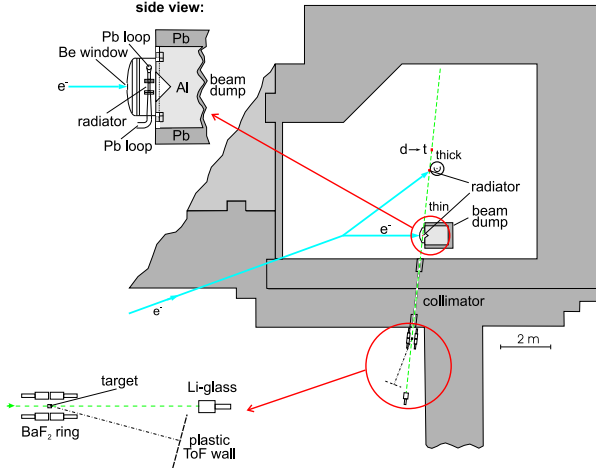
Fig. 1: *Floorplan of the ELBE nToF setup in the neutron cave. Inserts show a side view of the neutron radiator and the planned experimental site.*

Fig. 1 shows the floorplan of the ELBE nToF facility. The set up essentially consists of a liquid lead radiator confined by a molybdenum channel which is accommodated in a vacuum chamber, the beam dump absorbing the unused radiation (electrons, photons, neutrons), the collimator, and the tof detectors. The liquid lead target (through a heat exchanger) and the beam dump need to be cooled by a water circuit.

The electron beam hits the radiator, where simultaneously bremsstrahlung photons are produced and neutrons are emitted from (γ, n) reactions. The source strength can be as high as $2.7 \cdot 10^{13} \mathrm{s}^{-1}$ for an electron energy of 40 MeV and an average current of 1 mA. After a flight path of only 3.6 m the neutron flux on target is about $1.7 \cdot 10^6 \ (\mathrm{cm}^2 \mathrm{s})^{-1}$ with a beam repetition rate of 1.6 MHz.

A 3D rendering of the proposed design is shown in Fig. 2. The target + beam-dump assembly is located on a spindle lift platform and for radiation protection it can be lowered into a lead house when not in use. This mechanism also allows the operation of the Tungsten neutron target and the DT neutron generator sharing the same cave. The electron beam enters the Pb-Mo radiator housing through a Beryllium window, especially designed for good thermal stability and low scattering.
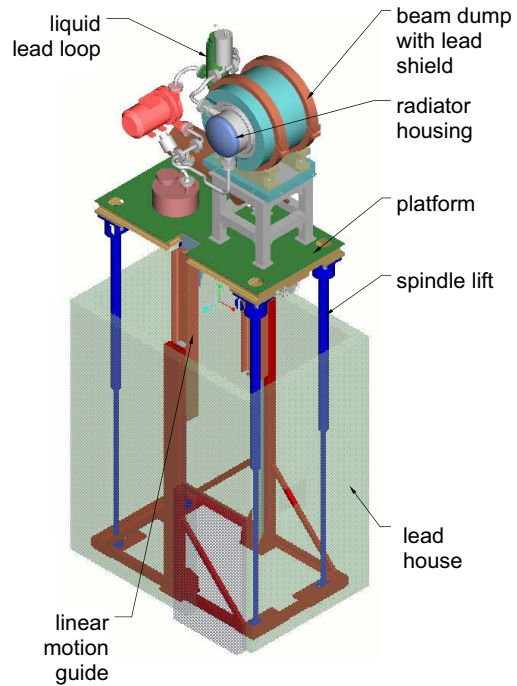
Fig. 2: *3D rendering of the ELBE nToF facility.*

The construction of the single components has started as well as the assembly of the main mechanical parts. A spindle lifter was constructed to lift the whole production target 3 m up from its rest position in a lead shield to the level of the electron beam line. The design of the instrumentation and control system including the interfaces with the ELBE LINAC has been finished. Thermal hydraulic and structural mechanic calculations were necessary to improve the design of the lead/water heat exchanger in order to allow for a faster response to changing heat deposition in the lead target and to exclude freezing or overheating of the lead in the circuit. A hot lead test experiment (400-500°C) is

[1]Institut für Sicherheitsforschung, FZ Rossendorf
[2]Institut für Kern- und Hadronenphysik, FZ Rossendorf
[3]Institut für Kern- und Teilchenphysik, TU Dresden

run in a dedicated loop to gather long term experience with the behaviour of those components and materials that are in permanent contact with the liquid lead. The key issues are related to the materials compatibility of molybdenum and stainless steel on the one side and the hot lead on the other side.

Monte Carlo calculations were performed with MCNP to optimise the collimator. The optimisation aimed at lowering the background of inelastically scattered neutrons and of photons at the experiment site. It was found that collimator insertions made from borated PE together with Pb to absorb the photon flash coming from the radiator represent the best solution, see Fig. 3. They lower the background and do not disturb the time-of-flight to energy correlation of the neutrons. Because of the scattering of photons off the edges of the lead, an additional lead absorber should be used to shield γ sensitive detectors, e.g. the BaF$_2$ detector array.
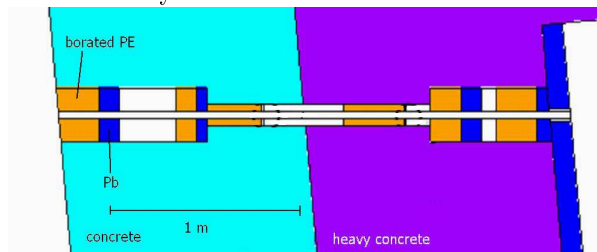
Fig. 3: *Collimator geometry*

The correlation between neutron energy and time of flight is shown in the MCNP spectrum, see Fig. 4. The main ridge in the spectrum is from neutrons with a correct energy to time-of-flight correlation. Neutrons that have lost their undisturbed correlation between energy and time-of-flight form a tail to the main ridge. They are supressed by two to three orders of magnitude, and constitute only 4% of all events. The low intensity ridge approx. 20 ns above the distribution of unscattered neutrons is due to scattering off the stainless steel windows of the vacuum housing surrounding the Mo-radiator, and contains only a fraction of $6 \cdot 10^{-4}$ of all neutrons. The inset shows a horizontal cut through the spectrum at 230 ns. The energy width (FWHM) of the peak for neutrons with a time of flight of 230 ns is 1.2 keV. This corresponds to an energy resolution of 0.1% at a neutron energy of 1.51 MeV.

For measurements of neutron-induced reactions, different detector types are being developed. For neutron-capture γ rays, a BaF$_2$ scintillation detector array of up to 60 crystals is being built, see Fig. 5. The crystals have a length of 19 cm and a hexagonal cross section with an inner diameter of 53 mm. They are read out by fast Hamamatsu PMTs R2059, which are UV sensitive to be able to measure both the slow and the shorter wave-length fast component of the BaF$_2$ scintillation light. This allows to use pulse shape discrimination (PSD) to separate photon signals from intrinsic α-particle background. The time resolution reached

with a ^{60}Co γ source is typically 0.65 ns (FWHM).
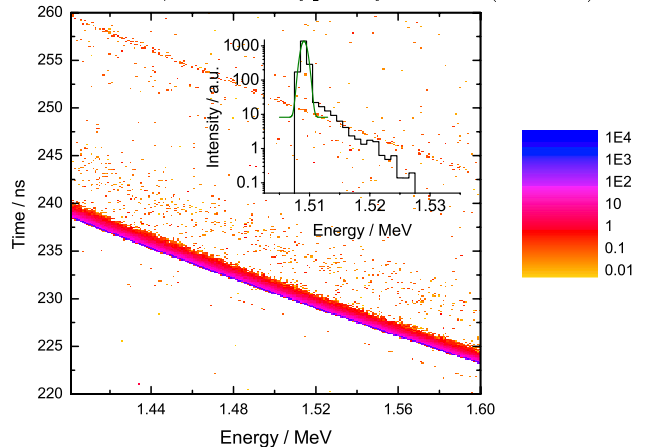
Fig. 4: *Time of flight vs. energy correlation calculated with MCNP 4C2. The plot only shows a part of the neutron spectrum between 1.4 to 1.6 MeV. The calculation was done with a realistic geometry using a nominal flight path of 3.90 m. Note the logarithmic scale of the cluster plot. The inset shows a horizontal cut of the tof-energy correlation at a time-of-flight of 230 ns.*

The read out will be performed with dedicated ADC/TAC modules [3] that allows a simultaneous measurement of timing and energy signals including PSD in VMEbus standard. The system will be controlled by a RIO3 real-time unix computer.

For neutron detection, Li-glass scintillators and a plastic scintillator wall is being built. The plastic scintillator wall will allow detection of fast neutrons from approx. 500 keV neutron kinetic energy through proton recoil in the scintillation material. The wall will cover an active area of approx. 1 m^2 consisting of 10 scintillation panels read out on both ends by fast PMTs R2059. For neutron energies below 500 keV Li-Glass Scintillators are used. They are enriched with ^{6}Li up to 18% and allow detection of low-energy neutrons mainly through the reaction ^{6}Li(n,t)^{4}He.
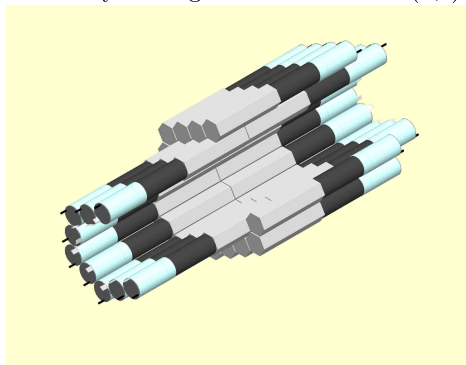
Fig. 5: *BaF$_2$ scintillation detector array. The target position is in the center of the cylindrical ring of hexagonal BaF$_2$ crystals.*

With a ^{252}Cf neutron source time-of-flight measurements have been made with one panel of a plastic scintillator read out on both ends by PMTs. The fission was triggered by the γ rays detected with a BaF$_2$ de-

tector close by the ^{252}Cf. With a flight path of ca. 10 cm, fission neutrons can be clearly separated from photons, see Fig. 5 The time resolution of the plastic szintillator from the photon peak is ca. 0.9 ns (FWHM).
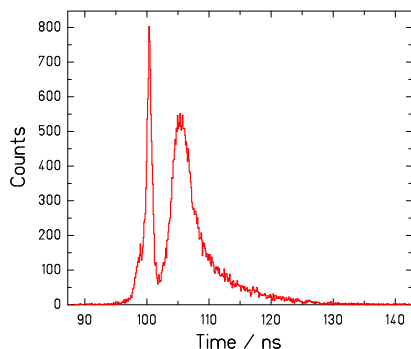
Fig. 5: *Time of flight spectrum of a ^{252}Cf neutron source measured with a plastic scintillator panel of 1 m length. The left peak is from photons, while the right peak is due to fission neutrons.*

As can be seen in the table below, ELBE is especially suited to do measurements in the energy range of 0.2 to 8 MeV; it is very competitive with all existing high resolution neutron beams in its luminosity - including nTOF at the CERN-PS. The proton accelerator based neutron sources at Los Alamos and the planned Oak Ridge Neutron Spallation Source loose a big portion of their intensity advantage over ELBE, when they increase their flight path such that they match the energy resolution of < 1 % expected for ELBE nToF. The neutron beam properties predicted on the basis of the present e-beams at ELBE are listed in the first of the three columns dealing with ELBE. The next one shows the improvements expected when the planned

laser driven photo-cathode electron injector allows to increase the number of electrons in each bunch to drive the accelerator to its design beam power at the above-mentioned 1.6 MHz.

When the repetition rate is reduced by another factor of 8, undisturbed tof-spectroscopy with even slower neutrons of 3 keV up to 200 keV becomes feasible. There, the use of a moderator is required and simulations with MCNP for a scheme of partial thermalisation of the faster neutrons emitted from the Pb radiator are on the way. These energies are of major interest for the understanding of the cosmic creation of the heavy elements by the successive accumulation of neutrons. Theoretical arguments predict several scenarios for this accumulation: Slow s-processes at stellar temperatures equivalent to 15 - 30 keV follow the 'valley of stability' in the isotopic landscape. Laboratory experiments to determine the crucial nuclear data have been performed largely at ORNL-Orela and especially at FZK-VdG at Karlsruhe. The comparison of their n-beam properties shows the potential for improved data from ELBE. The required reduction of the repetition rate is counteracted by the increase in the neutron capture cross sections to be measured. In addition, also experimental neutron capture data at energies above 100 keV allow to make an important contribution to the nucleosynthesis reaction networks.

For many neutron-rich nuclides a much higher neutron flux than obtainable in stars is needed; it is expected to exist during short periods of a super-nova event or during the close encounter of a neutron star with another star. Here temperatures are expected to reach 300 keV and cross-section measurements of importance for the understanding of such processes may profit from both the neutron tof alternatives described above.

Tab. 1: Parameters of operational and planned neutron time-of-flight facilities.

n-ToF-facility	CERN nTOF	LANL NSC	ORNL SNS	FZK VdG	ORNL Orela	IRMM Gelina	ELBE	ELBE with photo-gun
bunch charge / nC							0.1	1
power / kW	45	64	2000	0.2	8	7	6	40
rate / s^{-1}	0.4	20	60	$25*10^4$	525	800	$16*10^5$	$16*10^5$
fligh path / m	183	20	20	0.8	40	20	4	4
n-bunch length / ns	> 7	125	350	2	8	$\gtrsim 1$	≈ 1	≈ 1
E_{min} / eV	1	1	1	$3*10^3$	10	10	$2*10^5$	$2*10^5$
E_{max} / eV	$5*10^8$	$5*10^8$	10^8	$2*10^5$	$5*10^6$	$4*10^6$	$8*10^6$	$8*10^6$
$\Delta E_n/E_n(\%)$	≤ 0.3	5	13	3	≤ 0.5	0.2	≤ 1	≤ 1
n-flux /s^{-1}cm^{-2}	$\approx 10^5$	$5*10^6$	10^8	10^4	$4*10^4$	$2*10^5$	$2*10^6$	$15*10^6$

[1] E. Altstadt et al., Proc. Int. Conf. Nucl. Eng., ICONE12, Arlington VA, U.S.A., April (2004)
[2] Long Term Needs for Nuclear Data Development, comp. M.Herman, INDC(NDS)-428, IAEA Nuclear Data section, Vienna Austria (2001)
[3] C.P. Drexler, U. Thöring, W. Bonn, et al. IEEE Trans. Nucl. Sci 50:969-973 (2003)

EPOS – an intense positron beam project at ELBE

R. Krause-Rehberg[1], S. Sachert[1], G. Brauer[2], A. Rogov[2][3], K. Noack[2]

EPOS is an acronym from ELBE Positron Source and describes a running project to build an intense pulsed beam of monoenergetic positrons (0.2 ? 40 keV) for materials research applications. The system will be an external, user-dedicated facility of the Martin-Luther-University Halle-Wittenberg at Forschungszentrum Rossendorf. An outline of the positron production site, the projected positron beamline, and the capital equipment planned is sketched in Fig. 1.

The positron beam will be bunched for positron lifetime spectroscopy. It makes use of the primary bunch structure of the ELBE electron beam (77 ns repetition time of 5 ps bunches, cw-mode, 40 MeV, 1 mA). Positrons will be created via processes of pair production from Bremsstrahlung from the electron beam when hitting a radiation converter consisting of a stack of 50 tungsten foils (0.1 mm thick) flown through by cooling water. It was estimated to collect about 6x109 positrons having their energy in the range 1-250 keV in a tungsten moderator foil of about 0.03 mm thickness (30 mm diameter) which is floated by high voltage of +2 kV. This is necessary in order to extract the moderated positrons via electrostatic lenses and to form a positron beam which then is magnetically transported to the target position. The efficiency of the moderation process is of the order 10^{-4} only, and furthermore the originally very sharp bunch structure of the electron pulses is weakened by all mentioned processes at the beginning of the positron beamline. This time spread is planned to be retracted as much as possi-

ble by repeated chopping and bunching of the formed positron beam. An accelerator stage in front of the target is designed to vary the positron energy in order to allow depth dependent measurements of materials properties. Because a change in positron energy will also change the time focus of the positron beam which has to be on the target, this needs to be compensated by a drift path as indicated. The positron annihilation radiation provides the signal indicating the death of a positron. The appearance of this signal will be related to the machine signal indicating the appearance of an electron bunch, and thus the birth of a positron. This way it is evaluated to achieve a time resolution of about 100 ps (FWHM). It is planned to build a fully remote controlled setup (via internet) by using fully digital data collection and processing. In addition, a ^{22}Na positron source, combined with another tungsten moderator, will provide a continuous positron beam for special time-consuming experiments at times when the electron beam is not available but occupied by other users at ELBE. Construction and build-up of the EPOS facility are underway and it is planned to be able to conduct first tests of the positron beamline in 2006 when the electron beam will be available at Cave 111b at ELBE.
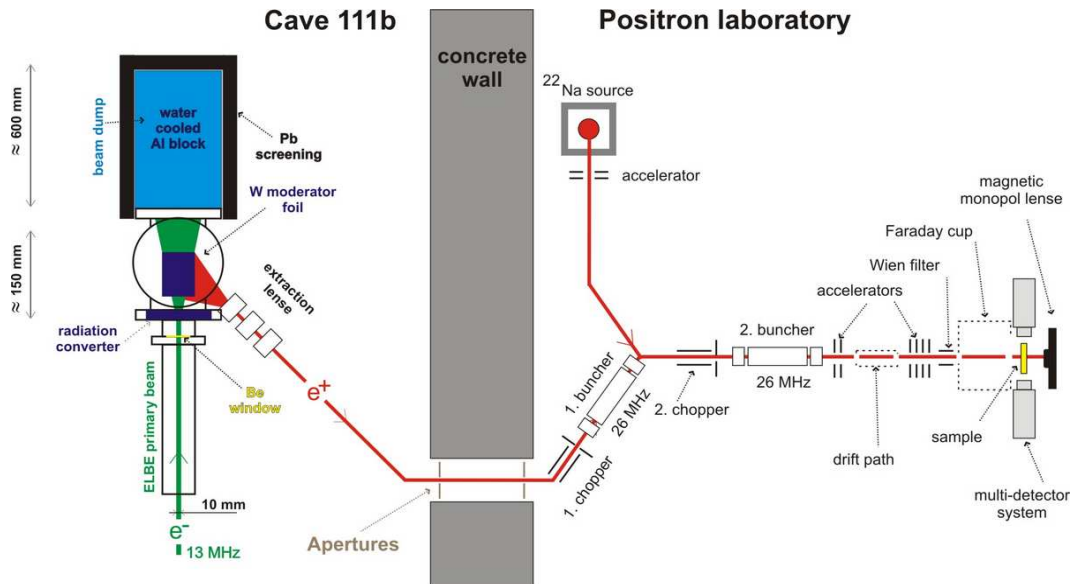
Fig. 1: *Sketch of the EPOS positron production site, beamline and capital equipment.*

[1] University Halle-Wittenberg, Department of Physics
[2] FZ Rossendorf, FWI
[3] Joint Institute for Nuclear Research, Dubna

Dynamics of matrix–isolated molecules

J.A. Piest

Gaining insight in molecular reactions is an important issue in order to understand the physical, chemical, and biological reactions in both micro- and macroscopic systems. Such reactions determine the way molecules interact with their environment. For instance, it has recently been verified in the field of laboratory astrobiology that formation of amino-acids takes place already in the interstellar medium and in particular in ice-analogues mimicking those covering interstellar dust grains [4,6]. A process that can be studied in more detail with available spatially and temporally resolved spectroscopic data in the infrared spectral range [3]. In a matrix-isolation MI setup such processes can be observed for molecules isolated in an inert gas ice, thus, with a minimum of interaction between the molecules and atoms in the ice-matrix, and at temperatures close to the absolute minimum.

The advantage of doing experiments in the region slightly above zero Kelvin is clear: molecules have much lower internal energies than at room temperature. Generally, in the spectra of such cold molecules there are 1) less transitions present, and 2) the bandwidth per transition is smaller. Thus, spectra for these molecules are less complicated than those recorded for warm species and can be interpreted with less ambiguity. In particular, time-resolved spectral data of cold molecules may lead to knowledge of the timescales on which *intramolecular vibrational re-distribution* (IVR) takes place, which informs us about the time-response of physical or chemical reactions in molecular systems. Due to lack of bright IR short-pulse light sources, time-resolved spectral data in the sub–nanosecond domain for matrix-isolated species are scarce, where spectra available in the μs region do not yield relevant information [1,2,3] on IVR. Therefore, during the last two years a Matrix-Isolation Setup for Time-resolved THz-experiments (MISTTe) has been under construction in room 113E of building 40 to be used in combination with the free-electron laser (FEL).

MISTTe consists of three chambers ($\varnothing$ ~15cm) two of which are pumped by two Varian V301 Navigator turbo–molecular pumps, with a pump capacity of ~300 l/s each. One Varian SH100 scroll pump provides a sufficiently low ($<10^{-2}$Torr) roughing pressure to drive the two turbopumps. The third chamber ($\varnothing$ ~35cm) provides room for diagnostics and IR pulse modulation and is pumped by another Varian SH100. The low- and high-vacuum compartments are separated by a KBr or a poly-ethylene window, depending on the used central wavenumber of the FEL. A liquid helium cooled cold–head taken from an Oxford Instruments Optistat setup is capable of operating in a continuous temperature range of 1.5K through 300K. With a cooling power of several Watts at 5K

it has been adapted to fit on one of the HV chambers. Thus, with an assumed FEL output of ~50W the summed column widths of molecular absorption lines, present under the IR spectral profile, can be as large as a few percent of the column–width of the FEL–pulse without melting the inert gas matrix.

In situ sample generation takes place via a gas-mixing compartment, consisting mainly of SwageLok parts, on a transparant (KBr or poly-ethylene) surface mounted on the tip of this cold–head. Purified gases, *e.g.*, Ar 6.0/Ne 5.0/N_2 6.0, are mixed with sample species to well defined concentrations, before being deposited on the cryogenically cooled window. The deposition rate is controlled with a micro–flow meter. A liquid nitrogen trap prevents backflow of the sample species in the gas–lines towards the clean gas–buffers, additionally, in the opposite flow direction it dries the purified gases before mixing with the sample species.

After passing through the sample the IR pulse is coupled out of the HV compartment via a LV-line connected to a Bruker 66v vacuum FTIR to be analyzed spectrally.

The species that can be studied in MISTTe are limited to those that can be brought in the gas–phase at room or elevated temperature with any method provided that no substantial fragmentation or polymerization of the sample molecules takes place.

Possible pump-probe methods to be applied vary from simple one-color pump-probe in direct absorption, to sophisticated methods taking advantage of background free detection schemes such as: two or three pulse photon echo experiments, transient grating in transmission, and laser-induced fluorescence.

After the arrival of the SwageLok parts and the vacuum components in February and March 2003 the setup has been build and first evacuated in May 2003. Also in May 2003 the LV diagnostic tank was saved from an old setup that literally had to be trashed. It was cleaned and modified to the needs of MISTTe. The purchase of a desired cryostat was cancelled due to its high weight on the investment budget. Instead, the coldhead of an existing cryostat was modified to be mounted in the vacuum. Due to the larger physical dimensions of this coldhead compared to those of the desired (Janis) UHV coldhead there is hardly room available in the HV compartment for adjustment, which could give problems when cooling down the coldhead. Presently the coldhead is mounted on the HV chamber in a fully (360°) rotationable way, thus, the sample window can be accessed from four orthogonal directions without breaking the (high)vacuum.

In the summer of 2003 besides constructing MISTTe an investigation was done on commercially and non-commercially available molecular modelling software.

Packages that have explicitly been under study were: Spartan'02, Gaussian'03, and Gamess v2003 [8]. These three packages claim to compute molecular wavefunctions via the density functional approach (DFT). Also other approaches (Hartree-Fock, Moeller-Plesset perturbation theory) are available via these packages. Spartan'02 goes with a graphical interface. For the other two packages such an interface has to be purchased, however, nice graphical interface packages are available as freeware for the Unix and Mac operating systems. From these three packages Gaussian offers the most versatile package. A good alternative and well suited for quick runs on geometry optimization and frequency computations of vibrational modes offers Gamess. Spartan goes with too less freedom of choice in setting of molecular and environmental parameters. Furthermore, it was found that the group-theoretical characterization of energy-levels, at least when computing vibrational modes, is not reliable. In August 2003 the ICAVS conference happened in the same week as the THz-bridge meeting both in Nottingham. Visiting several posters and talks, and having discussions with theoretical chemists/physicists it was verified that Gaussian is *the* standard in professional molecular modelling software.

In the fall of 2003 the Gamess package, which is free of charge but still licensed, has been installed on the servers of FZR. After two months of validation it was setup to compute the potential surface of the torsion mode in the electronic groundstate of neutral aniline. Two different approaches of the torsion path were implemented as depicted in figure 1 (middle panel). Computations were run at the B3LYP/D95(d,p) level via DFT. The results of which are shown in figure 1. The (v=1)⟵(v=0) transition of this torsion mode has previously been computed at $277 cm^{-1}$. This was done in the harmonic approximation in the minimum of the potential [7]. Though, the barrier for 180° torsion is estimated not higher than $2\,500 cm^{-1}$, therefore, severe tunnelsplitting is expected particularly for the vibrationally excited states of this mode. Com-

bined with the strongly anharmonic potential the transition mentioned is expected at a considerably lower wavenumber. Computations on wavefunctions and eigenstates are presently running.

Except from the aniline tunnel mode, which has been documented well and shows similar an-harmonic spectral characteristics, the other normal modes have previously been computed well in the harmonic approximation and have been documented [7]. Therefore, aniline has been selected to run the first validation experiments both to be able to compare the spectra observed to recently recorded MI spectra [5] and to investigate the spectral properties of the torsion mode, of which mode no evidence has been found in literature that it was observed before in the IR spectrum of groundstate aniline.

Despite only 40% of the estimated budget for a complete and running setup of 50000 €has been spent, the present construction status of MISTTe is close to conduction of these validation runs. Under the assumption that the lacking 60% (30% in case no UHV cryostat is purchased) of the estimated budget can be spent, it will take a fulltime employee between half a year and one year to finish the validation runs on aniline and set up a pump-probe experiment in order to be prepared for experiments on selected peptides and amino-acids.

[1] Allamandola and Nibler, Chemical Physics Letters, 28 (1974) 335–340

[2] Allamandola *et al.*, Journal of Chemical Physics, 67 (1977) 99–109

[3] Allamandola, L.J., NASA/Ames Research Center, private communications

[4] Bernstein *et al.*, Nature, 416 (2002) 401

[5] Gée *et al.*, Chemical Physics Letters, 338 (2001) 130

[6] Muñoz Caro *et al.*, Nature, 416, 403, 2002

[7] Piest *et al.*, Journal of Chemical Physics, 110 (1999) 2010–2015

[8] www.wavefun.com (Spartan'02);
www.gaussian.com (Gaussian'03);
www.msg.ameslab.gov (Gamess v2003)
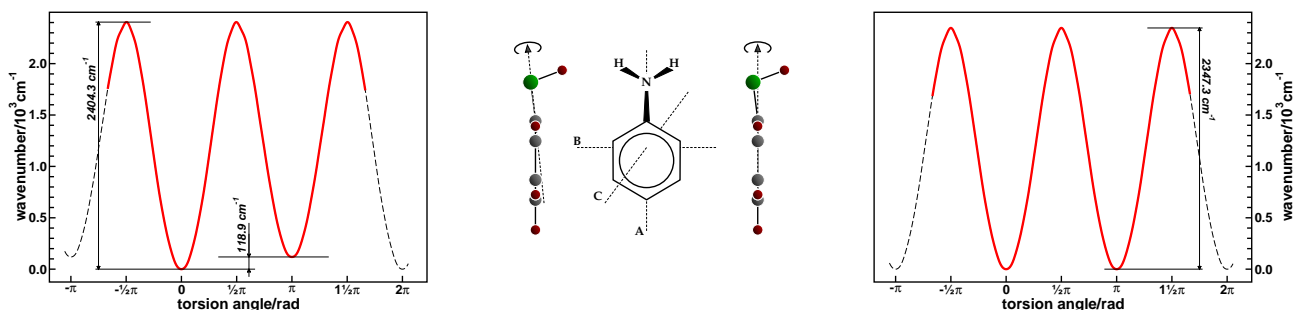
Fig. 1: *Left panel – Potential of aniline torsion mode when rotating the amine group rigidly around the N—C axis, thus non-symmetrically, of the optimized geometry (middle left scheme). The barrierheight is computed 2 404.3 cm^{-1}, with a difference between the potential-minima of 118.9 cm^{-1} for a full rotation. Right panel – Same potential as in the left panel but now the amine group is rotated symmetrically around the A principal axis of inertia of the optimized geometry (middle right scheme), yielding a barrierheight of 2 347.3 cm^{-1}. Computations were run with DFT at the B3LYP/D95(d,p) level.*

Accelerator and Technical Development at ELBE

In the two years under report the ELBE facility has made a huge step forward. With the first accelerator stage and beamline being fully operational in fall 2002 routine user operation of the bremsstrahlung facility started in January, 2003. In the same year the radiation physics beamline was completed and generation of channeling radiation demonstrated October 28th, 2003.

Now, full effort could be put to finish the FEL beamline and it's optical resonator. Already in 2003 the electron beam was threaded through the U27 undulator but completion of the optical beamline took until May, 2004. Than, it was a very rapid progress from seeing spontaneous radiation, setting up the optical beam transport the diagnostics lab, fine-tuning the optical resonator to first lasing at May 7th, 2004. The carefull design of the whole system and accurate work aligning all components has seriously payed off. It has shown, nevertheless, that lasing with the low available beam energy was difficult and always required tedious work to be reproduced. Once started, however, the laser was running very stably.

During summer and fall 2004 a new accelerator module was built. It will be installed in January, 2005, boosting the available beam energy to the design value of 40 MeV, thereby, extending the IR and X-ray spectral range.

Along with the increasing experience in operating the facility many technical systems were improved and upgraded. When browsing through the operation protocols of both years it becomes obvious, that initally machine stability and reliability have been a serious issue. Several problems have now been adressed, others like the energy drift are avoided by adapting the operational regime. Still, further effort is needed to improve the reliability of the machine.

Experiences on ELBE operation

P. MICHEL

At ELBE now three of the initially planned five secondary radiation facilities are available to the user. Since January, 2003, the bremsstrahlung facility, the channeling X-ray source and the mid-IR free-electron laser step by step have gone into routine operation. In total, 2523 hours of beam time were available for scientific work by the users, another 958 hours were used for machine development and comissioning of the radiation production (see Fig. 1). In the following, some experiences with the operation of the particular beamlines shall be described.
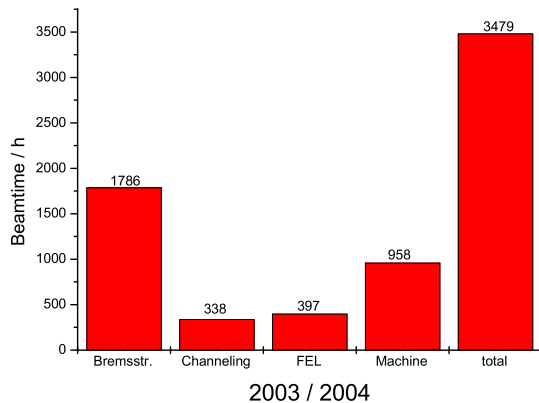

Fig. 1: *Beam time usage at ELBE.*

The bremsstrahlung facility

Since the startup of the operation, in total 1786 hours of beamtime were provided for the bremsstrahlung facility. Electron energies from 7 to 16 MeV and beam currents up to 600 μA were run on niobium radiators of 4 and 7 μm thickness. The photon beam was primarily used for investigations in nuclear spectroscopy. Besides that, first measurements were performed on photon activation and on nuclear spectroscopy using polarized photon beams. These types of experiments are characterized by long continuous runs with constant beam energy and current. To allow for the further construction of the whole ELBE facility these experiments at large were run in afternoon and night shifts. As a stable and reliable operation could be achieved single-operator runs became possible for the night shifts. Some typical problems encountered are:

- The available diagnostics to determine and to reproduce the beam energy (which is important for threshold reactions) needs an improvement.
- The beam current is limited due to heating of beamline components by electrons that were scattered at the radiatior.
- One main source of interruptions were RF shutdowns caused by interlock events originating from the RF windows in the accelerator cryomodules.

The channeling X-ray source

After completion of the radiation physics beamline generation of channeling radiation [1] was demonstrated for the first time at October 28th, 2003. Since than, about 338 hours of beamtime were provided which almost exclusively were used to characterize crystals for channeling and to optimize the radiation production and to study the radiation background. The following problems were encountered:

- Because of the very sensitive X-ray detectors most experiments were run at extremely low beam currents, thus, disabling major parts of the online beam diagnostics. Therefore, it is difficult to compensate the beam energy and target spot drifts over long measuring runs.
- Beam-loss in the dispersive sections of the beamline leads to high radiation background which can be avoided minimizing the energy spread.

Typically beam stability is required for a timescale of one hour which is needed to acquire radiation spectra or to perform angular scans to determine channeling planes. Due to the more complex beam transport and many necessary operator actions the experiments were mostly run in daytime shifts by an accelerator physicist or engineer.

The mid-IR free-electron laser

At May 7th, 2004 for the first time infrared light was generated with the mid-IR free-electron laser of ELBE [2]. With the limited beam energy range (at max. 17 MeV until the end of year 2004) infrared wavelengths from 15 to 22 μm were available. The majority of the provided beamtime was used to optimize the laser and to characterize the beam properties. A total of 397 hours were provided for experiments with the FEL. As the startup of the laser has proven to be quite difficult with the low electron beam energy and as the operation requires frequent parameter changes (wavelength, intensity...) the FEL shifts were mostly run during daytime by accelerator physicists. The following problems occured:

- At the beginning of the FEL runs some (up to 4) shifts were needed just to get the laser started. The major difficulty lies in the controlled adjustment of the longitudinal beam properties but also in the reproducibility of the optical resonator of the FEL.
- In the first few hours after turn-on the beam energy and accelerator rf-phases are drifting. To avoid the impairment of operation the accelerator was run 24 h a day in the weeks of FEL usage.
- With the high accelerating gradients required, RF interlocks due to arcs at the RF windows were a frequent source of interruptions.

[1] this report, p. 15
[2] this report, p. 32

First Lasing of the ELBE mid-IR FEL

U. Lehnert for the whole team

First lasing of the mid-infrared free-electron laser at ELBE was achieved on May 7, 2004. At 19.6 μm an optical power of 3 W was outcoupled using an macro-pulsed electron beam with an energy of 16.1 MeV and an energy spread of less than 100 keV. The bunch charge charge was 50 pC. For characterization of the FEL operation the minimum gap of 13.8 mm ($K_{RMS} = 0.7$) was used. This was the long-awaited final step of sustained tedious work wich shall be outlined here.

Setting up the electron beam

One of the first steps in the FEL commissioning was the electron beam characterization done at a beam energy of 16 MeV. The electron beam profile and position in the undulator are measured with the help of OTR view screens. The beam transport was tuned according to the design calculations to possibly match the envelope of the optical beam inside the undulator.

ELBE is equipped with a strip-line beam position monitor (BPM) system. The resolution of the system is about 10 μm. There are two phenomena, which make this system very useful during the FEL operation. First, there is an energy drift observed for the first 2–3 hours every time the linac is switched on. A BPM located in a dispersive region is used to monitor the electron beam energy and to compensate the drift. The second phenomenon is the dependence of the R_{56} of the "S" shaped beam line on the electron beam path through it. Both phenomena are to be investigated more detailed in the future.

The transverse emittance was measured in the injector with the multislit method, while the emittance of the accelerated beam was measured with the quadrupole scan. At the maximum design bunch charge of 77 pC the emittance is measured to be 8 mm mrad. The gain reduction factor due to the finite emittance was 0.97 at first lasing, i.e., is almost negligible.

Since the FEL gain is linearly proportional to the beam peak current it is highly desirable to minimise the electron bunch length in the vicinity of the undulator. Previously, the bunch length was measured to 1.5 ps (rms) immediately at the accelerator exit using a Martin-Puplett interferometer (MPI). At the undulator with the beam tuned for lasing this value is however different. One can groupe the beam line elements, which influence the bunch length, between the accelerator exit and the undulator in three groups. These are the magnetic chicane, the "S"–shaped part of the beam line and drift spaces. The chicane can be used to adjust the R_{56} of the FEL beam line. For the FEL commissioning the MPI was installed right downstream of the undulator. Additionally a single Golay cell detectors was installed upstream of the "S" shaped part of the

beam line to measure the total power of the coherent transition radiation, which is in the first approximation inversely proportional to the bunch length. Note that the two Golay cells installed at the interferometer can be used in the same way for the bunch length minimisation without scanning the interferometer. One of the key elements to tune the longitudinal phase space is the second accelerator cavity. Adjusting the cavity phase one changes the electron beam energy spread and the bunch length in the undulator vicinity because of the non-zero R_{56} of the beam line. For that reason the energy spread and the Golay cell signals were measured as a function of the second cavity phase. Fig. 1 shows results of the measurements. The bunch length at its minimum can be measured with the help of the interferometer. Here the FWHM of the interferogram is about of 2.5 ps.

The most important observation to note is the following: adjusting the cavity phase to have minimum energy spread drastically increases the bunch length in the undulator . In fact at the energy spread minimum the bunch length is so long that it cannot be measured with the MPI. It turnes out, however, that for lasing at the used (rather long) wavelength it is more critical to minimize the energy spread of the beam than to minimize the bunchlength.
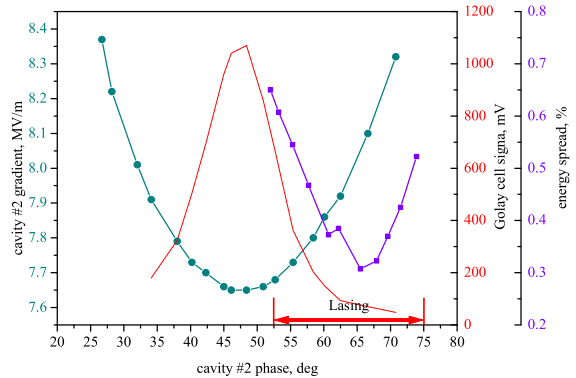
Fig. 1: *Electron beam parameters dependence on the second cavity phase (dots show the cavity gradient needed for constant energy, squares the energy spread and the line the bunchlength signal).*

Observation of spontaneous radiation

The general idea for the first FEL turn–on was to observe the spontaneous undulator radiation and to maximize it by systematic adjustment of the optical cavity and the electron beam parameters. First, the spontaneous radiation was observed downstream of the undulator so that the optical cavity was not incorporated in the measurements. For that purpose a mirror was inserted in to the beam line behind the last dipole

deflecting the beam to the dump. The spontaneous radiation was outcoupled off the beam line through a KRS–5 window and focused by a parabolic mirror on a liquid nitrogen cooled MCT detector. An accurate alignment of the setup was essential for the spontaneous radiation measurements. For the first observation of the spontaneous radiation we had to use an extremely strong averaging of the data, however, that was an important step for the commissioning, since once the spontaneous radiation was observed we could optimize the machine using it as a tune signal.

Setting the optical cavity length

The adjustment of the FEL cavity to the correct length is an important prerequisite for the achievement of lasing. The cavity length of the FEL has been determined by employing an external frequency stabilized fs mode-locked Ti:sapphire laser (Femtolasers, Austria). The fs laser is operated at 78.0 MHz, i.e. the 6th harmonic of the FEL. A 390 MHz reference signal is derived from the RF electronics of the gun, which is used for stabilizing the repetition rate of the fs laser with a phase-lock loop at its 5th harmonic. This synchronization scheme reduces the timing jitter of the fs laser to 500 fs. The pulse train of the fs laser operating at 800 nm with 15 fs pulse duration is directed through the outcoupling hole into the FEL cavity. The light re-emitted through the outcoupling hole is detected via a beam splitter and a fast photodiode. When perfect synchronism of the fs laser and the FEL cavity is achieved, the detected optical pulse is enhanced due to constructive superposition of pulses circulating in the cavity. This results in an increase of the detected pulse intensity by a factor of five. The correct cavity length is determined by this method with an accuracy of some μm, i.e. a relative accuracy of 10^{-7}. Since the expected FEL operation covers a cavity detuning range of several 10 μm, this accuracy was sufficient to start lasing at the preset cavity length.

First lasing observations

Initially, we operated the FEL in a pulsed mode only using an MCT detector to measure the FEL power as a function of time. In that mode the small signal gain is measured by fitting an exponential function to the rising slope of the MCT signal in its very beginning. The amplitude of the MCT detector close to the macropulse end is associated with the saturated power. The saturation power as well as the small signal gain

are measured as a function of the optical cavity detuning. Typical results of such measurements are shown in Fig. 2.
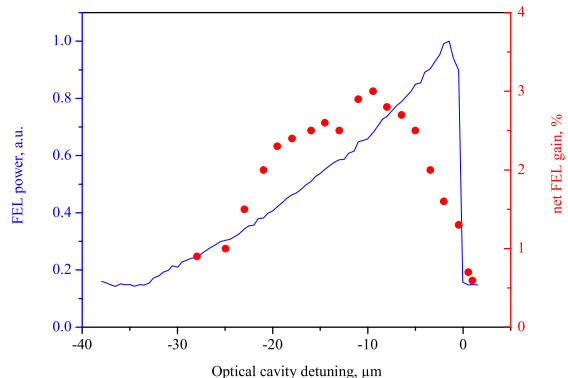
Fig. 2: *The saturation power (line) and the FEL net gain (dots) vs. optical cavity detuning.*

The FEL spectra were measured with a Czerny-Turner type spectrometer (SpectraPro-300i from ARC) which contains a turret with three different gratings (75 l/mm, blazed at 8 μm; 60 l/mm, blazed at 15 μm; 30 l/mm, blazed at 30 μm). For these measurements we used the side exit slit equipped with a single MCT detector. Fig. 3 shows how the spectral width decreases with the detuning of the cavity length.
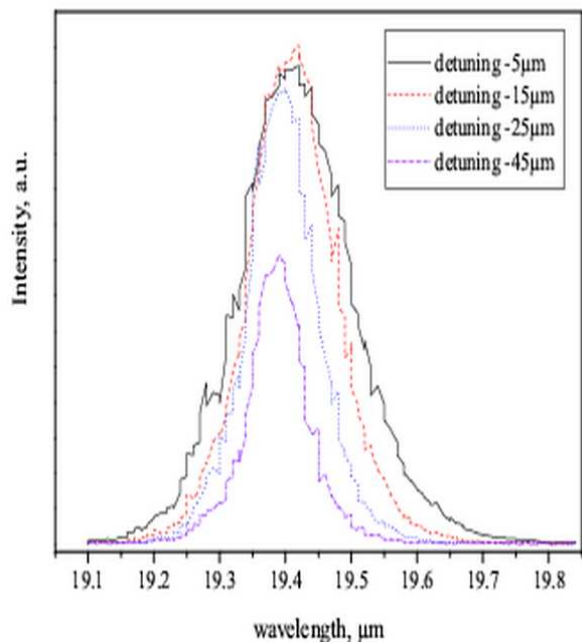
Fig. 3: *FEL spectra measured at different optical cavity detuning.*

A New Undulator (U100) for the Far Infrared at ELBE

Th. Dekorsy[1], K. Fahmy[1], E. Grosse[1], U. Lehnert, P. Michel, W. Seidel[1], A. Wolf[1], R. Wünsch[1]

Starting from May 2004 the U27 undulator at the radiation source ELBE has produced IR light between 16 and 22 μm at electron energies around 16 MeV. Now a second accelerator unit is being installed. The higher electron energy (up to 40 MeV) extends the range down to 3 μm. To enlarge the range to the far infrared ($\lambda \lesssim 150\,\mu$m) another undulator with a larger period will be installed.

In the far infrared a FEL constitutes a unique radiation source. Radiation quanta with this energy (10 - 100 meV, 2 - 20 THz) are appropriate for the spectroscopy of low-energy elementary and collective excitations. Such excitations are observed in solid-state quantum-structures and in complex biomolecules as well. Their study establishes the basis for understanding complex phenomena in solids and liquids and for elucidating processes in biological material. Technological and medical innovations are the long-term output of such investigation.

To produce radiation in the THz region by means of the ELBE beam an undulator with a period λ_u of several centimeters is needed. To avoid the use of electron energies below 20 MeV, where the energy spread is larger than 0.3%, we use an undulator with the period of $\lambda_u = 10$ cm. To get a sufficiently high single-pass gain 38 undulator periods are envisaged resulting in a total undulator length of approximately 4 m. The design of the electron beam line requires an asymmetric installation of this long undulator. Its middle is located 85 cm downstream from the resonator center. The maximum parameter $K_{\rm rms}$ of this hybrid Sm/Co undulator is about 2.5.

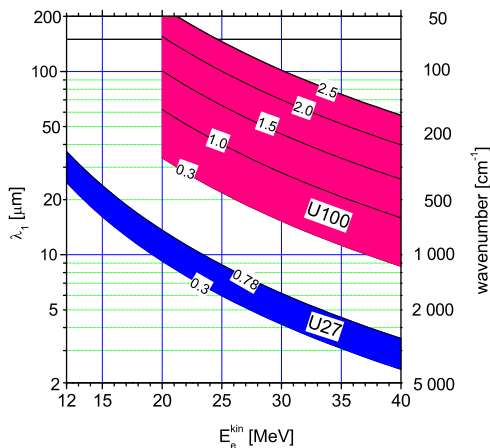Fig. 1 shows the wavelength range covered by this undulator at the beam of ELBE. It slightly overlaps the range of the U27 undulator and allows to produce light up to 200 μm. Above 150 μm the diffraction losses in the presently designed IR beam line diminishes the power available in the user laboratories considerably. Above roughly 50 μm the diffraction of the IR beam has seriously to be taken into account. It increases the beam size and reduces the coupling with the electron beam in the undulator (filling factor). Big resonator mirrors, large diffraction losses and a small laser gain are the result. Therefore, a vertical beam compression by means of a rectangular waveguide (10 mm high) spanning from the undulator entrance to the downstream resonator mirror will be applied (see Fig. 2). To avoid ohmic losses in the side walls the waveguide has to be broad enough (5 cm in the undulator and 10 cm at the mirror) to allow a free beam propagation in the horizontal direction [1]. The free propagation on the upstream side of the resonator simplifies the passage through the dipole and quadrupole magnets and provides an approximately round beam profile at the out-coupling mirror (M1). To optimize the coupling between the waveguide and the free optical mode a bifocal mirror with appropriate radii of curvature has to be used (see ref. [2]). The downstream mirror (M2) is a cylindrical one. The proposed setup is similar to that used at the FELIX facility [3].
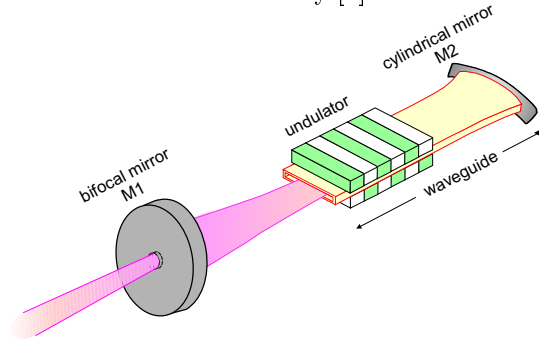
Fig. 2 *Optical mode compression by means of a resonator with partial waveguide.*

To minimize the optical beam cross section in the undulator we shall use an asymmetric resonator with the horizontal beam waist located in the undulator center and a Rayleigh length of 180 cm. The height of the waveguide and the resulting minimal pole gap are large enough for the electron beam and guarantee a sufficiently large magnetic field on the axis.

The undulator will be available at the beginning of the year 2006. Waveguide and resonator should be installed one year later.

Fig. 1 *Wavelength ranges (first harmonic) λ_1 of the existing U27 and the planned U100 undulator of ELBE as a function of the kinetic electron energy E_e^{kin} calculated for the indicated values of the undulator parameter $K_{\rm rms}$.*

[1] L.R. Elias and J. Gallardo, Appl. Phys. B31 (1983) 229
[2] R, Wünsch, Wiss.-Techn. Berichte FZR-423 (2005)
[3] http://www.rijnh.nl

[1] FZR, Institute of Nuclear and Hadron Physics

34

Gain and Power of the Far Infrared FEL (U100) at ELBE

R. Wünsch[1]

To ensure a satisfactory work in the envisaged wavelength region ($15\,\mu m \lesssim \lambda \lesssim 150\mu m$) we have estimated the single-pass gain and the outcoupled optical power of the U100 undulator at the ELBE beam. The calculation is based on a scheme developed by S. Benson [1] for the Jefferson Laboratory. Electron beam, undulator and resonator parameter are the input. Beam and undulator parameters are summarized in table 1. The resonator is considered in Ref. [2].

Table 1: *Parameters of the ELBE beam and of the U100 undulator*

Electron beam	
Kinetic energy	20-40 MeV
Pulse charge	70 pC
Energy spread	60 keV
Norm. transv. emittance	13 mm mrad
Undulator	
Undulator period	10 cm
Number of periods	38
Magnetic field amplitude on axis	$\lesssim 0.4$ T
Undulator parameter (K_{rms})	$\lesssim 2.5$
Minimum pole gap	20 mm

The single-pass laser gain depends strongly on the length of the electron pulse. We assumed a longitudinal Gaussian charge distribution and calculated the
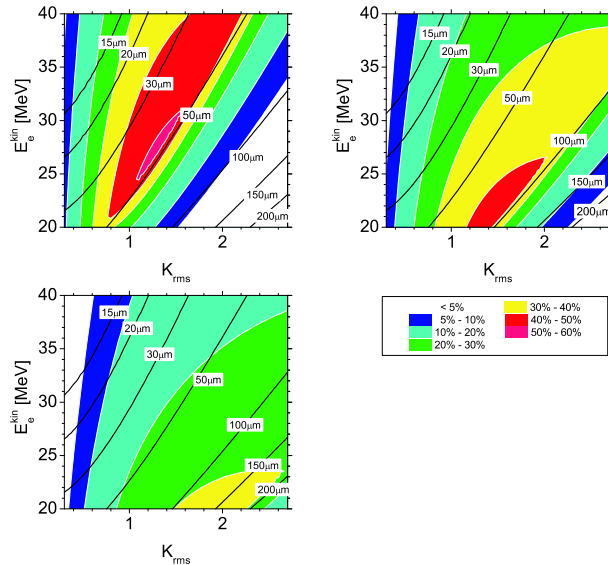

Fig. 1: *Small-signal single-pass gain calculated for the U100 undulator at the ELBE beam for 3 values of the rms electron pulse length τ as a function of the undulator parameter K_{rms} and the kinetic electron energy E_e^{kin}. The figure displays the maximum gain with respect to resonator desynchronization.*

Upper left panel: τ=1 ps; *Upper right panel:* τ=2 ps;
Lower left panel: τ=4 ps;

gain for 3 values of the rms pulse length. Fig. 1 shows that the gain is larger than the optical losses considered in Ref. [2] in the whole wavelength range. Choosing the appropriate electron pulse length the gain is ever larger than 30%. The larger the wavelength the longer the electron pulse should be.
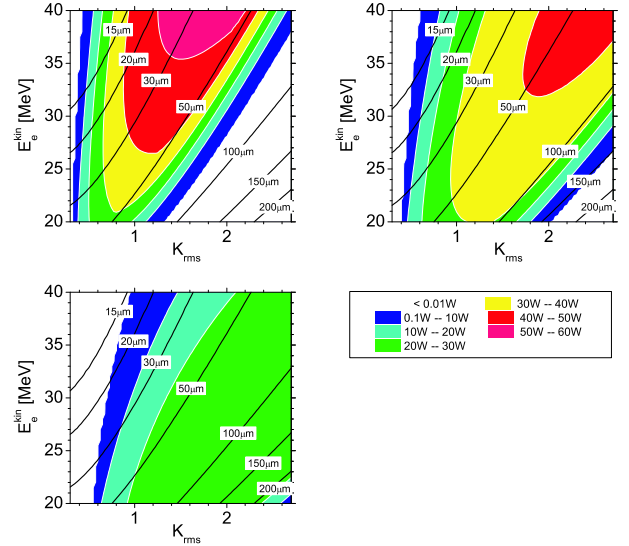
Fig. 2: *Outcoupled average laser power as a function of the undulator parameter K_{rms} and the kinetic electron energy E_e^{kin} with the same pulse lengths as in Fig. 1.*

Outcoupling and resonator desynchronization have been assumed to be optimal. To realize this outcoupling the radius of the outcoupling hole has to be varied from 1.5 mm around $15\,\mu m$ up to 6 mm around $150\,\mu m$. For a fixed outcoupling hole the power is smaller in general. To cover the whole wavelength region 3 different outcoupling holes are necessary at least.

According to the results of Ref. [2] we assumed resonator losses fixed to 8%. They include mode-coupling, absorption and dispersion losses. The outcoupling was considered separately according to the size of the hole. Around $30\,\mu m$ the average outcoupled power may achieve 50 Watts. At wavelength around $150\,\mu m$ the predicted power is still 25 W.

Fig. 2 shows the maximum gain with respect to the resonator desynchronization. This desynchronization is significantly smaller than the desynchronization resulting to the maximum gain, which is displayed in Fig. 1.

[1] S.V. Benson, CEBAF TN#94-065
[2] R. Wünsch, Wiss.-Techn. Berichte FZR-423 (2005)

[1] Institute of Nuclear and Hadron Physics

Radiation Sensor System for the Undulator U27 Using Optical Fiber

W. Seidel[1], J. Kuhnhenn[2], U. Weinand[2], A. Schamlott

Permanent magnets as components of a Free-Electron Laser (FEL) undulator are irradiated with high-energy electrons and bremsstrahlung X-rays, especially in the initial beam conditioning and in the beam positioning with screen monitors. Several authors have reported radiation damage of permanent magnet materials used in undulators at synchrotron radiation facilities [1, 2]. Because extremely high accuracy of the strength of magnetic fields on the path of an electron beam in the undulator is required, a modification of the field strength would be a serious problem for the lasing process. It is of even more importance in high-duty cycle machines using superconducting accelerators such as the ELBE facility with the high average current.

An undulator such as the U27 at ELBE, with NdFeB permanent magnet material can show some degradation in field quality with as little as 10^5 Gy and a dose of 10^6 Gy probably leads to unacceptable undulator performance [2]. This is the reason why we have to be very careful with beam loss around the magnet material. The radiation exposure was continuously monitored in the initial commissioning phase of the FEL by TLD-100-type thermoluminescense dosimeters, placed in between the poles directly at the magnets. Due to the limited linear range of the TLD's (10 Gy) we had to replace the dosimeters every shift. Such a procedure is not feasible in the routine operation of the FEL. Furthermore, we noticed a possible missteering or runs with high dark current levels not until the analysis of the TLD's. To overcome this, an integrating radiation detector placed near to or in the undulator will monitore the dose on-line. If the dose approaches a predefined threshold, the beam loss must be reduced. We have installed a system based on the radiation-induced attenuation in optical fibers. Using radiation sensitive P-doped optical graded-index fibers the ionizing radiation leads to a local increase of the attenuation which is measured with a commercial Optical-Time-Domain-Reflectometer (OTDR). In contrast to other optical fibers, P-doped fibers have several advantages for dosimetry purposes. Their radiation-induced attenuation increases linearly with dose before it saturates for doses higher than 1000 Gy. Additional, they do not show a fast fading of the induced attenuation, so they integrate the dose over beam interuptions. Also the induced loss is independent of the dose rate. Since the linear correlation coefficient between dose and attenuation depends on many production parameters of the specific fiber one has to determine this for each fiber separately. At the Co-60 sources of the INT this coefficient was measured for the used fiber. The

radiation-sensitive fiber was wound to spools around an Al-plate which fits between the beam pipe and the undulator magnets without restriction of gap tunability. The sensor spools were spliced to radiation hard fiber leads which connected the spools to each other and finally to the OTDR which was located in a neighboring room. To calculate the dose it is necessary to know the exposed length of the fiber. Since the radiation generated at the undulators is not specifically located the exposed length of the fiber has to be determined. This could be done, e.g. with several TLDs which are located perpendicular to the beam axis. This has not been possible so far, thus the exact length of the exposed fiber is not known. Therefore, the doses in Fig. 1 are given in arbitrary units. Further details on the experimental details and data analysis can be found in [3].

In Fig. 1 the measured doses for 3 positions in the undulator are shown. The measurements were performed during the commissioning of the accelerator. Although the absolute doses are unknown, the relative scale is correct. One can clearly identify three major dose depositions: at around 15:30, at 18:30 and at 21:00. This also corresponds to conventional dose-rate measurements which were done using ionization chambers near the entrances of both undulator units (in 5 cm distance from the beam pipe). Both results can be correlated with the operation conditions of the electron beam.
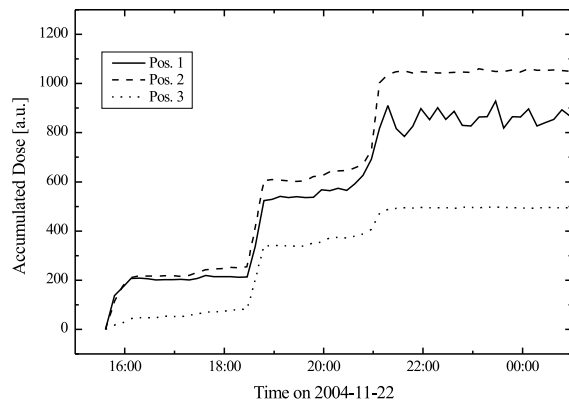
Fig. 1: *Accumulated dose during accelerator commissioning measured by a fiber optic dosimetry system at 3 positions in the undulator at November 22, 2004.*

[1] J. Chavanne, et al., ESRF Machine Technical Note 1-1996/ID (1996)
[2] M. Petra, et al., Nucl. Instr. Meth. A 507 (2003) 422
[3] H. Henschel, et. al., Nucl. Instr. Meth. A 526 (2004) 537

[1] *Institute of Nuclear and Hadron Physics, FZR, Dresden, Germany*
[2] *Fraunhofer INT, 53879 Euskirchen, Germany*

A Goniometer for Channeling Radiation Experiments at ELBE

W. Wagner[1], F. Müller[2], A. Nowack[3], M. Sobiella[1], J. Steiner[1], W. Enghardt[1]

Channeling radiation (CR) is emitted by relativistic electrons travelling through a single crystal along a main lattice plane or axis. For channeling the particles have to be captured by the average planar or axial potential. This happens when their angle of incidence with respect to the plane or axis is smaller than the critical (Lindhard) angle Θ_{cr}.

At ELBE energies $\Theta_{cr} \approx 2\,\mathrm{mrad}$ can be given as a typical value. Considering a beam of sufficiently small divergence ($\approx 0.1\,\mathrm{mrad}$), the angle of incidence has to be adjusted by means of a goniometer which carries the crystal. The goniometer must have at least two rotational axes oriented perpendicular to each other and allowing for a reproducibility of the angular setting better than Θ_{cr}, i.e. $\leq 0.05°$. Since the goniometer operates in line with the superconducting cavities of the ELBE accelerator, it has to meet the rather strong demands for an extremely clean UHV. This concerns the composition of the residual gas as well as the absence of microparticles.

At commercial UHV goniometers the precise angular setting ($\approx 0.001°$) is usually reached by means of worm gears. The mechanisms for translatory movement include spindle drives and roller bearings. It is recommended by the producer that gears and bearings have to be lubricated either with UHV grease or with Molybdenum. A gas analysis made by means of a quadrupole mass spectrometer showed that the remaining atmosphere in an UHV chamber housing such type of goniometer contains plenty of masses larger than 32 amu (O_2^+) originating from radicals of higher carbonic hydrogens, fluorinated hydrocarbons etc.

Furthermore, a measurement of microparticles produced from dryly operating worm gears resulted in concentrations of 10^3–10^4 cft^{-1}. Such values are to large by several orders of magnitude and could be diminished by the use of lubricants only.

To overcome the difficulties mentioned above we, therefore, decided to construct a goniometer which bases on another principle (Fig. 1). All drives are implemented as linear ones using ball bearing screw thread spindles which are driven by Phytron UHV stepping motors and sway a nut element. The translatory movement of the nut is transformed by a connecting rod to the rotation of a frame which carries the crystal holder. All ball bearings used for the bearing of rotating elements are dryly running miniature ones. Special measures have been taken to avoid the propagation of minimal tilt clearance of the also dryly running spindle-nut drive to the rotary motion of the frame. The screw thread rising of the subtle spin-

dles amounts to only $0.25\,\mathrm{mm}$ resulting in an angular resolution of $\Delta\vartheta \leq 0.005°$ per motor step (MS) at a maximum nonlinearity of the angular scale of 2.5 % .
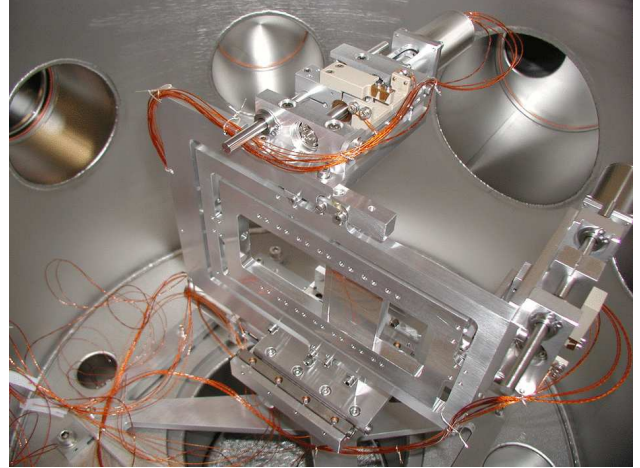

Fig. 1: *The goniometer without target holder at opened UHV chamber.*

The combination of two such nested mechanisms whose axes of rotation are perpendicular to each other allows to simultaneously rotate (ϑ) and tilt (ψ) the crystal around the vertical and the horizontal axis, respectively, up to angles of $\vartheta = \psi = 25°$ with respect to the normal of the frames at zero position. The special construction of the crystal holder which fixes the crystal to the inner frame of the goniometer, guarantees the reproducibility of the angular orientation of the crystal even after multiple changes of the target.

The two rotary mechanisms are mounted onto a sliding carriage which allows shifting (X) of the crystal out of the beam. At a second target position an 18 μm thick Al foil serves as an OTR view screen for the beam setting.

The goniometer is remote- controlled via programmable Phytron OMC/TMC 93-70 MINI stepmotor control units. The software allows absolute as well as relative positioning of the goniometer coordinates ($X;\vartheta,\psi$) in units of MS. The once defined zero position serves as a relative reference. The endpoints of the drives cannot be used for that. The practical scales (X/μm, ϑ/degrees and ψ/degrees) have been obtained by a calibration procedure.

The goniometer runs well at pressures down to 10^{-9} mbar. The reproducibility of angular positioning has been checked by measurements of planar CR from diamond. It can be estimated from angular scans to be ≈ 1 mrad (10 MS). This accuracy is enough for CR production experiments.

---

[1] FZR, Institute of Nuclear and Hadron Physics
[2] FMB GmbH, Berlin, Germany
[3] FZR, Department of Research Technology

Dose Rate Measurement around the ELBE Channeling X-Ray Beam Line

J. Pawelke[1], U. Lehnert, A. Schamlott, W. Wagner[1], W. Enghardt[1]

A main objective of building the channeling radiation (CR) source at ELBE is its application to determine the RBE of X-rays by cell irradiation. Reliable studies of radiobiological effects on living cells need a maximum irradiation dose rate of about 1 Gy/min where a sufficiently low level of background radiation at the irradiation site is required. However, CR has been produced at ELBE only with low intensity by an electron beam of 1 to 50 nA current so far in order to measure photon energy spectra and to study the dependence of the CR energy and yield on the electron beam energy and on the diamond crystal thickness [1], [2]. To yield the required maximum dose rate for cell irradiation from the 1-0 transition of (110) planar channeling in a diamond crystal an average electron beam current of 100 μA would be necessary.

In a first attempt to increase the CR intensity by raising the electron beam current by about four orders of magnitude the photon radiation background (polychromatic bremsstrahlung) at the irradiation site has been measured. Four air filled ionisation chambers (IC) connected to an UNIDOS electrometer (PTW Freiburg), each, were placed around the beam line (Fig. 1). Three Farmer IC (M30001, PTW Freiburg, position I, II and III) and a rigid stem IC (M23332, PTW Freiburg, position IV) have been chosen because of their energy and dose rate range as well as size and handling [3]. In addition, the LB6701 IC (Berthold, Bad Wildbach) was used at position V which is part of the radiation protection system of ELBE.
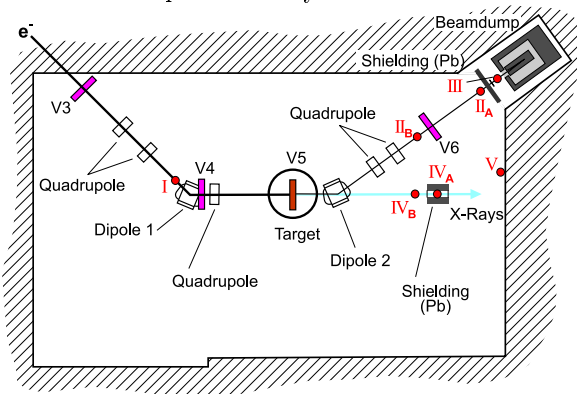

Fig. 1: *Position of the ionisation chambers in the radiation physics cave. The electron beam comes from the accelerator (left) and is stopped in the dump (right).*

After tuning the electron beam of 17.0 ± 0.2 MeV energy and up to 130 μA current, photon dose rates were measured without any target in the beam. The measurement was repeated with an 18 μm thick Al foil inserted into the beam in order to study the influence of electron scattering in the target on beam loss and the corresponding radiation background. The Al foil

has been chosen for practical reasons. since it is used as an optical transition radiation viewer for observation of the electron beam profile and position at the CR target and results in a roughly comparable electron scattering as the thicker diamond crystals used for CR generation. Two sets of dose rate measurements were done moving the IC's II and IV from position A to B, in both cases, with and without target in the beam.

Tab. 1: *Comparison of photon dose rates at different positions measured for an electron beam current of 100 μA.*

Position	Exp. no.	Dose rate / (mGy/min)	
		no target	18 μm Al target
I	1	1	1
	2	1	1
II_A	1	286	660
II_B	2	1	814
III	1	829	1042
	2	896	1638
IV_A	1	0	409
IV_B	2	1	450
V	1	74	890
	2	85	1478

Without passing a target the electron beam can be transported to the dump without loss. The corresponding high bremsstrahlung background at the dump (see Table 1) is considerably attenuated by the 10 cm thick Pb shield in front of the dump and by the concrete wall in which the dump is inserted. This results in a very low level of background radiation at the cell irradiation site (position IV_A and IV_B, respectively). In contrast, the electron scattering in the target results in a considerable beam loss and a corresponding overall rise of the background radiation level. However, the high radiation intensity at the cell irradiation site is mainly caused by bremsstrahlung generated in the target and emitted in forward direction of the electron beam. Only a rather small contribution of bremsstrahlung generated at the beam line reaches the irradiation site, as indicated by the about 10 % lower dose rate at position IV_A, i.e. when the IC is shielded by a Pb hollow cylinder against photons arriving from lateral direction, compared to site IV_B. But the about 60 % dose rate variation measured for the target in the beam at position III and V, respectively, also shows the difficulty of reproducible beam tuning behind the second dipole magnet.

[1] W. Wagner, A. Panteleeva et al., Wiss.-Techn. Berichte FZR-401 (2004) 56
[2] W. Wagner, B. Azadegan et al., this report, p. 16
[3] J. Pawelke, T. Mikuletz, A. Panteleeva, Wiss.-Techn. Berichte FZR-401 (2004) 58

---

[1]FZR, Institute of Nuclear and Hadron Physics

Beam Monitoring at the Radiation Physics Beam Line

W. Neubert, K. Heidel, J. Pawelke, W. Wagner, W. Enghardt

The current monitors installed at the beam line of the electron accelerator ELBE are induction devices suitable for beam intensities $\geq 1\,\mu A$. Experiments to ascertain the conditions for generation of channeling radiation by proper crystals require a precise monitoring of beam intensities from about 1 nA to some hundreds of nA. A commonly used device in the MeV region is the secondary electron monitor (SEM). Such type of monitor constructed in the past and described in [1] was installed at $\simeq 20$ cm behind the the crystal position in the goniometer chamber of the radiation physics beam line. The SEM can be removed from its measuring position by a pneumatic driven UHV bellow without breaking the vacuum.

The SEM must be calibrated by a Faraday cup (FC) positioned as close as possible to the SEM in order to minimize the loss of beam electrons scattered away by the SEM. The installation of such a FC at a distance of $\simeq 20$ cm from the SEM was only possible by the construction of a dedicated adapter flange which substitutes the former one at the exit of the goniometer chamber. The disponable space inside this flange, the required application to beam energies of 20 MeV as well as the realisation of in-beam and out-of-beam positions allowed only a very compact construction. It was realised using ranges in the CSD approximation supported by simulations using the program package GEANT 3.2. The body where the electrons are slowed down consists of a conical cylinder of Al terminated by a Cu disc. Although the ratio of backscattered electrons in the energy range from 15 MeV to 20 MeV is about 10^{-3} as a precaution two magnetic pieces of hard sinter ferrits (BaFe/SrFe, type R1212) were inserted into the Al corpus near to the aperture of the FC. They supply a magnetic induction of 5.6 ± 0.2 mT perpendicular to the beam axis which avoids to escape backscattered electrons from the FC. The cylindric body of the FC (diameter = 53 mm, length = 86 mm) is insulated from the outer Al screen by 4 Marcor sticks. It was checked that a negative biased screen is unnecessary due to the implemented ferrits. The FC is holdered by a Vitronit construction which insulates it from the ground potential of the beam tube.

The beam absorbed in the FC is measured by a current integrator based on the operation amplifier OPA-129 as already described in [2]. The calibration carried out using a precision current generator confirmed a linear response in the dynamical range from zero to $1\,\mu A$ with an offset of -0.35 mV. The efficiency of the SEM was measured with the same integrator type. Fig. 1 shows that a voltage ≥ 10 V applied to the outer collecting foil electrodes provide for full efficiency. The response of the SEM related to the FC was measured as function of the beam intensity using different pulsing regimes. Fig. 2 demonstrates a linear behaviour in the range of interest.

The calibration factor of the SEM obtained with removed target amounts to $R = I(SEM)/I(FC) = (4.29 \pm 0.08) \cdot 10^{-2}$ at the incident energy 14.6 ± 0.2 MeV. The accuracy of the current measurement in the FC was estimated to be $\simeq 1\,\%$ as follows from GEANT 3.2 simulations taking into account electron losses caused by scattering in the SEM and electron escape from the FC corpus. An analog setup described in ref's. [3,4] yielded at 15 MeV the ratio $R = (4.16 \pm 0.04) \cdot 10^{-2}$ in fair agreement with our result.

[1] W. Neubert, K. Heidel et al., Wiss.-Techn. Berichte FZR-341 (2002) 16
[2] W. Neubert, J. Pawelke et al., Wiss.-Techn. Berichte FZR-423 (2005)
[3] V.J. Vanhuyse, E.D. Wattecamps et al., Nucl. Instrum. Meth. 15 (1962) 59
[4] V.J. Vanhuyse, R.E. Van De Vijver, Nucl. Instrum. Meth. 15 (1962) 63
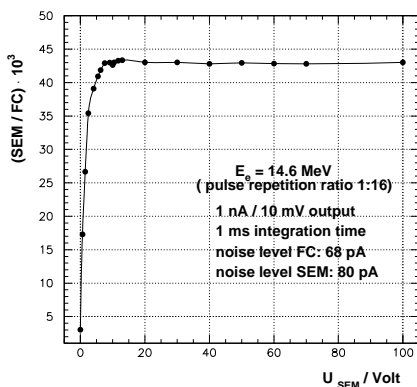
Fig. 1: *Efficiency of the SEM related to the FC as function of the voltage applied to the outer foil electrodes.*
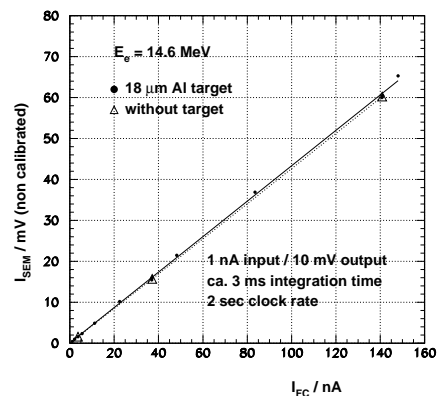

Fig. 2: *Response of the SEM as function of the beam intensity measured with the FC. The solid and dashed lines are fits to the points measured with 18 μm Al and without target, respectively.*

GEANT Simulations for the Beam Monitors at the Radiation Physics Beam Line

W. Neubert, J. Pawelke, W. Wagner, W. Enghardt

The beam monitors described in the preceding contribution [1] have been used to determine absolute yields of channeling radiation produced by electron impact in diamond and other crystals. Measurements of the relative current obtained by the secondary electron monitor (SEM) compared with the corresponding one from the Faraday cup (FC) were performed in subsequent runs at beam intensities which cover more than 2 orders of magnitude. The obtained ratios are shown in fig. 1 together with the main setup parameters.
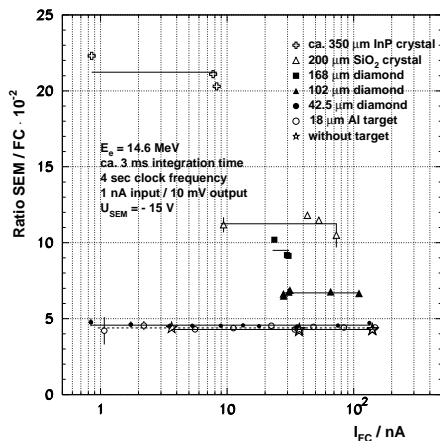

Fig. 1 *Ratios of the beam current measured with the SEM and the Faraday cup as function of the beam intensity.*

The ratio $R = I(\text{SEM})/I(\text{FC})$ was found to be constant for a given target, but the thicker the crystal the larger the measured ratio. Simulations using the program package GEANT 3.2. were performed in order to find out the reason of this behaviour and to quantify the deviations from the calibration ratio $R = 4.29 \pm 0.08$. The beam spot observed at the OTR 18 μm Al screen in target position was imitated by a parallel beam with a Gaussian profile $\sigma_x, y = 0.415$ mm.
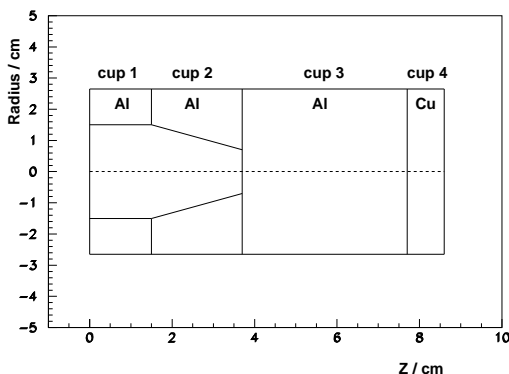

Fig. 2 *Dimensions of the cylindric Faraday cup and its representation as 4 bodies in the simulations.*

The diamond crystal was approximated by amorphous carbon with the average density of diamond $\varrho = 3.516$ g/cm^3. The SEM was represented by a compact Mylar disc with the sum thickness of the 3 foil electrodes surrounded by a iron ring corresponding to the construction dimensions of the stainless steel holders. The geometry of the FC is shown in fig. 2. In the simulations all relevant electron interaction processes were taken into account.

The lateral spread of the electron beam caused by the SEM decreases from $\sigma_{x,y} \simeq 1$ mm at 12 MeV to $\simeq$ 0.4 mm at 32 MeV in front of the FC. Thus the main beam intensity fits always into the aperture of the FC. But to a greater extend beam electrons are lost by scattering in the target crystals. The fraction of simulated beam electrons found in the aperture of the SEM and detected in the FC are assembled in table 1. Incoming electrons of $\simeq 15$ MeV are completely stopped in cup 3 of the FC (cf. Fig. 2) but affected by copious electrons mainly produced by inelastic interactions producing δ-rays. In order to avoid double-counting a cut set at 8 MeV allowed to eliminate most of such secondaries. The fraction of electrons assigned to the incoming beam are given in table 1. They allow to correct the measuring data from both the SEM and the FC for electron losses due to scattering mostly in the target. The corrected ratios R_{corr} agree within the estimated errors with the calibration ratio $R = 4.29 \pm 0.08$ measured without target. The multiple scattering in thick targets adulterates mainly the measurement of the beam current in the Faraday cup unlike the SEM, closer located to the crystal. This monitor requires only moderate corrections as seen in table 1. These corrections are nearly independent of the beam profile because dedicated simulations performed with other Gaussian or asymmetric profiles showed that the width of the outcoming beam is almost the same even after passing a moderate thickness. Therefore, the corrections are basically determined by the target thickness.

Table 1 *Results of simulations at 14.6 MeV. The fractions of the started beam electrons counted within the aperture of the SEM and detected in the FC are given in columns 2 and 3, respectively. The ratios R_{exp} in column 4 correspond to Fig. 1 whereas column 5 gives these ratios corrected for calculated losses by electron scattering.*

target	SEM %	FC %	R_{exp} $\cdot 10^{-2}$	R_{corr} $\cdot 10^{-2}$
only SEM	100	99.9	4.29	4.29
18 μm Al	99.0±0.4	93.7	4.36	4.1±0.2
42.5 μm C	98.8±0.8	87.9	4.7	4.2±0.2
102 μm C	95.7±0.8	64.9	6.7	4.6±0.5
168 μm C	90.6±0.6	47.5	9.5	4.8±1.1
200 μm SiO$_2$	84.0±1.0	36.6	11.24	4.6±1.4

[1] W. Neubert, K. Heidel et al., this report, p. 39

Establishment of a Laboratory for X-Ray Experiments at ELBE

J. Pawelke[1], S. Eckert[2], W. Enghardt[1]

At the ELBE facility intensive quasi-monochromatic X-rays are produced by channeling of the ELBE electron beam in diamond crystals [1] in the radiation physics cave (room 112, cf. Fig. 1). The channeling X-ray source ($E_\gamma \approx 10 - 100$ keV) is planned to be used for radiobiological experiments by the Radiation Physics Division of the Institute of Nuclear and Hadron Physics [2] and for imaging of phase transition and flow phenomena in liquid metals by the Magneto-hydrodynamics Department of the Institute of Safety Research [3].

For the preparation of the experiments including the necessary detector tests without requiring ELBE beam time and not occupying the irradiation site in the radiation physics cave, a separate X-ray laboratory with two conventional X-ray tubes (see Tab. 1) has been established in the ELBE building (room 112a, cf. Fig. 1).

Tab. 1: *Main parameters of the two X-ray tubes.*

	Isovolt 320 HS	XS225D OEM
Tube voltage [kV]	5 to 320	10 to 225
Tube current [mA]	0.1 to 45	0.005 to 3
Maximum anode dissipation [VA]	4200	1400
Beam angle [°]	40	25
Anode material	W	W, Cu
Focal spot size	4.0 / 1.5 mm	$\geq 3\ \mu$m
Inherent filtering	7 mm Be	0.5 mm Be
Minimum focus-object-distance	13 cm	4.5 mm

The high stability constant potential X-ray tube Isovolt 320 HS (Agfa NDT Pantak Seifert, Ahrensburg) is very well suited for dosimetrical experiments and will be used as a reference X-ray source for the radiobiological studies, whereas the X-ray unit XS225D OEM (Phoenix X-ray Systems, Wunstorf) meets the requirements of feature recognition down to μm spatial resolution.

Important features of the laboratory are: circulating air cooling, argon gas and cooling water (20 l/min, 30°C) supply as well as access control system. The front wall stands back from the adjacent rooms giving place for the X-ray tube control units (Fig. 2). For radiation shielding, the laboratory steel structure has intermediate lead panels (thickness in the front wall of 28 mm, in the side wall toward the positron laboratory of 100 mm and in the ceiling of 5 mm).

Perspectively, the use of the quasi-monochromatic X-ray beam from the radiation physics cave in the X-ray laboratory is possible.

Fig. 2: *Control unit of the Isovolt X-ray tube in front of the laboratory.*

[1] W. Wagner, A. Panteleeva et al., Wiss.-Techn. Berichte FZR-401 (2004) 56

[2] W. Neubert et al., Proc. Conf. Monte Carlo 2000, Lisbon, Eds.: A. Kling et al., Springer-Verlag (2001) 123

[3] S. Eckert et al., FZ Rossendorf, Wiss.-Techn. Berichte FZR-341 (2002) 96
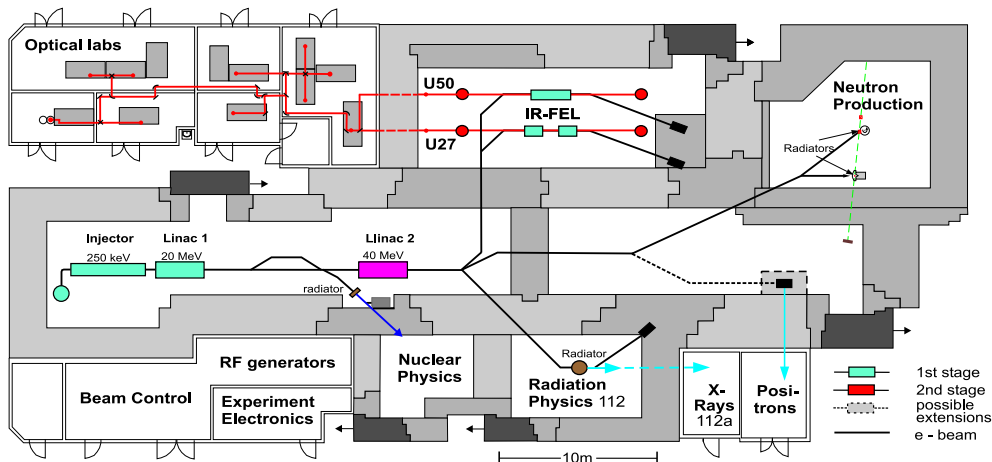
Fig. 1: *General layout of the radiation source ELBE with the radiation physics cave (112) and the X-ray laboratory (112a).*

---

[1] Institute of Nuclear and Hadron Physics
[2] Institute of Safety Research

Improvements of the Bremsstrahlung Facility at ELBE

K.D. Schilling[1], M. Döring[1], M. Erhard[1], E. Grosse,[2] A. Hartmann[1], A.R. Junghans[1], K. Kosev[1], R. Matjeschk[1], T. Riedel,[3] G. Rusev[1], W. Schulze[1], R. Schwengner[1], W. Seidel[1], J. Steiner[1], A. Wagner[1]

In continuation of the status report presented in [1] and based on the methodical experiences gathered during extensive beam time periods with the bremsstrahlung facility at ELBE, further improvements have been realized. They are displayed in Fig. 1 and will be described in the following:

• The Al window mentioned in [2] that separates the ultra-high vacuum in the accelerator (electron) beam tube from the vacuum system of the bremsstrahlung beam line was exchanged for a quartz window of 3.3 mm thickness and 35.6 mm effective diameter. In this way, a system for the laser alignment of the beam tube between the last bending magnet on the left of the steering magnets (not shown in Fig. 1) and the γ beam dump including the bremsstrahlung collimator [3] has been realized. Thus, the collinearity of the collimated bremsstrahlung beam with the incident electron beam can be achieved.

• The polarization monitor [4,1], which houses the target of deuterated polyethylene (CD_2) of about $50\,\mu$m thickness, was moved upstream to a position in front of the third Pb wall (in beam direction) in the experimental cave (Fig. 1). This led to a considerable γ-background reduction observed in the HPGe (+ BGO) detector array as a result of the essential shielding effect of the third Pb wall.

• A EUROBALL cluster detector [5] consisting of 7 individual hexagonal shaped HPGe crystals has been installed at an average angle of $\Theta = 140°$ relative to the photon beam direction in order to detect γ radiation emitted to the backward hemisphere.

• A photon-beam position monitor [6] consisting of four segmented scintillation detectors has been constructed and installed at the entrance of the γ beam dump. It serves to monitor the position and the intensity of the bremsstrahlung photon beam.

• An essential new ingredient of the bremsstrahlung facility consists in the installation of a photoactivation setup [7]. It enables measurements of activation yields, e.g., of p-nuclei in order to determine photodisintegration cross sections of astrophysical interest [8]. The new setup is positioned inside of the iron casing of the electron beam dump (Fig. 1) downstream of the graphite cylinder utilizing a high bremsstrahlung intensity for activation purposes. A cylindrical Al tube contains an Al rod with a clamp-type target holder. The setup will be upgraded by a pneumatic-tube delivery system in near future. See [7] for more details.

• An automatic N_2-filling system for the HPGe detectors has been installed that gives a permanent information about the status via TV camera and sends an SMS in case of an alert signal.
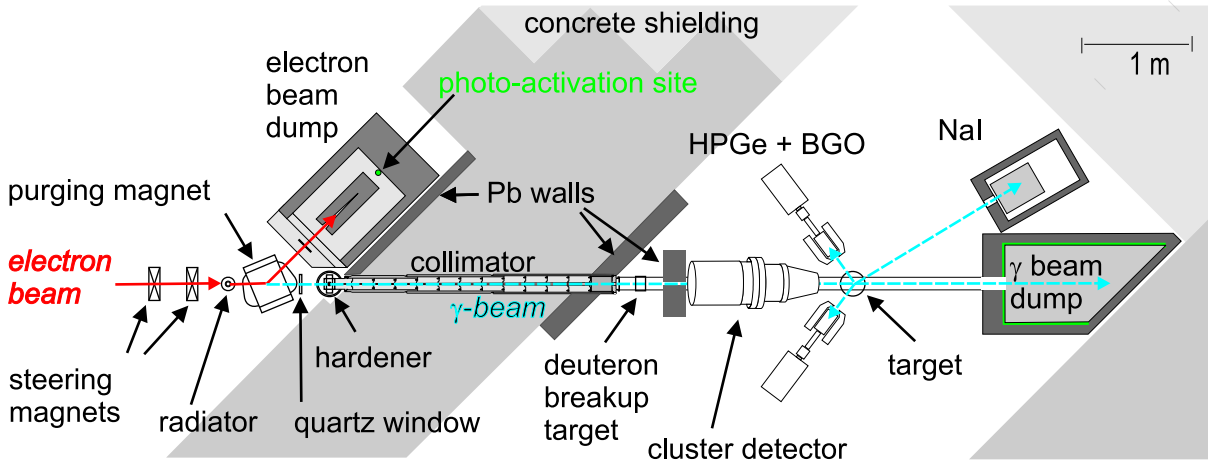

Fig. 1: *Current layout of the bremsstrahlung facility for nuclear-physics and astrophysics experiments at ELBE.*

[1] K.D. Schilling, F. Dönau et al., Wiss.-Techn. Ber. FZR-401 (2004) 5
[2] K.D. Schilling, A. Wagner et al., Wiss.-Techn. Ber. FZR-341 (2002) 41
[3] K.D. Schilling, R. Schwengner et al., Wiss.-Techn. Ber. FZR-341 (2002) 37
[4] R. Schwengner, H. Sharma, A. Wagner, Wiss.-Techn. Ber. FZR-341 (2002) 39
[5] J. Eberth, H.G. Thomas et al., Progr. Part. Nucl. Phys. 38C (1997) 29
[6] M. Döring, R. Matjeschk et al., Wiss.-Techn. Ber. FZR-423 (2005) p. 23
[7] M. Erhard, E. Grosse et al., Wiss.-Techn. Ber. FZR-423 (2005) p. 14
[8] M. Erhard, E. Grosse et al., Wiss.-Techn. Ber. FZR-423 (2005) p. 13

[1] Institute of Nuclear and Hadron Physics
[2] also Technische Universität Dresden
[3] FZ Rossendorf, FWF

A Beam Position Monitor for Bremsstrahlung Photons at ELBE

M. Döring[1], R. Matjeschk[2], A. Hartmann[3], K.D. Schilling[1], W. Schulze[1], A. Wagner[1]

In order to monitor the position and intensity of the photon beam at the bremsstahlung facility at ELBE we constructed and tested a segmented scintillation detector. The detector should determine both misalignements of the photon beam inside the experimental area as well as intensity asymmetries caused by a non-centered electron beam spot at the bremsstrahlung radiator where photons are produced. The mechanical setup consists of four identical plastic scintillators, lightguides, and photomultiplier tubes. The four plastic scintillators of size $35 \times 35 \times 4 \, mm^3$ made of NE104 [1] are arranged symmetrically around the center of the photon beam. Scintillation light of each scintillator is registered by an individual $3/4''$ photomultiplier tube of type R3478 [2]. The mechanical setup of the detector is shown in Fig. 1.

Fig. 1: *Mechanical setup of the photon beam monitor. Each scintillator bar is read out by a separate photomultiplier tube via an attached lightguide. The projected photon beam distribution is indicated by a circle.*

In order to calibrate the light output we irradiated each detector with a ^{60}Co γ-source and determined the location of the Compton-scattering edge. Varying the high voltage bias setting for each detector individually we adjusted all four detectors to give the same energy signal. Results are shown in the following table.

Table. 1: *High voltage bias settings $U_{Compton}$ for each tube resulting at the same signal amplitude for the Compton-edge using a ^{137}Cs-source. U_{Rate} is the value for equal count rates obtained for a discriminator threshold setting of -52mV.*

Detector No.	Serial No.	$U_{Compton}$	U_{Rate}
1	KA 1651	-1535 V	-1614 V
2	KA 1753	-1525 V	-1570 V
3	KA 1692	-1580 V	-1600 V
4	KA 1751	-1800 V	-1725 V

With the aim of increasing the flux of ionizing particles inside the scintillator we wrapped them with several layers of thin aluminium foil working as converters of photons into electrons by Compton scattering. We found that for thicknesses between 0 and 500 μm there was no increase in count rate using a rather low-energy photon source of 667 keV(^{137}Cs). Moreover, the aluminium foil proved to be an absorber decreasing the detection efficiency by up to 20%.
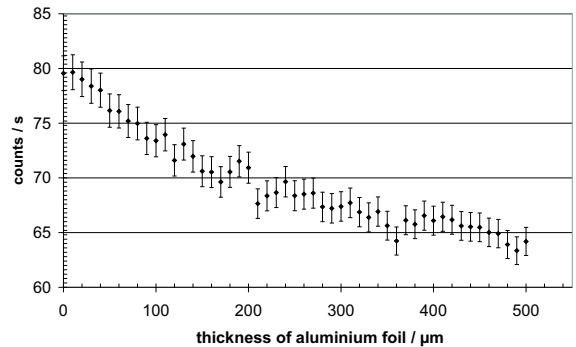

Fig. 2: *Count rate variation of the scintillating detector for different thicknesses of aluminium foil wrapped around.*

The position sensitivity has been determined by scanning the detector surface with a collimated photon beam. We used two linear stepper motor drives and we scanned across the detection area determining the count rate for each scintillation detector individually. The expected count rate variation has been calculated by folding the source's circular aperture of 10 mm diameter with the rectangular shape of the scintillator bar. The results are shown in Fig. 3 for a scan in one direction. The overall agreement between the measured and expected count rates is quite convincing. It enables us to use the device as a position-sensitive photon detector at the bremsstrahlung facility at ELBE.
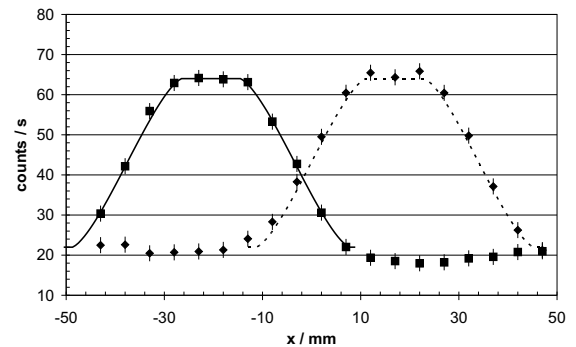

Fig. 3: *Count rate variations for scans over the detection area of two of the scintillators (filled squares and diamonds) using a collimated photon source. Lines indicate the expected distribution by folding the circular aperture with the geometrical size of the detector.*

The detector is now installed inside the photon beam dump of the bremsstrahlung facility at ELBE.

[1] Saint-Gobain Crystals & Detectors, Paris, France
[2] Hamamatsu Photonics, Hamamatsu City, 430-8587, Japan

[1] Technische Universität Chemnitz
[2] Technische Universität Dresden
[3] Institute of Nuclear and Hadron Physics

Progress of the Photoactivation Setup at ELBE

M. Erhard[1], E. Grosse[1], A. Hartmann[1], A.R. Junghans[1], C. Nair[1], K.D. Schilling[1], W. Schulze[1], R. Schwengner[1], A. Wagner[1]

The accomplishment of a photoactivation experiment consists of two steps: first, the activation itself, when a target is irradiated with bremsstrahlung and, second, the measurement of γ quanta from the decay of the activated nuclei in a well-shielded setup [1].

In 2004, the first activation runs were performed at the existing nuclear-resonance-fluorescence (NRF) setup at ELBE. We used high-purity germanium (HPGe) detectors to measure the photon flux and the shape of the bremsstrahlung spectrum with the six strongest transitions in an NRF target of boron acid ($H_3{}^{11}BO_3$) containing 97.3% enriched ^{11}B. The photon flux density amounts to $\approx 10^8/(s \cdot cm^2 \cdot MeV)$ at half of the end-point energy. In order to increase the intensity significantly, we placed the activation targets inside the electron-beam dump behind the vacuum steel vessel. A cylindrical Al tube was inserted, and a target holder consisting of an Al rod with a clamping bolt was mounted.

In order to determine the photon flux for photoactivation experiments, samples consisting of natural Au at two experimental sites were used as normalisation standards. The photon flux at the NRF site was measured utilising photon scattering from the boron target together with a gold activation target. Another Au disk sandwiched with the Mo target under investigation was placed behind the electron beam dump. The resulting activation yield ratio displayed in Fig. 1 increases linearly with the energy caused by the higher photon-flux at the beam dump site.
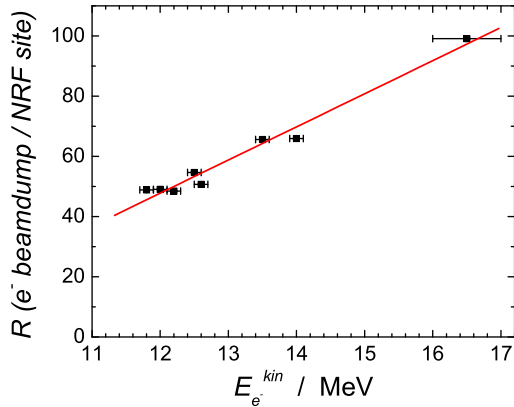

Fig. 1: *Activation yield ratio of the Au targets, activated in the electron-beam dump and at the NRF site simultaneously. The decay of ^{196}Au ($T_{1/2} = 6.2\ d$) was measured with a HPGe detector (356 keV transition in ^{196}Pt, $\sigma_R < 0.4\%$).*

The targets were prepared as circular discs with a diameter of 2 cm while their thickness was chosen according to the expected photodisintegration cross section with a maximum irradiation period of $\approx 16\ h$

and $\approx 500\ \mu A$ electron-beam current. Depending on energy and duration of the irradiation, we used Mo targets consisting of several 0.2 to 0.3 mm thick slices corresponding to masses of 0.63 g up to 0.98 g.

The activity of the Mo targets 20 min after shutdown of the electron beam was 5.2 kBq/g in the run with the highest energy (16.5 MeV), irradiated for 7 h, and the total target dose rate was measured to be 2.4 $\mu Sv/h$.
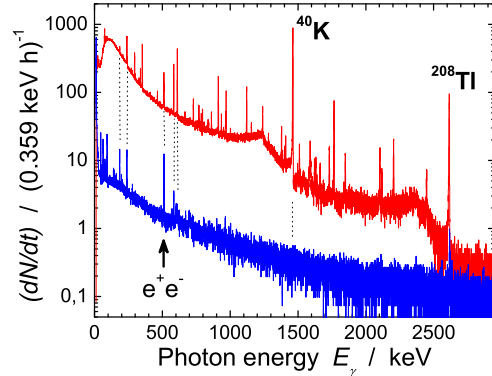

Fig. 2: *Background of an HPGe detector outside (upper curve, 12 h meas. time, overall count rate: $127\ s^{-1}$) and inside the lead castle (lower curve, 41 h, $2.9\ s^{-1}$). Background suppression is better than $1400\times$ for ^{40}K.*

For the measurement of very low activities, the reduction of radiation from surrounding materials is needed [2]. Fig. 2 shows the background suppression measured with a 60%-HPGe coaxial detector (n-type) inside and outside the lead castle shown in Fig. 3.
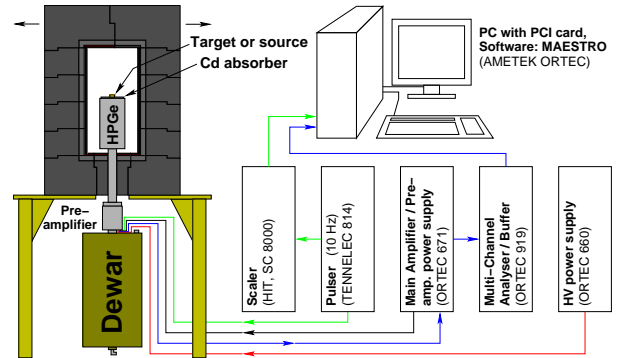
Fig. 3: *Low-level counting setup at ELBE with lead castle, HPGe detector and data acquisition system.*

The preamplifier-output signals are amplified and then processed by a multi-channel analyser. Deadtime and coincidence-summing corrections were done by applying a 10-Hz pulser signal to the preamplifier test input.

[1] M. Erhard, A. Wagner et al., Wiss.-Techn. Berichte FZR-401 (2004) 13

[2] P. Theodórsson, "Measurement of Weak Radioactivity", World Scientific Publishing Co. Pte. Ltd., 1996

---

[1]Institute of Nuclear and Hadron Physics

Measurement of the Beam Energy at ELBE via the Photodisintegration of the Deuteron

R. Schwengner[1], G. Rusev[1], K. D. Schilling[1], A. Wagner[1], E. Grosse[1], A. Hartmann[1]

During photon-scattering and photoactivation measurements it is important to monitor the electron energy, which defines the maximum energy of the bremsstrahlung spectrum. This monitoring can be done via the photodisintegration of the deuteron. The maximum energy of the incident photons can be deduced directly from the measured proton spectrum.

For the detection of the protons following the disintegration of deuterons we use a set-up of four silicon detectors placed perpendicular to the photon beam at azimuthal angles of 0°, 90°, 180° and 270° [1]. The detectors have sensitive areas of 600 mm^2 and thicknesses of 300 μm. They are mounted in a cylindrical reaction chamber at a distance of 6 cm from the beam axis. A polyethylene film, in which hydrogen is substituted by deuterium (CD2), is used as a target [2]. The CD2 film has a thickness of 40 μm and is positioned parallel to the incident beam such that it is observed by all four detectors under 45°.

The spectrum of the incident photons times the cross section for the disintegration of the deuteron can be obtained by rescaling the measured proton spectrum according to $N_\gamma(E_p + E_n + E_B) \sim N_p(E_p)$. Here, N_γ and N_p denote the photon and proton intensities at the given energies, respectively, $E_p \approx E_n$ are the energies of the proton and neutron, respectively, and $E_B = 2225$ keV is the binding energy of the deuteron. The photon spectrum is obtained by dividing by the disintegration cross section, σ_{dis}, for which the expression given in Ref. [3] was used.

The spectrum of incident photons obtained by rescaling a proton spectrum measured at $E_e^{kin} = 13.2$ MeV is shown in Fig. 1. This spectrum may be compared with spectra calculated (i) by using the formula given by Schiff [4], (ii) by using the programme GEANT4 [5], which applies a parametrisation of the data given by Seltzer and Berger [6], and (iii) by using the formula given by Bethe and Heitler (BH) [7], respectively. The increase of the experimental spectrum towards energies below 6 MeV is due to scattered photons hitting the silicon detectors. The calculations based on the Schiff formula and on GEANT4 do not reproduce the spectrum at the edge close to the maximum energy. The calculations according to Bethe and Heitler apparently reproduce the experimental spectrum fairly well and may thus be used to describe the photon flux.

[1] R. Schwengner, H. Sharma, A. Wagner, Wiss.-Tech. Berichte FZR-341 (2002) 39

[2] By courtesy of D. K. Geiger, SUNY Geneseo, NY 14454, USA

[3] H. Bethe, C. Longmire, Phys. Rev. 77 (1950) 647

[4] L.I. Schiff, Phys. Rev. 83 (1951) 252

[5] S. Agostinelli, J. Allison et al., Nucl. Instr. Meth. A 506 (2003) 250

[6] S.M. Seltzer, J. Berger, Nucl. Instr. Meth. B 12 (1985) 95, Nucl. Data At. Data Tables 35 (1986) 345

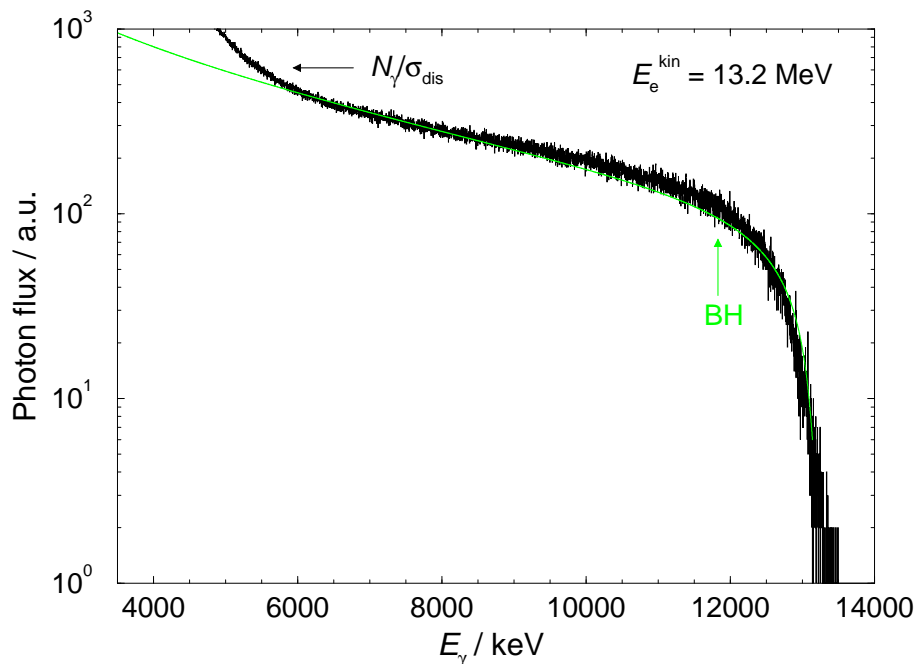[7] W. Heitler, *The quantum theory of radiation*, Dover publications, New York 1984, p. 242 ff.

Fig. 1: *Spectrum of incident photons recalculated from the proton spectrum over the cross section for the photodisintegration of the deuteron σ_{dis}. The experimental spectrum is compared with a spectrum calculated according to Ref. [7] (see text).*

[1] Institute of Nuclear and Hadron Physics

Testing Novel TOF Detectors for CBM at ELBE

F. Dohrmann, R. Kotte, L. Naumann, B. Kämpfer, E. Grosse

Testing of detectors often involves minimum ionizing particles (mips). Usually the intrinsic time resolution of the desired beam is quite broad such that additional reference counters are needed. For testing resistive plate chambers (RPC), which have a wide spectrum of application in particle physics and beyond [1,2], such reference counters need to have a time resolution comparable or better to that of an RPC detector. The time resolution of the RPC detector has to be corrected for contributions by electronics as well as reference counters and the pulse height dependence (walk) of the reference counter. If however the test beam itself has a very good time resolution, one may avoid these problems by referencing the test detector against the beam structure. The electron accelerator ELBE provides up to 40 MeV electrons. The beam packets with time spread of better than 10 ps are well suited for testing time resolutions. Moreover, electrons with energies of a few 10 MeV have very similar specific energy losses as mips and thus may simulate the behavior with respect to pulse height, time resolution and detection efficiency.

The focus of the RPC detector tests at ELBE will be time resolution. The challenge of this elegant method is to provide rather low intensity electron beams. E.g. the CBM experiment at the future FAIR facility at GSI considers hit densities between 20 kHz/cm^2 (near beam) and 1 kHz/cm^2 for acceptable time resolution as well as efficiency. Currently, beam diagnostics at ELBE require a minimal beam intensity of $\sim 1\,\mu A$. Beam experiments have been achieved with three orders of magnitude lower intensities, i.e. ~ 1 nA or $\sim 1 \times 10^{10}$ Hz , but this rate is still too high for detector tests even when distributed over a sufficiently large area. Currently a reliable solution is to reduce beam intensities by a scatterer if necessary.

First parasitic beam tests were performed at the radiation facility cave at ELBE. A 15 MeV electron beam was scattered off a thin Al foil. Electrons were detected under 45 degrees scattering angle. Fig. 1 shows the testing telescope. The background distribution was scanned with respect to the main scattering direction, as shown in Fig. 2. A second test in preparation will use scintillators with very good time resolution as have been used for testing RPC in other laboratories. We have contacted RPC developing groups within our JRA 12 for preparations on RPC tests and prepared the installation of a gas supply facility for gases required for RPC tests. This allows mixing and using these gases at the accelerator as well as in the laboratory. Moreover, cabling, acquisition of hardware and electronics has been completed and first test of an RPC prototype in the laboratory with ^{90}Sr source have been performed.

The test facility is set up for RPC tests. In addition we will set up a second experimental facility which will enable us to perform detector tests completely independent of the radiation facility cave. This second cave should be available for more intensive tests.

[1] http://www.gsi.de/zukunftsprojekt/forschung_e.html
[2] M. Petrovici et al., Nucl. Instr. Meth. A **508** (2003) 75.

Fig. 1: *The testing telescope for background studies. Two thin scintillators are fixed on a rotating step motor. A laser is used for position calibration.*

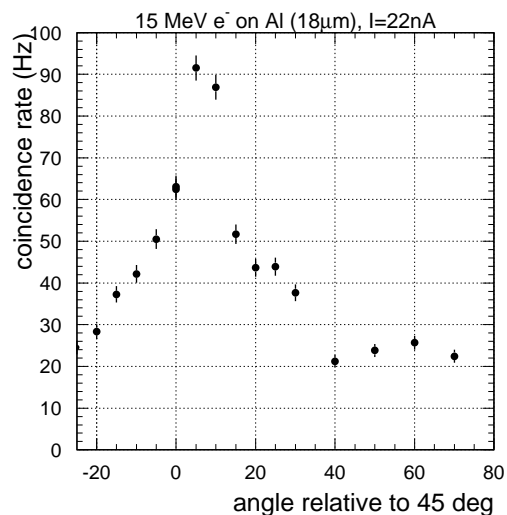**Fig. 2:** *Distribution of background relative to 45 degrees. The main peak corresponds to elastically scattered electrons observed under 45 degrees with respect to the beam direction.*

An Isolating Transformer for High-Resolution Electronics

K. Heidel[1], U. Wolf[1], W. Enghardt[1], A. Wagner[1]

High resolution electronics for experiments at ELBE need to have a clean power supply in order to reduce electronic noise and interference with other installations like, e.g. the superconducting accelerator.

Electronic noise can originate from various sources, like oscillating transients by electromagnetic pulses (EMP), electromagnetic field interference (EFI), radio frequency interference (RFI), low-frequency mains-borne interference (LFI), earth currents. Disturbing sources are generated inside or outside the electronics compartment coupling line-conducted or stray radiation to the experiment electronics.

For this purpose we installed an isolating transformer for nuclear physics, hadron physics, and radiation physics experiments at ELBE. While the experiments are located in the vaults in rooms 109, 111 and 112, the main electronics setup has been installed in the separate room 109 due to the high radiation background at the experiment locations. Care has been taken to avoid any connection between the experiment electronics (power supply, earthing, high voltage supplies) from the liquid helium plant and the accelerator electronics. The transformer follows the specifications for medical applications featuring a high-voltage guard protection and thermal protection [1]. The power supply is based on a three-phase transformer [2] with a separated neutral point contact. An electrical screen at the secondary winding reduces capacitively coupled external noise significantly. The overall power rating is 8.3 kW distributed evenly over all three phases.

Since the switching power supplies of the experiment had been identified as the major source of disturbing currents we disconnected the separate neutral point N (see Fig. 1) and changed from an asymmetrical supply to a symmetric one with phases L and L'. Both conductors feature a symmetric potential against ground and are isolated independently. Disturbing currents stemming from the filter capacitor of switching supplies are now prevented from disturbing the L and L' power lines.

The isolating transformer is rated in class protection 2 (4 kV isolating potential).

[1] European standard EN 60742 (DIN VDE 0551)
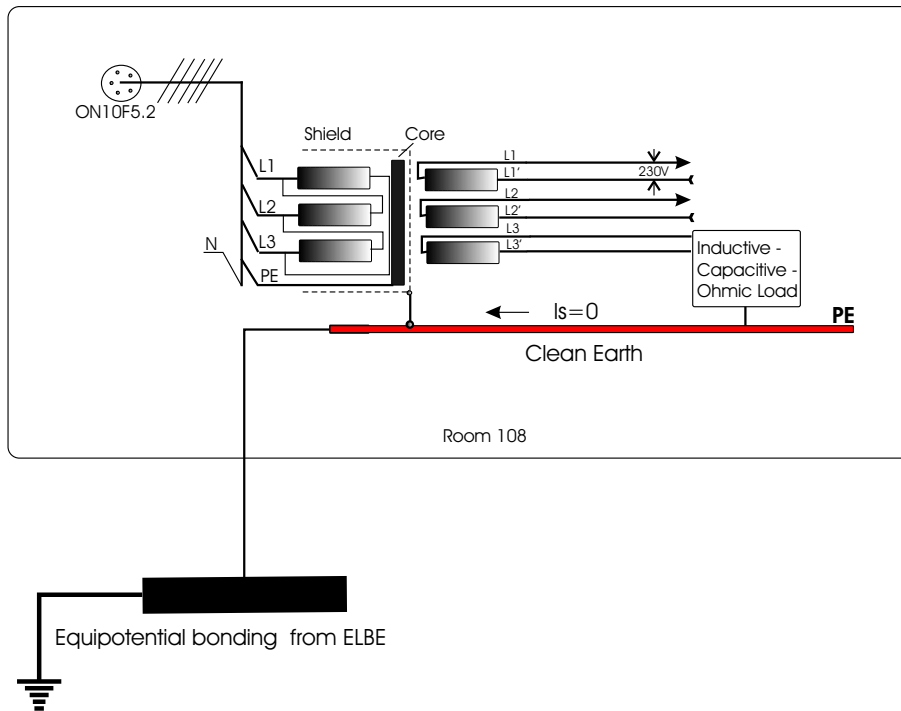[2] DT-MED, Moeller GmbH, Hein-Moeller-Str. 7, D-563115 Bonn, Germany

Fig. 1: *Layout of the isolating transformer for nuclear physics, radiation physics and hadron physics experiments at ELBE.*

---

[1] Institute of Nuclear and Hadron Physics

Fill level control and pressure stability of the ELBE cryostat

Ch. Schneider, F. Herbrand[1]

The major task of the pressure and fill level control is to keep a pressure stability in the Helium tank of the cavities in the range of ±0.1 mbar, not to shift the resonance frequency away from the HF 1.3 GHz main frequency. The pressure is controlled by two cold compressors, which are located in the cold box of the Helium plant. The cold compressors are directly connected to the valve box in the accelerator hall via a transfer line. The two ELBE cryostats are each connected via a separate L-transfer line to opposite sides of the valve box. The fill valves for Cryostat I and Cryostat II are located in the valve box.

It has been shown in the past that the control of the fill level valve alone could not compensate the dynamic load of the cavities to the liquid helium bath if the HF is switched on and off. A second difficulty in the fill level and pressure control is the fact, that the field emission of the ELBE cavities starts very early, see Fig. 1. The expected quadratic power loss to the helium bath with rising gradient is only true for up to 6 or 7 MV/m, after that the exponential rise due to field emission starts. For a gradient of 9 or 10 MV/m (depending on the cavity) a loss in the order of 50 W has to be considered.
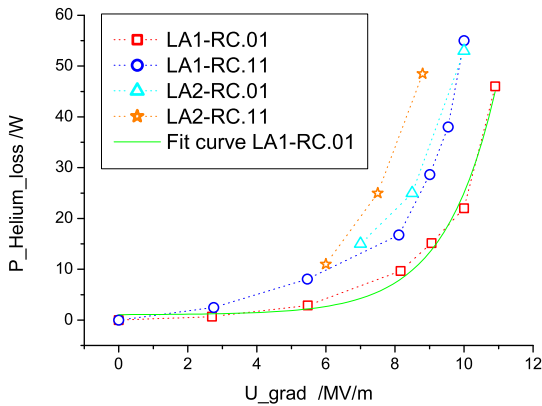

Fig. 1: *Power loss in the helium bath as a function of the applied gradient for the four cavities in the two cryomodules LA1 and LA2.*

All this leads to strong pressure fluctuations in the complete Helium return line out of the required range of ±0.1 mbar, especially in cases, when for security reasons the HF is switched of very fast. Therefore the cryostat design had been adapted in adding a separate pot and heater. An additional small fill level sensor is integrated into the pot to control the heater power. The measured fill level in the pot is than directly proportional to the power of the heater, see Fig. 2. A further opening of the fill valve requires a higher heater power and leads to a higher fill level in the pot. To adapt the fill level of the pot and therefore of the

complete cryostat a settable "Level Set value" is integrated in the controlling process of the heater. When the cavities are switched on the fill level starts to decrease and as a consequence the heater power decreases until the heat load of the cavities and the heater are in balance with the amount of filled Helium.
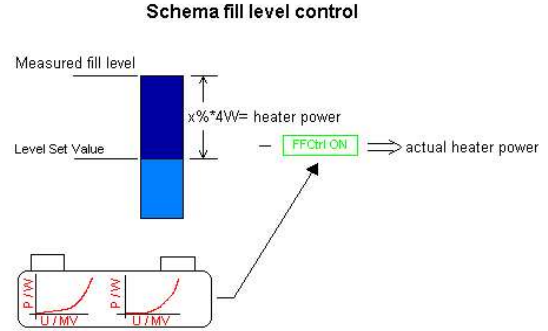

Fig. 2: *Scheme of the fill level control in a cryomodule.*

Since the measurement of the fill level is slower than the heat transfer of the cavities to the helium, especially for the high gradients, still the problem of to strong pressure fluctuations exists. Therefore a feedforward control has been established. From the measured power loss of the single cavities a fit curve had been determined, see Fig. 1 "fit curve LA1-RC.01", from which the expected power loss for an adjusted gradient can be extrapolated. The actual applied heater power is therefore the necessary total heater power determined by the measured fill level in the pot subtracted by the extrapolated value of the cavities. These leads to an over all satisfied pressure stability in the range of ±0.1 mbar, see Fig. 3. Included in Fig. 3 are those events, at which the HF was switched off and on. It is also remarkable that the system with two cryostats in operation works with the required pressure stability.
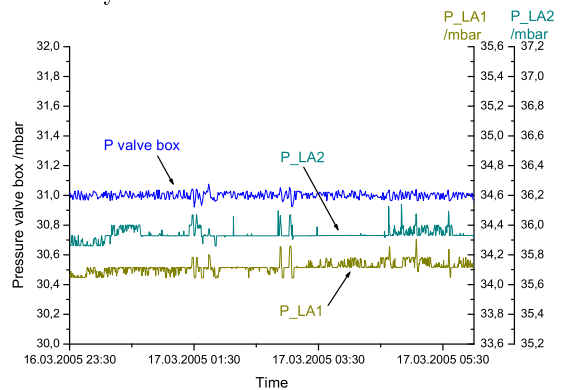

Fig. 3: *Pressure stability in the valve box, cryomodule LA1 and LA2 measured over a period of approx 6 hours (beam energy 28 MeV). Fast switch "off" and "on" of the cavities are included.*

---

[1]Department of Research Technology

An Interface for Online Beam Parameters at ELBE

A. Wagner[1], P. Evtoushenko, F. Herbrand[2], R. Jainsch[2], K. Leege[2]

Modern experiments at accelerators like ELBE quite often need online control and monitoring of accelerator parameters. For the electronic data acquisition system for nuclear physics experiments we developed a software scheme which enables to include various parameters into the online data stream of the experiment. The system uses a TCP/IP data communication stack on a dedicated Windows-based server machine which can be accessed from different data acquisition frontends simultaneously. The server machine communicates exclusively with the accelerator control system which is based on a SIMATIC S7[1]system and an interface on basis of WINCC[2] which prevents the accelerator control from getting locked by hanging processes or communications problems. The server is connected to the accelerator control system via Profibus[3] hardware and OPC[4] SimaticNET software.
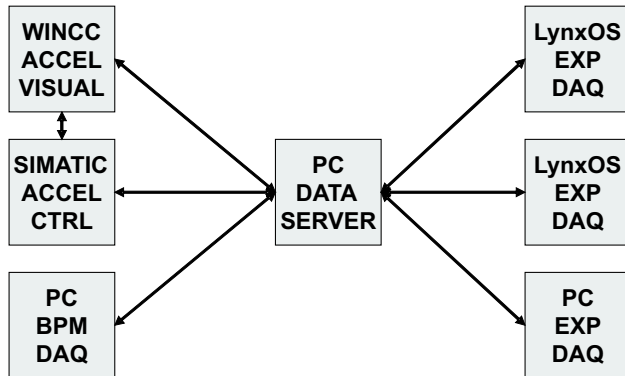

Fig. 1 *Data flow of online accelerator control information, beam position monitor (BPM) data into the data stream of the experiment data acquisition systems (EXP DAQ).*

The communication procedures are implemented in standard C-code using a standardized TCP/IP communication stack. The use of standardized libraries allows for easy integration into different data acquisition front ends. Data are being send by the data server on request from the front end. Each parameter from a predefined list can be accessed independently in either *read only* or *read write* mode. The binary readout data format consists of one 32 bit wide long word (LW) indicating the data quality followed by a

LW for the parameter data value and two LW for the time stamp of the last parameter value update.

Right now, the predefined list of parameters is shown in table 1 which can be extended on request by the experimenters.

Table. 1: *Available parameters for front end data acquisition systems (AC stands for accelerator control, NP stands for nuclear physics, RP stands for radiation physics).*

Data Source	Parameter
AC	acceleration field strengths
AC	injector current
AC	macro-pulse settings
AC	beam position monitor data
AC	NP beam line radiator setting
AC	NP beam shutter setting
AC	NP steerer magnet settings
AC	RP interlock status
AC	RP radiation monitors
NP	online detector count rates

The system has been used in various experiments. The average readout time for about 10 parameters delivered to the nuclear physics data acquisition system [5] is about 15±2ms. This system uses the real-time Unix operating system LYNX-OS[6] on several VME-based Power-PC processors[7].

[1] SIMATIC, Process automation systems, Siemens AG, Munich,
http://www.automation.siemens.com/simatic

[2] SIMATIC WinCC. Process visualization, Siemens AG, Munich.
http://www.automation.siemens.com/wincc

[3] PROFIBUS SIMATIC NET. S7/PC hardware interface, Siemens AG, Munich,
http://www.automation.siemens.com/net

[4] Open Connectivity data exchange standard,
http://www.opcfoundation.org

[5] H.G. Essel, N. Kurz: The General Purpose Data Acquisition System MBS, IEEE Trans. NS 47,2 (2000) 337 and http://daq.gsi.de

[6] Lynx-OS hard real-time operating system. Lynux-Works Inc.. http://www.lynuxworks.com

[7] Creative Electronic Systems, S.A.. http://www.ces.ch

---

[1]Institute of Nuclear and Hadron Physics
[2]Department of Research Technology

A web based electronic logbook for ELBE

C. Rücker[1], A. Schamlott

It is usual praxis in the operation of an accelerator to log all machine relevant parameters in a so called logbook. Usually, this is a paper book, written by different people whos handwritings are difficult to read later on. Quite often various diagrams and pictures have to be inserted and so on. This way, one often misses a continuous history of the operating times and, moreover, only one person can read it at a time. That is why we created a web based "electronic logbook" at ELBE which is in use since February 2003. It is also permitted as a machine diary by the "Sächsisches Landesamt für Umwelt und Geologie (LFUG)".

The electronic logbook found a broad acceptance. An advantage of the electronic logbook is the possibility to allow all interested people (who own access permissions) beside the operators an instant access to the actual machine state from all over the world simply using a web browser.

The electronic logbook is based on an Oracle database (Oracle version 10g), which resides on a central computer of the FZR. All data, pictures and so on are stored on the central fileserver taking advantage of the high availability and data safety.

People who have an account at Rossendorf are allowed to read the data but only the staff of ELBE has permissions to write into the logbook, special entries are designated for the users. The planning of the shifts and the beam time at the accelerator (which is done by the users them selves) is also also realized using a web form based on the Oracle database. The planned shift data are transferred into the logbook. So, at the beginning of the shift, it offers the right header data to the operator. However, it is also possible to create an additional logbook entry for an extra shift.

There are four main paragraphs in the logbook:

- Header data (time, operator, task, energy, beam current)

- Comments which are the main part of the logbook. That means the operator writes down all important notices here. It is possible to insert pictures, diagrams or links to external documents.

- Malfunction and faults (malfunction of the machine or supporting systems, faults means problems with the software or design problems)

- General comments independent of the shift, they are intended as a kind of notification for the whole staff

Most of the graphics (png, jpg, bmp) are immediately shown by the browser. External documents will start with the linked application if it is available on the computer of the user. A search function for the content of the electronic logbook is also implemented. It is also possible to create statistics for the distribution of beam time at the end of a month for instance.

The complete content of the electronic logbook is additionally stored in plain text form in an archive so that it is possible to look for details under unusual circumstances. As a future development it is planned to transfer machine data into the electronic logbook directly from the WinCC control system. A modified version of the electronic logbook for the SRF-Gun cathode preparation is under development.

---

[1] FZR, Department of Information Technology (FKTI)

E L B E - LogBook 07.05.2004 - 2. Schicht

	Protokollauswahl
Protokoll-Nr.: 526		Nutzer-Bemerkung || Aktualisieren
Schicht	07.05.2004 13:04	bis 07.05.2004 22:59
Schichtleiter	Lehnert Dr., Ulf; FWL
SSB	Lehnert Dr., Ulf; FWL
Schichtpersonal	Hartmann, Bernd; FWL (13)
Schichtpersonal	Büttig Dr., Hartmut; FWL (831)
Zusätzl. Personen	Schneider Dr.,Chr. FWL,
Nutzung	Machine Developement Ist-Strahlzeit: 08 Std. 00 min.
Aufgaben	Testbetrieb Optimierung FEL FIRST LASING !!!
Strahlenergie	16 MeV **Strahlstrom** 600 µA
Bemerkung	gestern: ---------------- RC.01 -85.1° 10.18 MV/m RC.11 48.5° 7.60 MV/m

Bemerkung	Die Transmission geht in den Keller!
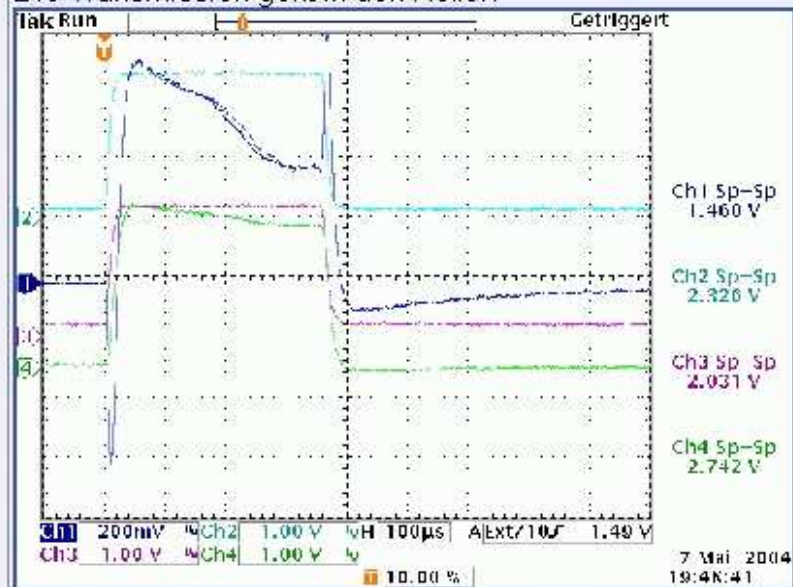
Bemerkung	7.5.2004 19:39 Uhr wir lasen !!!!!!

Fig. 1: *Screenshot of the electronic logbook from the First Lasing Shift at May 07, 2004.*

Remote Controlling of Measurement Instruments at ELBE

R. Schurig, J. Fromme

A variety of different instruments like spectrum- and network analysers, oscilloscopes, power generators and meters are employed at ELBE, during normal operation of the accelerator and especially when intermittent failures have to be traced down. It was required that all instruments can be controlled from anywhere within the FZR intranet, independent of the position of the instrument. Control applications were programmed using the graphical development software LabVIEW from National Instruments. The data is transferred between the control computer(s) and the instruments over Ethernet, GPIB or RS232, depending on what interface is available in the instrument. Every instrument that is equipped with an Ethernet interface is given an unique IP address. Where only a GPIB interface is available, National Instruments GPIB to Ethernet converters are used. One converter is fix installed in the electrical control room, two others can be placed to where needed. Each of the converters has its own IP address that can be addressed from anywhere. The principle of how it works is shown in Figure 1. The applications that control the instruments are usually running on an application server which is in the control room. The Operator can change all of the important instruments parameters, for instance sensitivity, output power, center frequency, etc. Measured data can be stored to user defined data files and can be distributed via data socket server. Any number of clients can read the data from the data socket server for further processing. Direct control over the instrument is also possible from any client within the intranet. It would be possible to control the instruments and read data over the internet, the FZR firewall rules had to be configured accordingly. As the result of this project ready to use control applications for the instruments shown in table 1 are available.

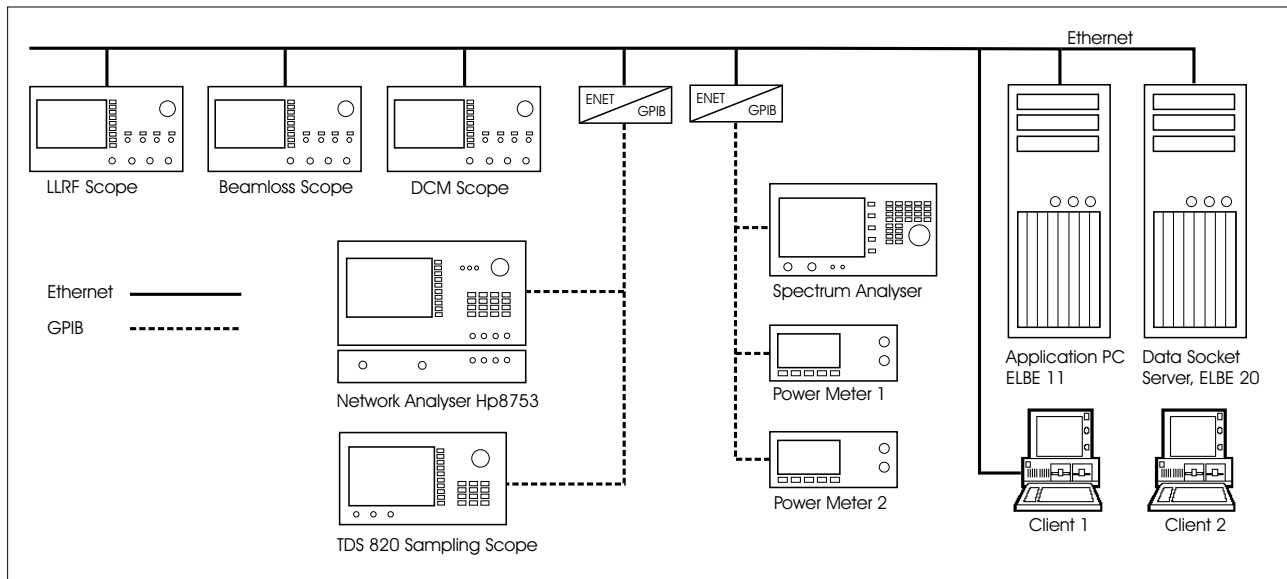| Multimeter | Fluke 45, Agilent 34410, K2000 |
Function Generator	Agilent 33120A, HM8130
Signal Generator	R&S SMT06, SMR20
Scope	TDS3014, 654, 694, 784, 820
Power Meter	Agilent E4419B
Network Analyser	Agilent 8753C, N5230A
Spectrum Analyser	Agilent 8591E, E4404B
Delay Generator	DG535

Tab. 1: *Measuring devices at ELBE.*

Fig. 1: *Principle of instrument remote control.*

Development of a Superconducting RF photo Gun

The Radiation Source ELBE is a place of research and development for superconducting radiofrequency photo injectors. During the last years very successful results have been obtained and the research topic has attracted high international attention. The highlight was the world-wide first operation of such a superconducting rf photo gun with a half–cell resonator in 2002.

For future SRF linear accelerator projects, FEL light sources or 4th generation synchrotron light sources with energy recovery, the development of high brightness electron injectors is one of the most important challenges. High current electron beams of highest quality must be produced by the source and its emittance preserved in the low energy region. The SRF photo gun is considered as one of the most promising candidates. For the BESSY-FEL in Berlin and the 4GLS at Daresbury such a source is intended to be used. The new SRF photo gun now under development will be a fully utilizable injector for the ELBE accelerator and will produce electron beams of much higher quality (higher bunch charge and lower emittance) than the existing thermionic injector. Due to its great relevance the SRF gun project is encouraged and supported by many national and international accelerator institutes. Especially the European Union supports the SRF gun development within the CARE project (Coordinated Accelerator Research in Europe) and a common national research project with BESSY Berlin, DESY Hamburg and Zeuthen, and the Max-Born-Institut Berlin has launched with financial support of the BMBF.

Design of the Cryostat, the Cavity Tuner and the Cathode Transfer Device for a $3\frac{1}{2}$ Cell superconducting RF Gun

H. Büttig, P. Evtushenko, D. Janssen, W.D. Lehmann, U. Lehnert, P. Michel, P. Murcek, Ch. Schneider, F. Staufenbiel, J. Stephan, J. Teichert, R. Xiang

After successful oeration of a half cell superconducting RF gun [1], the development of a new $3\frac{1}{2}$ cell super-conducting RF gun started at the Forschungszentrum Rossendorf.

The new gun will be installed at the ELBE electron accelerator. The design of the main component like cryostat, cavity, cavity tuners, and cathode transfer device was finished in 2004. A three-dimensional sectional view of the cryostat is shown in Fig.1. The working temperature of the cavity will be 2 K. In order to minimize the heat transfer to the room temperature level the cryostat contains an aluminium shield, which is cooled down to LN2 temperature. The LN_2 shield and the He tank are surrounded by multiple layers of superinsulation. The support of the helium tank is realized by eight thin titanium spokes. All together, the static heat transfer into the He bath should be about 3–4 W. The magnetic shield is located between the vacuum vessel and the LN2 shield. It is made of mumetal and prevents the entrance of the magnetic earth field into the superconducting niobium cavity.
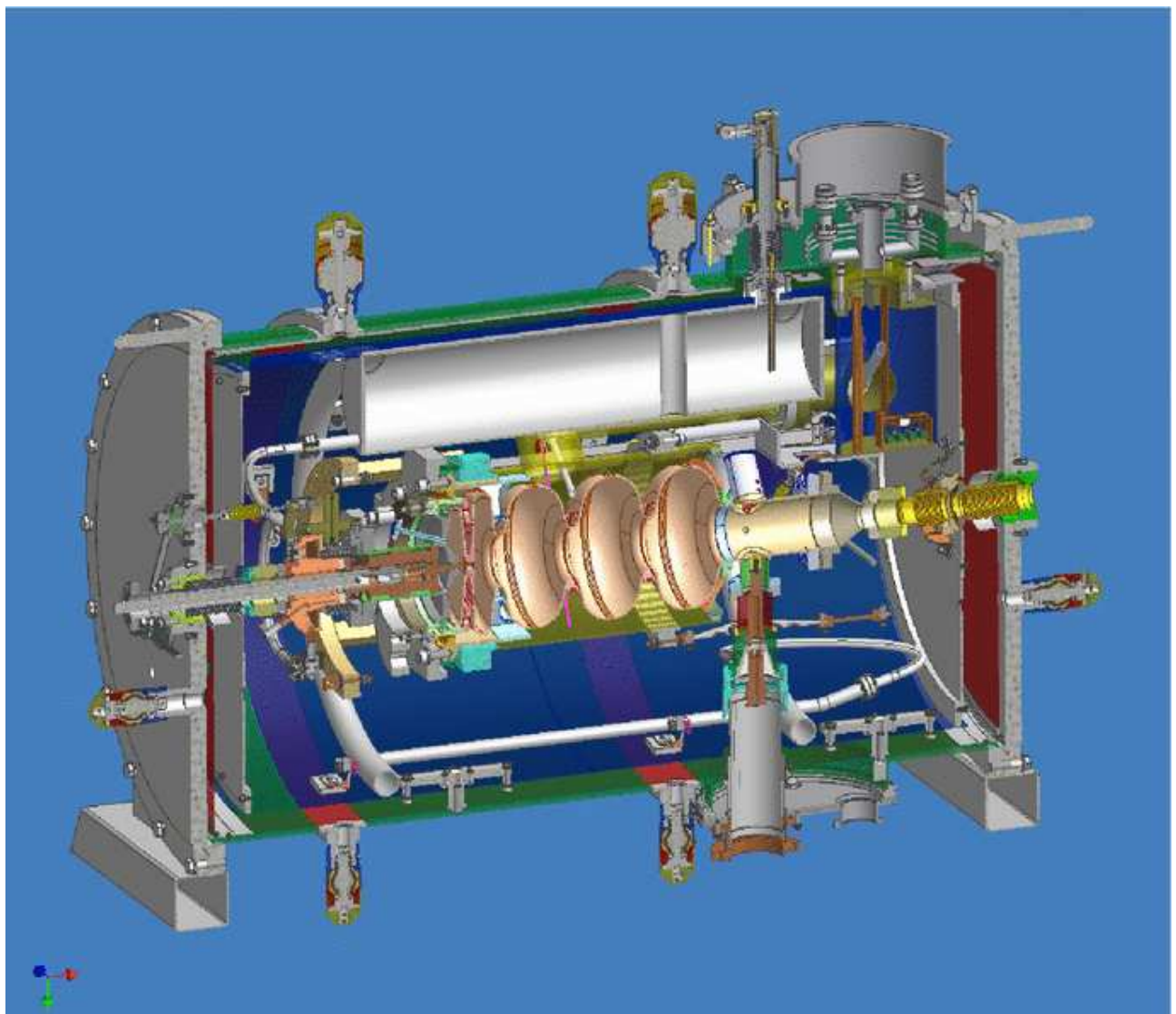

Fig. 1: *Sectional view of the SRF-gun cryostat.*

In order to tune the cavity to the operational frequency of 1.3 GHz and to obtain the optimal field balance between the different cells a special tuning system has been designed. The gun cell and the TESLA cells of the gun cavity have different stiffness constants and require two separate mechanical tuners. These tuners must be able to change the cell lengths in the order of several nanometers. They are designed following the design of the tuner in the ELBE cryostat [2]. The forces are transferred by bends of special parts only. The projected parameters are given in Tab.1 and an overview drawing of the tuning system is presented in Fig.2.
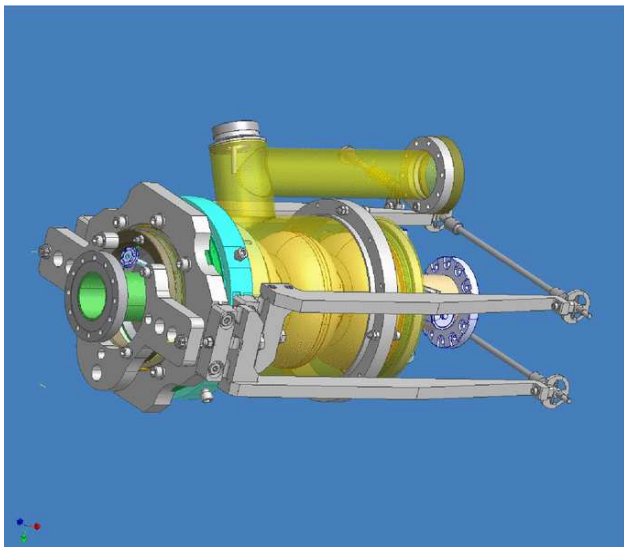

Fig. 2: *Tuning system of the cavity.*

Tab. 1: *Design parameters of the tuning system.*

design range	gun cell	TESLA cells
mechanical range [mm]	-0.25 ... 0.25	-0.3 ... 0.3
frequency shift [kHz]	-137 ... 137	-286 ... 286
force [N]	-2250 ... 2250	-2700 ... 2700

An essential part of the SRF gun is the cathode transfer device. It has the following functions:

- exact positioning of the cathode inside the cavity from outside of the cryostat

- exchange of cathodes without vacuum breakdown and particle production

- cooling of the cathode to liquid nitrogen temperature during gun operation

The design of this module is shown in Fig. 3. Three bridges made of thin titanium sheets connect the cathode cooling cylinder with the cavity flange and allow the adjustment of the cathode. The movement can be performed by means of three wheels from outside the cryostat. Their axes are connected via stainless steel bellows and levers with the Ti brigdes.
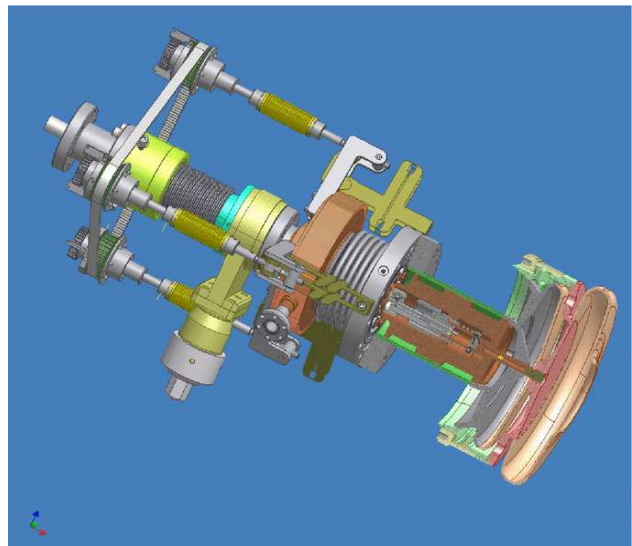

Fig. 3: *Cathode transfer device.*

[1] D. Janssen, et al., FEL-03, Tsukuba, Japan, Sept. 8-12, 2003, NIM A528 (2004) 305
[2] F.Gabriel ed., Internal design report, Forschungszentrum Rossendorf, Dresden 1995

Emittance Compensation in a Superconducting RF Photoelectron Gun by a Magnetic RF Field

D. Janssen, V. Volkov[1]

For compensation of the transverse emittance in normal conducting RF photoelectron guns a static magnetic field is applied. In superconducting RF guns such a static magnetic field cannot be used. Therefore we propose the application of a magnetic RF field (TE - mode) to that purpose which will coexist together with the corresponding accelerating mode in the superconducting cavity of the RF gun. Simulations have been carried out for the $3\frac{1}{2}$ cell cavity of the superconducting RF photo gun currently under development in Rossendorf. The shape of the cavity and the RF fields are shown in Fig. 1.
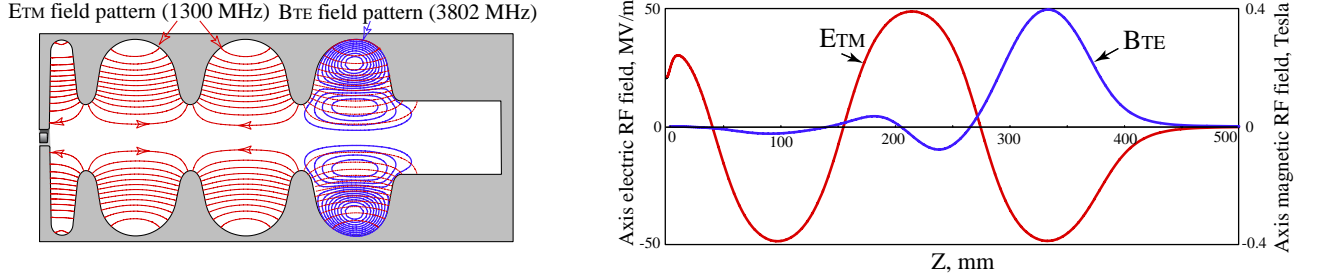

Fig. 1: *Shape and field distribution of the $3\frac{1}{2}$ cell superconducting cavity.*

The results of tracking calculation together with the corresponding peak values of the RF field are given in Tab.1 and Tab.2.

Tab. 1: *Peak values of RF fields in the RF gun.*

Peak of axis E_{TM010}, MeV/m	50
Peak of axis B_{TE021}, mT	324
Peak of surface B_{TE021}, mT	136
Peak of surface B_{TM010}, mT	115
Peak of surface $|B_{TM010} + B_{TE021}|$, mT	144

Tab. 2: *Results of the tracking calculation.*

Bunch transv. norm.emitt., mm mrad	$0.78 - 0.98$
Rms Beam Size, mm	3.06
Longitudinal Emittance, keV mm	72.4
Average Energy, MeV	8.82
Rms Energy Spread, keV	53.9
Rms Bunch Length, mm	2.79
Distance from the cathode, m	4.44
RF phase of TE 3802 MHz mode	$0 - 360°$
RF phase of TM 1300 MHz mode	$74.6°$
Laser spot size, mm	2.6

The main features of TE modes in superconducting RF cavities are the following:

- No obligate coincidence of its resonance frequency with any harmonic frequencies of the acceleration mode.

- The magnetic field of the TE mode is zero on cathode surface.

- Low RF power demands

- The peaks of the surface magnetic field of the TE mode are disposed between the peaks of the accelerating TM mode.

- The magnetic field vectors of the TM and TE mode are perpendicular to each other.

- As a result of the calculation the vector sum of the surface magnetic field is less than the 180 mT limit for RF superconductivity

- The transverse emittance can be reduced by the magnetic field of the TE mode by more than a factor of two

---

[1]BINP SB RAS, Novosibirsk, Russian Federation

New Photocathode Preparation Chamber for the SRF gun

R. Xiang, J. Teichert, M. Anton, C. Werner

The photocathodes play a key role in the photo-injector. We need a kind of photocathode material which fulfils the requirements of high quantum efficiency, short response time and long lifetime in the new $3\frac{1}{2}$ cell superconducting RF gun [1]. This made the establishment of a new laboratory for photoemission at FZR necessary.

Cs_2Te is the best choice among the present photocathode materials. The Cs_2Te photocathode will be produced remotely from the gun, to allow detailed measurements without interfering with the whole gun investigations. There is a UHV transportation system to transfer the prepared cathodes up to six pieces at one time from the chamber to the gun. The central equipments in the photocathode preparation laboratory are the preparation chamber, control system and the diagnostics system.

Fig. 1: *New preparation chamber.*

The preparation of Cs_2Te photocathode has to be undertaken in the vacuum of 10^{-11} mbar - 10^{-9}mbar region. In the new UHV preparation chamber, there are four evaporators of Cesium and Tellurium. A manipulator permits the movement of each of these sources in front of the cathode plug surface, making it possible to change the evaporators without breaking the chamber vacuum. All of these sources can be heated by passing a current through them. The shutter is controlled by a motor to shield the cathode surface while the sources are outgassing. The Cu or Mo cathode plug is fixed on the holder in the middle of the chamber and a halogen light can keep the cathode to 120^oC. During the fabrication process, a knife-edge aperture with the radius of 5mm is placed in front of the cathode as a mask. After the deposition, a special mask made of Molybdenum mesh will be placed in front of photocathode by manipulator, and the UV light beam as thin as 0.3-0.4mm is transported through the mesh to the cathode to measure the Quantum efficiency distribution.

A control software based on C^{++} has been developed to master the voltage on the anode or on the cathode, the temperature of the cathode substrate, the power of the evaporators, and also to control the rotate motor of shutter(see Fig. 2).
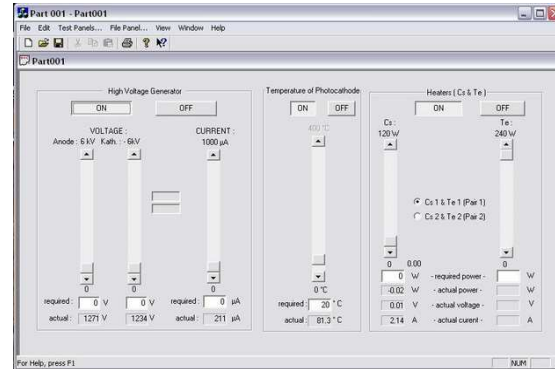

Fig. 2: *Interface of control software.*

The diagnostics tools include the thin film monitor for thickness measurement, the photocurrent meter, and the UV drive laser. To detect the process of the deposition process, we utilize a 262nm laser as the light source. There are some lenses and mirrors which transport the beam and allow adjustment of the beam size at the cathode. A cylindrical lens is used to collimate the asymmetrical laser. A mirror, mounted on a x-y-scanner which can be remoted controlled by piezo motors, allowing the spot on the cathode to be centered and scanned. A UV photodiode is used to measure the relative pulse energy, and the power meter can be inserted to measure the average power. A tiny part of the beam is delivered to the virtual cathode, which is placed at the same distance as the cathode to measure the laser spot size on the cathode. In the beam line, a group of lens work as telescope to adjust the beam size. By using the same laser with scanner, QE distribution of the photoemission layer can also be described in preparation chamber.

In standard evaporation process adopted in the first SRF gun test, not only Cs_2Te, but also other stable compounds formed in the process, which makes the quality of the cathode difficult to anticipate. When the ratio of Cs/Te atoms is controlled exactly, the co-evaporation will be a good way to get more proportioned Cs_2Te film than standard process, and this process will be studied in the new photocathode preparation chamber during 2005. There are still some open questions on the photocathode research. The physics performance of the cathode material in high RF field and low temperature condition needs to be theoretically and experimentally studied.

[1] J. Teichert, R. Xiang, Report on Photocathode. CARE/JRA-PHIN 2004

The ELBE Department
Zentralabteilung Strahlungsquelle ELBE

head: Dr. Peter Michel

      e-mail: P.Michel@fz-rossendorf.de

office: Jacqueline Kraatz

      phone: +49–351–260–2101
      FAX: +49–351–260–3690

Scientific Personnel
Dr. H. Büttig
Dr. P. Evtushenko
Dr. D. Janssen
Dr. U. Lehnert
Dr. Ch. Schneider
Dr. F. Staufenbiel
Dr. J. Teichert
Dr. R. Xiang

Technical Personnel
M. Anton
B. Eppendorfer
M. Freitag
B. Hartmann
M. Justus
J. Kraatz
P. Murcek
B. Reppe
A. Schamlott
R. Schurig
H. Taubert
J. Weiske
R. Wenzel
U. Wünsche

ELBE Facility Operation

C	control and data acquisition	<u>A. Schamlott</u> M. Justus
D	electron beam and diagnostics	<u>Dr. U. Lehnert</u> A. Schamlott Dr. Ch. Schneider R. Schurig
E	electrical installations	<u>R. Wenzel</u> R. Schurig
F	free-electron laser	<u>Dr. W. Seidel[1]</u> Dr. U. Lehnert U. Wolf[1]
G	electron gun	<u>Dr. J. Teichert</u> U. Wünsche
H	RF systems	<u>Dr. H. Büttig</u> R. Schurig R. Wenzel
I	infrastructure and media	<u>B. Eppendorfer</u> B. Reppe
K	cryogenics	<u>Dr. Ch. Schneider</u> J. Weiske U. Wünsche
S	radiation protection	<u>Dr. K. D. Schilling[1]</u> H. Taubert M. Freitag
V	vacuum and mechanics	<u>M. Freitag</u> B. Reppe J. Weiske

[1]Institute of Nuclear and Hadron Physics